Microscopic clustering in light nuclei

Martin Freer[*]

School of Physics and Astronomy, University of Birmingham, Birmingham B15 2TT, United Kingdom

Hisashi Horiuchi[†]

Research Center for Nuclear Physics (RCNP), Osaka University, Osaka 567-0047, Japan and International Institute for Advanced Studies, Kizugawa 619-0225, Japan

Yoshiko Kanada-En'yo[‡]

Department of Physics, Kyoto University, Kyoto 606-8502, Japan

Dean Lee[§]

Facility for Rare Isotope Beams and Department of Physics and Astronomy, Michigan State University, East Lansing, Michigan 48824, USA and Department of Physics, North Carolina State University, Raleigh, North Carolina 27695, USA

Ulf-G. Meißner[‖]

Helmholtz-Institut für Strahlen- und Kernphysik (Theorie) and Bethe Center for Theoretical Physics, Universität Bonn, D-53115 Bonn, Germany and Forschungszentrum Jülich, Institute for Advanced Simulation (IAS-4), Institut für Kernphysik (IKP-3), Jülich Center for Hadron Physics and JARA-HPC, D-52425 Jülich, Germany

(published 28 August 2018)

This review examines the tendency of light nuclei to exhibit clustering, where correlations between nucleons result in the formation of precipitates, typically α particles. The observation of clustering dates to the earliest days of the subject, where α particles were the building blocks of some nuclear models. The description of a nucleus in terms of clusters was attractive in terms of simplifying the computationally challenging problem through the reduction of the degrees of freedom. However, more recently it has been possible to develop *ab initio* methods which seek to build nuclei not from the clusters, but from the individual nucleons with a full account of the Pauli exclusion principle. This review links the development of the subject from the assumption of preformed α particles, through to the development of models which demonstrate the appearance of clustering from the A-nucleon wave function with realistic but effective interactions, to finally first principle approaches using interactions based on chiral effective field theory and the symmetries of quantum chromodynamics. This places the understanding of clustering as a cornerstone of the development of nuclear theory as it attempts to develop a complete understanding of light nuclei from the fundamental strong force.

DOI: 10.1103/RevModPhys.90.035004

CONTENTS

[*]m.freer@bham.ac.uk
[†]horiuchi@rcnp.osaka-u.ac.jp
[‡]yenyo@ruby.scphys.kyoto-u.ac.jp
[§]leed@frib.msu.edu
[‖]meissner@hiskp.uni-bonn.de

I. INTRODUCTION

Nuclear clustering describes the emergence of structures in nuclear physics whose properties resemble those of atomic molecules. In atomic systems there is a rich phenomenology of different types of chemical bonds, complex rotational and vibrational excitations, and intricate structural geometries. The potential for nuclear analogs is intriguing.

The attractive nucleon-nucleon interaction makes the highly symmetric four-nucleon system ^{4}He, the α particle, enormously stable, with a binding energy in excess of other light systems, and the large energy of the first quantum excitation makes the system difficult to perturb. These characteristics led to an early assumption that the α particle might form a stable subunit within the nucleus. However, the underlying physics is made more challenging by the democracy of particles involved in nuclear binding. Instead of heavy ions surrounded by light electrons, the protons and neutrons have nearly equal masses, and the clustering structures emerge from a delicate balance among repulsive short-range forces and Pauli blocking effects, attractive medium-range nuclear forces, and long-range Coulomb repulsion among protons.

Nevertheless, α-particle clustering is a reality in light nuclei. The clusterization has allowed a description of nuclear properties in terms of the geometric arrangement of the clusters, rotational properties of those structures, and even the covalent exchange of valence neutrons between the α-particle cores in an analog of the covalently bound atomic molecular systems.

Early models of nuclear clustering assumed a geometric arrangement of the clusters with a spectrum of excited states given by the dynamical symmetries. Later the models were improved to include the effects of the Pauli exclusion principle via antisymmetrization of the α-particle wave functions, acknowledging the bosonic description broke down at small separations of the α particles. However, the force between the α particles was an effective interaction and there was an explicit criticism of this approach that the α particles were assumed to preexist, which created a tension with those who preferred the single-particle shell-model approach.

This limitation was overcome through the development of techniques which modeled the nucleus as an A-body system in which there was neither an assumption of a mean field nor that the clusters preexisted. Indeed, the mean field could be created from the averaged interaction of the nucleons and clustering was not assumed. In principle, this approach could represent both single-particle shell structure and cluster correlations on an equal footing. Remarkably, the clustering assumed in the geometric α-particle models could be derived from these calculations.

Meanwhile, great strides had been made in developing realistic nucleon-nucleon interactions, some based on governing principles such as effective field theory (EFT). With accompanying advances in computational algorithms and hardware, one now has the chance to precisely describe both the structure of light nuclei and the emergence of clustering from first principles. The present review explores these developments.

The key elements associated with the development of the field are as follows. The experimental study of nuclear clustering really began with Rutherford's discovery by alpha radiation (Rutherford, 1899) and the development of quantum mechanics. Gamow (1928) and, independently, Gurney and Condon (1928) described the α particle as undergoing quantum-mechanical tunneling from inside the decaying nucleus. About a decade later, Wheeler (1937a) developed the resonating group method to describe α clusters and other cluster groupings within nuclei, while allowing protons and neutrons to maintain their fermionic quantum statistics. Afterward came the work of Hafstad and Teller (1938), which described even-even $N = Z$ nuclei in terms of an α-particle model with bonds connecting clusters. Following along the same lines, Dennison (1940, 1954) proposed a model of the

low-lying states ^{16}O in terms of four α clusters at the vertices of a regular tetrahedron. At a more microscopic level, Margenau (1941) used a Slater determinant wave function for α clusters to compute an effective α-α interaction.

Some years later, Morinaga (1956) suggested that nonspherical and even linear chains of α clusters could describe some states of α-like nuclei. One of the candidates for such a description was the second 0^+ state of ^{12}C postulated by Hoyle (1954) as responsible for enhancing the triple-α reaction in stars and experimentally observed soon after (Cook *et al.*, 1957). Concurrent with these theoretical developments, new experiments provided high-quality data on elastic α-α scattering (Heydenburg and Temmer, 1956; Nilson *et al.*, 1958; Afzal, Ahmad, and Ali, 1969). This in turn led to the development of an effective α-α interaction (Ali and Bodmer, 1966).

At around the same time, Brink (1966) used Margneau's Slater determinant wave function for the α cluster and the generator coordinate method to simplify calculations that were difficult in the more general formalism of the resonating group method. The equivalence of the generator coordinate method and resonating group method was later clarified by Horiuchi (1970). On the topic of α decays, Clark and Wang (1966) computed the probability of α clusters to form near the surface of heavy nuclei. Meanwhile Ikeda, Tagikawa, and Horiuchi (1968) noticed that α clustering appeared close to α-decay thresholds, and these were denoted schematically with the so-called Ikeda diagrams. Following these same concepts, the study of clustering was extended to proton-rich and neutron-rich systems with nearby open thresholds. The corresponding states are weakly bound systems of clusters and excess neutrons or protons.

There have been a number of reviews on clustering in nuclei (Akaishi *et al.*, 1986; von Oertzen, Freer, and Kanada-En'yo, 2006; Freer, 2007; Beck, 2010, 2012, 2014; Horiuchi, Ikeda, and Kato, 2012; Funaki, Horiuchi, and Tohsaki, 2015). The purpose of this review is to give a broad overview of the exciting developments in the past few years. Because of space limitations, it is not possible to cover all areas of research in depth. Nevertheless, we try to give a balanced view of the field as seen by a team of practitioners covering a range of methods and expertise. In the review of theoretical methods, we focus on microscopic clustering where clusters emerge from nucleonic degrees of freedom. As the field is dynamic and evolving, several key issues are not resolved at present, and there are disagreements among different methods. Furthermore, some of the most interesting results will likely come in the near future. This is to be expected in a growing field with important open questions and active research being pursued by many.

This review begins with an account of recent experimental results and future directions. We then discuss several theoretical approaches, including the resonating group and generator coordinate methods, antisymmetrized molecular dynamics, the Tohsaki-Horiuchi-Schuck-Röpke wave function and container model, no-core shell-model methods, continuum quantum Monte Carlo methods, and lattice effective field theory. We then conclude with a summary and outlook for the future.

II. RECENT EXPERIMENTAL RESULTS

A. Experimental observables

The experimental study of the role of clustering in nuclei dates back to the earliest observations of α decay of heavy nuclei. In the early models of nuclei, it was assumed by many that the α particle may play an important role, e.g., Hafstad and Teller (1938) describe the possible structures of nuclei such as ^{8}Be, ^{12}C, and ^{16}O as constructed from α particles. This early work also speculated on the existence of molecular structures in light nuclei, where neutrons, or even neutron holes, might be exchanged among α-particle cores. These basic ideas remain the drivers for much of the present experimental program. The "modern" era of nuclear clustering was catalyzed by the ideas of Morinaga (1956), who had suggested that the 7.65 MeV Hoyle state in ^{12}C, which had recently been experimentally measured, might be a linear arrangement of 3α particles. The concept that linear-chain structures might exist in nuclei has stuck with the subject until the present and remains to be resolved. Experiment has been substantially motivated by the desire to provide evidence for the types of structures envisaged by Morinaga and those calculated by Brink using the Bloch-Brink alpha cluster model (Brink and Boeker, 1967; Brink, 2008). For example, in the case of ^{12}C, the α-cluster model (ACM) finds two structures. The first is an equilateral triangular arrangement which historically has been associated with the ground state, and the second is a linear arrangement (or chain).

The ability of experiments to elucidate the cluster structures of light and heavy nuclei is determined by the range of experimental observables that may be extracted. From a simplistic starting point, the moment of inertia of a rotating nucleus gives insight into the deformation which can be at least shown to be consistent with a cluster structure, even if not direct evidence. If ^{8}Be is used as an example, then the ground-state rotational band has 0^+, 2^+, and 4^+ states at 0, 3.06, and 11.35 MeV. The ratio of the 4^+ to 2^+ energy is 3.7, very close to what one would expect for a rotational nucleus 3.33. The moment of inertia that one extracts from $E_{\rm rot} = J(J+1)\hbar^2/2\mathcal{I}$ is commensurate with that found in *ab initio* Green's function Monte Carlo (GFMC) calculations, which strongly reveal the cluster structure (Wiringa *et al.*, 2000). We discuss calculations using Green's function Monte Carlo in Sec. VII.B. As a simple guide, the value of $\hbar^2/2\mathcal{I}$ associated with the 2^+ state is 0.51 MeV, which even in a simple calculation yields a separation of two α particles by twice the α-particle radius. The observation of a series of states which lie on a rotational sequence is not convincing evidence of either clustering or deformation. Here measurements of electromagnetic transition strengths provide tests of the overlaps of initial- and final-state structures and the degree of collectivity. For the case of ^{8}Be, a measurement of the $B(E2)$ transition strength from the 4^+ to the 2^+ state provides a consistent description with both the rotational picture and the GFMC calculations (Datar *et al.*, 2013).

However, and as previously noted, this simplistic interpretation needs to be treated with care. First, all of the states in ^{8}Be are unbound and hence are embedded in the continuum

and will have continuum contributions. Second, the widths of the states are significant (see Sec. II.B.1), and correspondingly the lifetimes short, and thus an understanding of what collectivity means on such short time scales is unclear. Finally, many calculations use bound-state approximations and hence cannot be completely accurate. There is an interesting discussion of the meaning of rotational bands where the resonances are embedded in the continuum, with a focus on ^{8}Be, by Garrido, Jensen, and Fedorov (2013). The conclusion is that rotational bands embedded in the continuum may still be a meaningful concept, but that the continuum affects properties such as transition probabilities and hence here the continuum needs to be treated carefully. This is particularly important for the comparison with *ab initio* methods.

The width of a state reveals a significant amount of detail regarding the structure and the decay. The greater the overlap of initial structure with the decay partition then the shorter the lifetime and the greater the width. In the case of the 2^+ excitation of ^{8}Be, the width is tabulated as 1.5 MeV. The decay width is also affected by the barrier through which the decay must proceed, but if the Coulomb and centrifugal barriers are removed, then the reduced width may be compared with the Wigner limit. This is the value the reduced width should adopt if the α particles are fully preformed. For this particular state, it is found that the experimental width is very close to the Wigner limit, again indicating the existence of the cluster structure (Cerny, 1974; Overway *et al.*, 1981). A further signature, not available to the decay of the example states in ^{8}Be, is the measurement of the dominant decay channel. States with strong cluster-like properties should preferentially decay by cluster emission as opposed to proton or neutron decay, for example. In reactions, this structural similarity is described in terms of a spectroscopic factor or an asymptotic normalization coefficient (ANC).

In the following sections we explore many of the recent developments in the experimental study of nuclear clustering. In many cases the recent work builds on significant historical work. There are many review articles that describe the development of the subject and we refer the interested reader to Freer and Merchant 1997), von Oertzen, Freer, and Kanada-En'yo (2006), Freer (2007), Beck (2010, 2012, 2014), and Freer and Fynbo (2014).

B. Status of studies of light nuclei

1. Alpha-conjugate systems, *N*-alpha structures, and chains

By far the most experimental attention has been devoted to the study of the cluster structure of α-conjugate nuclei. Here the challenges have been to first provide deeper insight into the nature of the cluster structures and ultimately to determine if the chain states really exist in light nuclei or not. The eventual aim is to determine experimental characteristics such that they may be tested against *ab initio* or other microscopic calculations.

^{8}Be: As already described, one of the best examples of the comparison between *ab initio* theory and experiment is the measurement of the gamma decay of the 4^+ state in ^{8}Be to the 2^+ state (Datar *et al.*, 2013). This was a *tour de force* where a gamma decay branch of $\sim 10^{-7}$ was observed. The experiment involved the use of a helium gas-jet target, and the 4^+ state was resonantly populated with a ^{4}He beam. The emitted gamma ray and the subsequent emission of the two α particles from the decay of the 2^+ state were detected in a triple coincidence. A cross section of 165(54) nb was observed which translated to a $B(E2)$ of 25 ± 8 e^2 fm^4. This is remarkably close to the value most recently calculated in the GFMC approach of 26.0 ± 0.6 e^2 fm^4 (Datar *et al.*, 2013) [see also Avila *et al.* (2015) and Wiringa *et al.* (2000)]. These latter calculations found the ground state of ^{8}Be to be highly clustered and predicted with significant precision the excitation-energy spectrum (Wiringa *et al.*, 2000). Given that the $B(E2)$ is sensitive to the overlap of the charge distribution and the collective behavior, such a result could be taken as evidence of both the cluster and collective behaviors. However, that being the case, this raises a rather interesting conundrum.[1] The widths of both the 2^+ and 4^+ states are large (1.5 and 3.5 MeV, respectively). From the uncertainty principle, these would correspond to lifetimes of the order of 10^{-22} s. This is the transit time of a nucleon with the Fermi energy to cross the nucleus. How is it possible for collective processes to develop and for rotational behavior to occur given the apparent mismatch in time scales, and what do rotations mean in such systems (Fossez *et al.*, 2016)? It is therefore possible that what is observed experimentally is simply patterns more generally linked to the underlying symmetry of a dumbbell-like structure. When it comes to precisely describing the properties of such states embedded in the continuum, the influence of the continuum on transition properties need to be fully accounted for (Garrido, Jensen, and Fedorov, 2013), and it is vital that *ab initio* methods be developed for such unbound systems.

^{12}C ground state and rotational band: Similar questions are pertinent for the next α-conjugate system ^{12}C. The effect of the continuum on the rotational bands in ^{12}C was discussed by Garrido, Jensen, and Fedorov (2016). Here the transitions between states are found to be consistent with the rotational picture. For ^{8}Be all the states lie above the α-decay threshold and hence, by definition for the emergence of clustering developed by Ikeda, have the ingredients for the formation of clusters (Ikeda, Tagikawa, and Horiuchi, 1968). However, the ground state of ^{12}C lies $\sim$7.3 MeV below the decay threshold, and hence the cluster structure would be suppressed. However, as shown in Fig. 1, antisymmetrized molecular dynamics (AMD) calculations indicate that states above the decay threshold (Hoyle band) clearly have a cluster structure, but even within the ground state this component may not be insignificant (Kanada-En'yo, 2007). This is supported by recent calculations using nuclear lattice simulations (Epelbaum *et al.*, 2012).

We discuss AMD methods in some detail in Sec. IV and lattice methods in Sec. VIII. The experimental $B(E2)$ for the transition from the first 2_1^+ state at 4.4 MeV to the ground state has been determined to be 7.6 ± 0.4 e^2 fm^4, which compares favorably with that calculated within the AMD framework of

[1]W. Nazarewicz, private communication at the 2015 Gordon Research Conference, New Hampshire, USA.

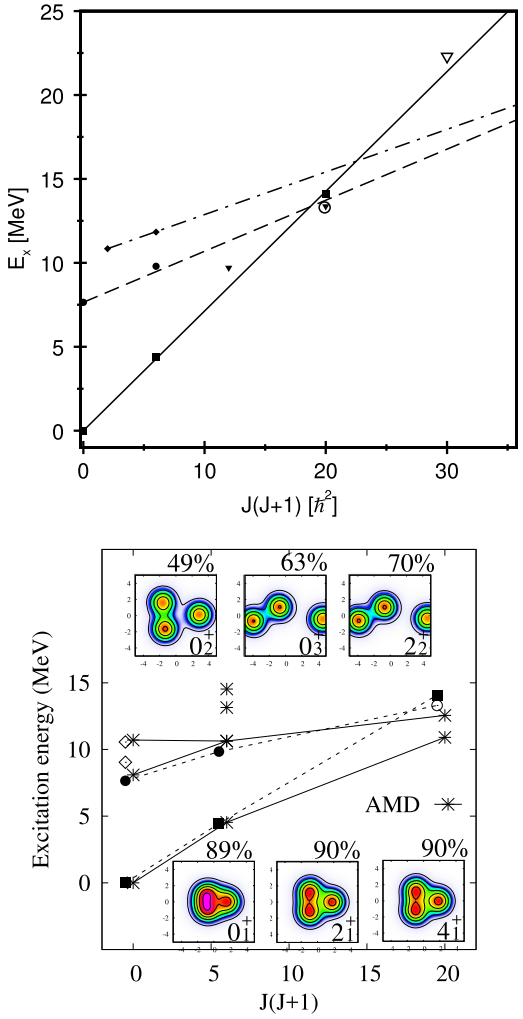

FIG. 1. (Upper) Experimental energy-spin systematics of states in ^{12}C. Filled symbols are strong assignments, and open symbols are tentative assignments which are yet to be confirmed. The squares correspond to the ground-state rotational band 0^+, 2^+, and 4^+. Triangles are the 3^-, 4^-, and 5^- states. Circles are states associated with the Hoyle band (0^+, 2^+, and 4^+), and diamonds are the 1^- and 2^- states. The various lines correspond to best fits to the rotational systematics. (Lower) Energy levels of the 0^+, 2^+, and 4^+ states in ^{12}C and matter density distributions obtained by antisymmetrized molecular dynamics (AMD) with variation after projection using the modified Volkov No. 1 (MV1) force (Kanada-En'yo, 2007) (asterisk symbols) are compared with the experimental energy spectra from Ajzenberg-Selove (1990), Freer *et al.* (2007, 2011), and Itoh *et al.* (2011). The intrinsic density distributions are shown together with percentages of the dominant component in the final wave functions. The 4_2^+ state has dominantly the same intrinsic component as that of the 2_2^+ state. The states with strong $E2$ transitions are connected by solid lines. Dashed lines correspond to the tentative assignments of experimental levels in the upper panel.

8.5 e^2 fm^4 (Kanada-En'yo, 2007). The calculated value for the transition from the 4_1^+ state is similar to a value of 16 e^2 fm^4. To date there is no experimental measurement, but this would in principle confirm if these states are rotationally linked.

This raises the question whether it might be experimentally possible to observe the intrinsic cluster structure shown in the AMD calculations for the ^{12}C ground state. One possibility might be via ultrarelativistic $^{12}\mathrm{C} + {}^{208}\mathrm{Pb}$ collisions where differences between the α clustered and uniform ^{12}C nucleus may be visible in quantities such as the triangular flow, event-by-event fluctuations, or the correlations of the elliptic and triangular flows (Broniowski and Arriola, 2014). A similar approach, e.g., examination of the properties of the fragmentation of ^{12}C at high energy, was explored by Artemenkov *et al.* (2017). Another possibility is via α-particle knockout from the ground state. The measurement of the $^{12}\mathrm{C}(p, p\alpha)$ reaction using polarized beams found analyzing powers which were strongly indicative of α particles being preformed in the ground state (Mabiala *et al.*, 2009). This provides no information on any geometric arrangement or otherwise. Alternatively, it may be possible to exploit the dynamical symmetries associated with the triangular arrangement of the three α particles. The early work of Hafstad and Teller (1938) paved the way for the more recent work of Bijker and Iachello (2014). The dynamical symmetries of the 3α system correspond to a spinning top with a triangular point symmetry (D_{3h}). The rotational properties of these states are given by

$$E_{J,K} = \frac{\hbar^2 J(J+1)}{2\mathcal{I}_{\mathrm{Be}}} - \frac{\hbar^2 K^2}{4\mathcal{I}_{\mathrm{Be}}}, \tag{2.1}$$

where $\mathcal{I}_{\mathrm{Be}}$ is the moment of inertia corresponding to two touching α particles, which can be determined from the ^{8}Be ground-state rotational band (Hafstad and Teller, 1938). K is the projection of the angular momentum onto the symmetry axis of the 3α system. One would expect that there should be a number of rotational bands with different values of K. For $K^\pi = 0^+$, the rotations will be around an axis which lies in the plane of the three α particles, generating a series of states $0^+, 2^+, 4^+, \ldots$. These correspond to the rotation of a ^{8}Be nucleus, the rotation axis passing through the center of the third α particle. The next set of rotations corresponds to the rotation around an axis perpendicular to the plane of the triangle, with each α particle having one unit on angular momentum, thereby giving $L = 3 \times 1\hbar$; $K^\pi = 3^-$. Rotations around this axis and those parallel to the plane combine to give a series of states $3^-, 4^-, 5^-, \ldots$.

The ground-state band described, with 2^+ and 4^+ states at 4.4 and 14.1 MeV, corresponds to the $K^\pi = 0^+$ rotational band. A candidate for the $K^\pi = 3^-$ bandhead is the 9.6 MeV 3^- state. The 13.3 MeV state presently tentatively labeled with $J^\pi = 2^-$ in tabulations has recently been shown to almost certainly have $J^\pi = 4^-$ (Freer *et al.*, 2007; Kirsebom *et al.*, 2010). Moreover, the 3^- state has been shown to have a reduced α width which indicates a cluster structure (Kokalova *et al.*, 2013). The observation of a candidate for a 5^- state at 22.5 MeV (Marin-Lambarri *et al.*, 2014) appears to complete the systematics and is also consistent with the AMD calculations (Kanada-En'yo, 2007). Widths of the negative parity states have not been calculated with AMD. However, Uegaki's 3α GCM [generator coordinate method (GCM)] calculations describe well the widths of the 3^- at 9.64 MeV and 4^- at 13.35 MeV (Uegaki *et al.*, 1979). The former and the latter are

dominated by the $^8\mathrm{Be}(0^+)+\alpha$ and $^8\mathrm{Be}(2^+)+\alpha$ partial decay widths. The width of the 5^- may be dominated by the $^8\mathrm{Be}(2^+)+\alpha$ partial decay width, but as yet there are no calculations to confirm this.

As with ^{8}Be, the widths of the unbound states in ^{12}C influence the possible collective interpretation. The 14.1 MeV, 4^+, state has a width of 270 keV and the 9.6 MeV 3^- state has a width of 46 keV, both of which may not affect the collective time scale. However, the states associated with the Hoyle state (see next) have large widths of the order of MeV or greater and a simple rotational picture may be an oversimplification.

The Hoyle state and collective excitations: The Hoyle state in ^{12}C is one of the best known states in nuclei given its rather crucial role in the synthesis of carbon through the triple-α process. The recent review of this state (Freer and Fynbo, 2014) provides a comprehensive description of its role in synthesis and its experimental properties. Suffice it to say, from an experimental perspective those properties have been well characterized. On the other hand, its structure is less well understood.

The fact that no-core shell-model calculations fail to reproduce the energy of the Hoyle state (Navrátil, Vary, and Barrett, 2000b; Navrátil *et al.*, 2007), without resorting to a significantly expanded harmonic oscillator basis, indicates already that the structure lies beyond that readily described by the shell model. The first *ab initio* calculation of the Hoyle state was performed only a few years ago by Epelbaum *et al.* (2011). These latter calculations were able to explicitly capture the α clusterization that appears in this state. The AMD calculations (Fig. 1) indicate that the Hoyle state is an extended three α system and that the associated 2^+ and 4^+ excited states are not rigid, rotational, excitations and that a loose assembly of α particles, an α gas, may be a better description. A similar conclusion was reached in the fermionic molecular dynamics (FMD) calculations for the same states (Neff and Feldmeier, 2014). Here it was suggested that the 2^+ and 4^+ resonances might be considered as members of a rotational band built on the ^{8}Be ground state with the third α particle orbiting around the ^{8}Be nucleus with relative orbital angular momentum of 2 or 4, respectively. The origin of nuclear clustering with relevance to the formation of the Hoyle state was also discussed by Okolowicz, Nazarewicz, and Ploszajczak (2013).

It was observed by Barker and Treacy (1962) that in order to reproduce the width of the Hoyle state, one has to use an unusually large radius: with a radius of 1.6 fm $A^{1/3}$, a width of 9.3 eV corresponds to a dimensionless reduced width $\theta^2 = \gamma_\lambda{}^2 M_{\mathrm{red}} R^2/\hbar^2$ as large as 1.5. Hence, the width of the Hoyle state is very large; this can be understood only if there is a large degree of α clustering. The presence of this cluster structure enhances the α-capture cross section. But its existence within the Gamow window results in the overall capture cross section being boosted by a factor of 10^8. Without the precise location of this state the abundance of carbon-12 would be greatly reduced, and thus it is intimately related to the existence of organic life. The rather deep question is if this is a happy accident, or if there is some reason why states with strongly developed cluster structure should exist close to the corresponding decay thresholds (Epelbaum *et al.*, 2013a, 2013b; Okolowicz, Nazarewicz, and Ploszajczak, 2013; Freer and Fynbo, 2014).

Beyond the fact that the Hoyle state has a 3α-cluster structure, the nature of that structure remains to be resolved. The AMD calculations in Fig. 1 indicate a dominance of $^8\mathrm{Be}+\alpha$ configurations in a loose assembly such that the 2^+ and 4^+ excitations do not possess a clear rotational behavior. The FMD calculations of the Hoyle state yield similar conclusions (Chernykh *et al.*, 2007). An extension of these ideas is that the state may be described by a gas or condensate of α particles (Funaki *et al.*, 2009). In principle, it may be possible to gain insight into the structure through the decay properties of the state. In this instance there are two decay modes open: sequential and direct. In the latter the system does not decay through the ^{8}Be ground state. An upper limit for nonsequential α decay of 4% was first determined by Freer *et al.* (1994). Subsequently, a measurement of the $^{40}\mathrm{Ca}+{}^{12}\mathrm{C}$ reaction at 25 MeV/nucleon suggested that the branching ratio was in fact higher at $7.5\% \pm 4\%$. This was challenged by further measurements where upper limits as low as 5×10^{-3} (95% C.L.) (Kirsebom *et al.*, 2012; Manfredi *et al.*, 2012) and $9(2)\times10^{-3}$ were put forward (Rana *et al.*, 2013). This was improved to be 0.2% (Itoh *et al.*, 2014). These measurements have now reached a sensitivity at which the phase space effects cease to be the dominant factor and it may be possible to probe the structure with limits of 0.047% (Smith *et al.*, 2017) and 0.043% (Dell'Aquila *et al.*, 2017), compared with the predicted phase space limit of 0.06% (Smith *et al.*, 2017).

A second approach is to probe the charge distribution through electron inelastic scattering (Strehl and Schucan, 1968; Sick and Mccarthy, 1970; Horikawa *et al.*, 1971; Nakada, Torizuka, and Horikawa, 1971). In such measurements the transition form factor is determined, which probes the overlap of the ground state with the Hoyle state. To interpret such measurements a model is required that can describe both the ground and excited states. Both the condensate (Funaki *et al.*, 2006) and FMD descriptions (Chernykh *et al.*, 2007) indicate that the Hoyle state is associated with a radius larger than that of the ground state by a factor of 1.35 to 1.60 (depending on the model used to analyze the data), which would correspond to an increase in volume by a factor of 2.5 to 4. Figure 2 shows the calculated electron inelastic scattering distribution for the condensate model (Funaki *et al.*, 2006).

A third approach to deduce the structure of the Hoyle state is to search for collective excitations, in particular, the 2^+ excitation. Inelastic scattering measurements (Freer *et al.*, 2009; Itoh *et al.*, 2011; Zimmerman *et al.*, 2011) were the first to provide evidence for such an excitation. A common analysis of the evidence for a 2^+ resonance from the proton and α-particle scattering data is given by Freer *et al.* (2012a), and a discussion of the impact of these measurements is given by Fynbo and Freer (2011). The 2^+ line shape, which is found in the inelastic scattering measurements of $^{12}\mathrm{C}(\alpha,\alpha')$ and $^{12}\mathrm{C}(p,p')$ (Freer *et al.*, 2012a), determined the properties to be $E_x = 9.75(0.15)$ MeV with a width of 750(150) keV. The existence of the 2^+ resonance was confirmed by a measurement of the $^{12}\mathrm{C}(\gamma,3\alpha)$ reaction at the HIγS facility (Zimmerman *et al.*, 2013). The excitation function for these

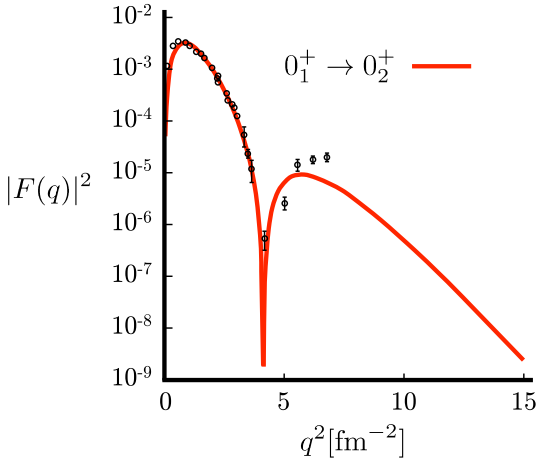

FIG. 2. The calculated inelastic form factor for electron inelastic scattering from the 0_1^+ ground state to the 0_2^+ excited state (Funaki *et al.*, 2006) for the Bose-Einstein condensate approach (red), compared with the experimental data from Strehl and Schucan (1968), Sick and Mccarthy (1970), Horikawa *et al.* (1971), and Nakada, Torizuka, and Horikawa (1971).

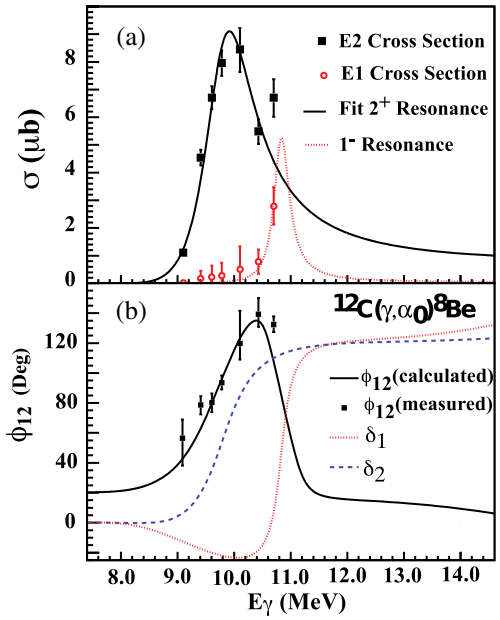

FIG. 3. (a) The measured $E1$ and $E2$ cross sections of the $^{12}C(\gamma,\alpha_0)^8Be$ reaction. (b) The measured $E1$-$E2$ relative phase angle (ϕ_{12}) together with the phase angle calculated from a two-resonance model. A reanalysis of the data by Fynbo *et al.*[2] indicates for a channel radius $R_0 = 1.6$ fm the resonance energy is $E_R = 10.025 \pm 0.050$, $\Gamma = 1.6 \pm 0.13$ MeV, and $\Gamma_\gamma = 220^{+26}_{-36}$ meV. From Zimmerman *et al.*, 2013.

measurements is shown in Fig. 3 and gives resonant parameters of $E_x = 10.13(6)$ MeV and $\Gamma = 2.1(3)$ MeV (Zimmerman, 2013).

These measurements have now been extended to higher energies and continue the expected trend for the 2^+ excitation.[3] If the state has a rotational behavior then there should also be a 4^+ state close to 14 MeV. There exists tentative evidence for such a state at 13.3 MeV with a width of 1.7 MeV (Freer *et al.*, 2011; Jyväskylä, 2013; Ogloblin *et al.*, 2014). The existence of this latter state has yet to be definitively confirmed. It appears to decay strongly to the ^{8}Be ground state as opposed to the 2^+ excited state, which might provide an insight into the way the angular momentum is constructed, i.e., through the orbiting of the α particle around a $^8\mathrm{Be}(0^+)$ core. Although much progress has been made in terms of understanding the structure of ^{12}C, the measurements are typically challenging and often far from unambiguous. As such, the need for detailed spectroscopy continues. Here the approach of the Aarhus group (Kirsebom *et al.*, 2014) in measuring electromagnetic properties points the way for those future studies. The $p + {}^{11}\mathrm{B}$ capture reaction is used to resonantly populate states in ^{12}C, and their decay after emitting an unobserved gamma decay is recorded through the subsequent charged particle channel.

The Hoyle state, although extended, is not consistent with a linear-chain structure arrangement that would require the 2^+ state to lie $\sim$1 MeV lower than observed experimentally. Guidance from theory (Kanada-En'yo, 2007) suggests that the 10.3 MeV, 0_3^+ state is the best possibility. This state has a width of 3 MeV and a 2^+ state corresponding to a linear-chain structure would be expected close to 11.5 MeV and would have a very large width. As yet, such a state remains to be observed. Recently, the possibility of two 0^+ states around 10 MeV was experimentally reported by Itoh *et al.* (2011) and supported by the extended Tohsaki-Horiuchi-Schuck-Röpke (THSR) calculation (Funaki, 2015; Funaki, Horiuchi, and Tohsaki, 2015).

Figure 4 shows the compilation of theoretical spectra and transitions for 0^+ and 2^+ states compared with the experimental data. Although there are many nonmicroscopic and semimicroscopic 3α calculations, we show only microscopic calculations with fully antisymmetrized wave functions and nucleon-nucleon interactions. It is difficult to directly compare the reproduction quality of microscopic calculations with nonmicroscopic calculations where interactions (or the Hamiltonian) are usually phenomenologically adjusted to fit the energy spectra of ^{12}C. It should also be noted that we do not discuss *ab initio* calculations obtained from the realistic nuclear forces on the same footing with the calculations using phenomenological effective nuclear interactions. Details of the theoretical frameworks and interactions are explained in later sections. In the 3α RGM [resonating group methods (RGM)] (Kamimura, 1981), extended THSR (Funaki, 2015; Funaki, Horiuchi, and Tohsaki, 2015), 3α GCM (Uegaki *et al.*, 1979; Descouvemont and Baye, 1987; Suhara and Kanada-En'yo, 2015), and $3\alpha + p_{3/2}$ (Suhara and Kanada-En'yo, 2015) calculations, phenomenological effective nuclear interactions of the Volkov forces (Volkov, 1965) are used. The interaction parameters of the Volkov forces are tuned to reproduce α-α scattering, although there are minor differences in the parameters among these calculations. The AMD results (Kanada-En'yo, 1998, 2007) are obtained by using the

[2]Hans O. U. Fynbo, private communication.

[3]M. Gai, private communication.

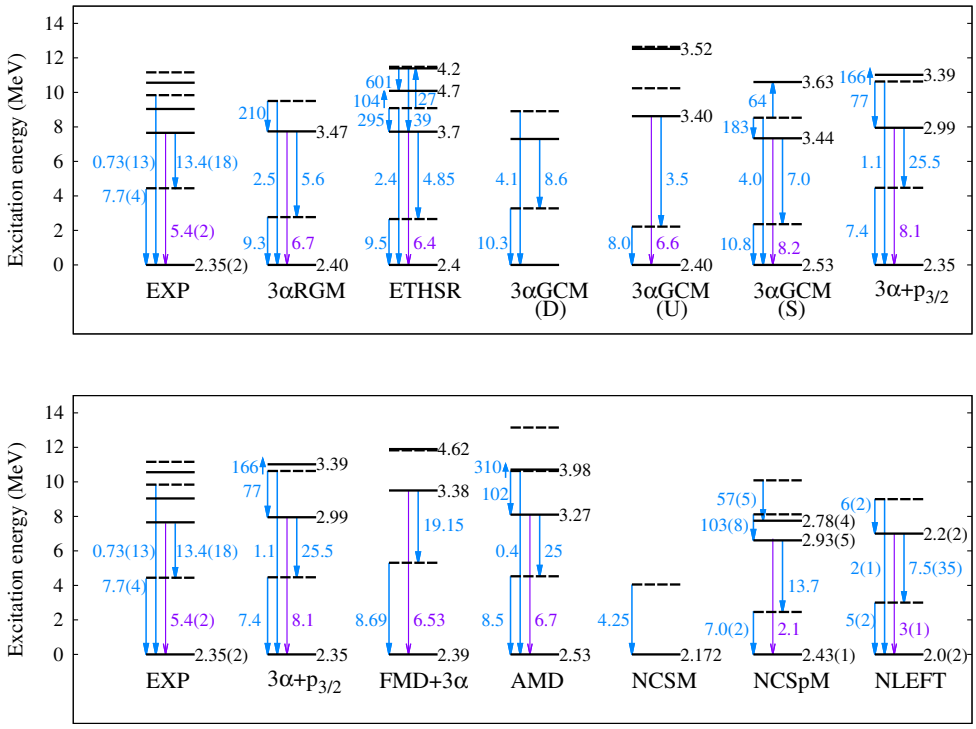

FIG. 4. Theoretical and experimental energy levels $E0$ and $E2$ transitions, radii of ^{12}C. The energy levels of 0^+ and 2^+ states are shown by solid and dashed lines, respectively. $B(E2)$ values (e^2 fm^4) are shown by the corresponding arrows (cyan text and arrows). $M(E0)$ values for $0_2^+ \to 0_1^+$ are shown by the arrows from 0_2^+ to 0_1^+ (purple text and arrows). Root-mean-square radii of point-proton distribution in 0^+ states are shown at the right side of the energy levels (black text). Experimental data are from Ajzenberg-Selove (1990), Chernykh *et al.* (2007), Itoh *et al.* (2011), Angeli and Marinova (2013), and Zimmerman *et al.* (2013). Theoretical results of the microscopic 3α models, 3α RGM (Kamimura, 1981), the extended THSR (Funaki, 2015; Funaki, Horiuchi, and Tohsaki, 2015), 3α GCM(D) (Descouvemont and Baye, 1987), 3α GCM(U) (Uegaki *et al.*, 1979), and 3α GCM(S) (Suhara and Kanada-En'yo, 2015) are shown in the upper panel, and those of the 3α GCM + $p_{3/2}$ (Suhara and Kanada-En'yo, 2015), the FMD + 3α (Chernykh *et al.*, 2007), AMD (Kanada-En'yo, 1998, 2007), NCSM (Navrátil *et al.*, 2007), NCSpM (Dreyfuss *et al.*, 2013), and NLEFT (Epelbaum *et al.*, 2012) calculations are shown in the lower panel. For comparison, the 3α GCM + $p_{3/2}$ results are also shown in the upper panel. The NLEFT energies have about 2 MeV errors and can be improved in future work using new methods as described by Lähde *et al.* (2015).

modified Volkov No. 1 (MV1) force (Ando, Ikeda, and Tohsaki-Suzuki, 1980), which is a phenomenological effective nuclear interaction modified from the Volkov force to describe the saturation properties, whereas the FMD + 3α results (Chernykh *et al.*, 2007) are obtained based on the realistic Argonne V18 potential with phenomenological tuning. For the no-core shell model (NCSM) (Navrátil *et al.*, 2007) and nuclear lattice effective field theory (NLEFT) (Epelbaum *et al.*, 2012) calculations, the results obtained with the realistic NN and NNN forces derived from the chiral effective theory are shown. In the no-core symplectic model (NCSpM) calculation (Dreyfuss *et al.*, 2013), a simplified effective Hamiltonian is used.

In general, the 3α calculations describe well the energy spectra of cluster states above the 3α threshold and the electron-scattering form factors for the 0_1^+ state and $0_2^+ \to 0_1^+$ transition, but they are not sufficient in describing some properties of low-lying states such as the 0_1^+-2_1^+ level spacing, $E2$ transition strength for $2_1^+ \to 0_1^+$ and $0_2^+ \to 2_1^+$. Hybrid calculations of the $3\alpha + p_{3/2}$ and FMD + 3α models as well as the AMD can reasonably describe the ground band properties and excited spectra for cluster states. The NCSM calculation fails to describe the excited cluster states above threshold since those states are beyond the model space, whereas the NCSpM, which contains higher shell configurations for cluster excitations, and the NLEFT calculations describe cluster structures in excited states above the threshold. The *ab initio* calculations (NCSpM and NLEFT) tend to much underestimate the size of the ground state, and also give small values of the size and $E0$ matrix element for the Hoyle state. The α-decay widths are calculated in the 3α RGM (Kamimura, 1981) and 3α GCM(D) (Descouvemont and Baye, 1987) by solving ^{8}Be + α scattering, and evaluated in the extended THSR (Funaki, 2015; Funaki, Horiuchi, and Tohsaki, 2015), 3α GCM(U) (Uegaki *et al.*, 1979), and AMD (Kanada-En'yo, 2007) within bound-state approximations using reduced-width amplitudes. The available data for the α-decay widths are reproduced quantitatively or qualitatively by theoretical calculations.

Although much progress has been made in understanding the structure of ^{12}C, it is apparent there is both need and scope for measurements to more precisely constrain the properties of the states presented in Fig. 1. In particular, this requires the measurement of electromagnetic transition rates where possible.

States in ^{16}O, dynamical symmetries and chains: One way of further testing our understanding of cluster correlations and the structure of ^{12}C is through the extension of that understanding to ^{16}O, which now is within the reach of *ab initio*

approaches; see, e.g., Epelbaum *et al.* (2014). Although much work has been done in both experiment and theory for this nucleus, here we provide some historical perspective first and then reflect on the most recent developments.

The work by Hafstad and Teller (1938) indicates the collective properties of the 4α system should be described by the tetrahedral symmetry group T_d. Here the characteristics are those of a spherical top, with equal moments of inertia and independent of rotation axis. If one assumes the separation between the α particles is that which is associated with the ^{8}Be ground state $\mathcal{I}_{\mathrm{Be}}$, then the rotational energies are given by

$$E_J = \hbar^2 \frac{J(J+1)}{4\mathcal{I}_{\mathrm{Be}}}. \tag{2.2}$$

The rotation of the tetrahedral structure corresponds to the equivalent rotation of two ^{8}Be nuclei around their symmetry axis, and hence the $4\mathcal{I}_{\mathrm{Be}}$ in the denominator. The symmetry then dictates that all values of J are permitted except $J = 1$, 2, and 5; states with $J = 0$, 4, and 8 have even parity and $J = 3$, 7, and 11 have negative parity. A key feature of this structure is degenerate 6^+ and 6^- states. A similar conclusion can be found in the recent work of Bijker and Iachello (2014) as shown in Fig. 5, which was triggered by related work performed using lattice simulations by Epelbaum *et al.* (2014). The algebraic cluster model of Bijker and Iachello (2014) generates energy eigenvalues and eigenvectors obtained by diagonalizing a finite-dimensional matrix, rather than by solving a set of coupled differential equations in coordinate space (Bijker, 2015). The model then describes the relative motion of the clusters.

The potential similarity between the structural properties of ^{12}C and ^{16}O and the underlying dynamical symmetries is compelling. However there are other models, e.g., the α-cluster model (Bauhoff, Schultheis, and Schultheis, 1984), that provide a good description of the energy spectrum of ^{16}O

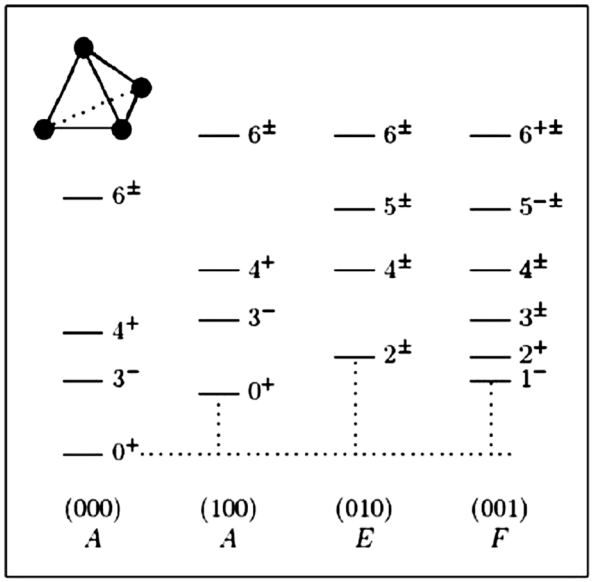

FIG. 5. The calculated spectrum of ^{16}O states assuming a T_d dynamical symmetry, obtained using the algebraic cluster model. From Bijker and Iachello, 2014.

states. Hence, it is important to examine the decay properties. The experimentally observed states at 6.130 MeV, 3^-; 10.356 MeV, 4^+ ($\Gamma = 26$ keV); and 21.052 MeV, 6^+ ($\Gamma = 205$ keV) have been linked by Bijker and Iachello (2014) to the collective excitations of the tetrahedral structure. These same calculations predicted states at 6.132, 10.220, and 21.462 MeV and electromagnetic transition strengths $B(E3)$ and $B(E4)$ of 181 and 338 $e^2\,\mathrm{fm}^{2L}$ compared with experimental values of 205(10) and 378(133) $e^2\,\mathrm{fm}^{2L}$. The comparison between experiment and theory is clearly compelling. The widths of the unbound 4^+ and 6^+ states are similar to those for the ground-state band in ^{12}C. Nevertheless, caution is required when interpreting transition rates for such states.

The alternative theoretical approach provided by the ACM calculations of Bauhoff, Schultheis, and Schultheis (1984) offered a different perspective. These calculations identified a number of cluster structures, including a tetrahedral arrangement of the four α particles in the ground state. In addition, a planar arrangement of α particles is found for the first excited 0^+ state, which can be associated with a $^{12}\mathrm{C} + \alpha$ structure. We note the similarity to the lattice results from Epelbaum *et al.* (2014). The main difference between the ACM and the algebraic cluster model (ACM′) of Bijker and Iachello (2014) is evident in the assignment of the 10.356 MeV 4^+ state to rotational bands. The ACM assigns it to the planar rotational structure, whereas the ACM′ links it to the tetrahedral ground state.

The algebraic cluster model reproduces the $B(E4)$ for the 10.356 MeV to ground-state transition, while the α-cluster model would place this state in a different band. This is clearly contradictory. What is clear from measurements of the α-decay branching ratios for decay to the ^{12}C ground state and first excited states is that the states in the ACM planar band, above the α-decay threshold, all have very similar decay properties. They predominantly decay to the ground state (Tilley, Weller, and Cheves, 1993; Wheldon *et al.*, 2011). Moreover there is also a negative parity band built on the 7.12 MeV, 1^- state with similar decay properties. This similar structure of this group of states conflicts with the tetrahedral interpretation and indicates a collective excitation built around a $^{12}\mathrm{C} + \alpha$ cluster structure where the total angular momentum of the state is generated by the orbital motion of the α particle around the ^{12}C core. These two different perspectives on the nature of the low-lying states in ^{16}O need to be resolved. Precision measurements of the *complete* electromagnetic decay patterns are likely to be the way forward. Measurements of the ANCs of the states close to the decay threshold in ^{16}O have recently been reported (Avila *et al.*, 2015). ANCs provide a model-independent assessment of the cluster structure and as such are also a key ingredient in refining the understanding of ^{16}O as a test case for nuclear theory.

One of the longest-standing questions related to ^{16}O is the existence of the 4α chain state. The 4α decay threshold is at 14.4 MeV and thus a chain state would exist close to or above this energy. The 15.1 MeV 0^+ state is a potential candidate, although the state has been identified as the analog of the Hoyle state (Funaki *et al.*, 2009). The proximity of this state to the decay threshold means that the 15.1 MeV state cannot decay strongly to the 4α final state. There are, however, a number of resonances that decay to the $^8\mathrm{Be} + {}^8\mathrm{Be}$ or

^{12}C(Hoyle) + α final states. The pioneering measurements of Chevallier *et al.* (1967) revealed both the excitation energy and dominant angular momenta of the ^{16}O resonances that decayed to ^{8}Be + ^{8}Be as populated in the ^{12}C(^{4}He, ^{8}Be)^{8}Be reaction. Remarkably, the energy-spin systematics of selected narrow resonances fell onto a $J(J+1)$ trajectory with moments of inertia commensurate with a structure where the α particles are arranged in a linear fashion: an α-particle chain. This work was published in 1967 and until the present has been held as an example of extreme α clustering. Confirmation of such an exotic structure is clearly vital. There are a number of possible approaches. One is to confirm the details of the excitation function, and the second is to search for higher spin members of the 4 α-particle chain band. The band was observed only up to spin 6. Subsequent measurements by Brochard *et al.* (1976) found no evidence for the 8^+ member. The measurements of Chevalier *et al.* were revisited (Curtis *et al.*, 2013), as displayed in Fig. 6. The highly detailed excitation functions for the ^{12}C(α, ^{8}Be)^{8}Be and ^{12}C(α, ^{12}C[7.65 MeV])α reactions presented by Curtis *et al.* (2013) show that the original structure that was interpreted as resonances in the earlier work (Chevallier *et al.*, 1967) was more complex and that no evidence for an 8^+ state could be identified. This most recent study contained over 400 measurements at different energies, with significant coverage of the angular distributions which should permit the components from resonances and transferlike processes to be disentangled. A measurement of ^{13}C(α, ^{8}Be + ^{8}Be)n was recently published which provides some insight as to what are resonant features in the ^{12}C + α excitation function (Curtis *et al.*, 2016). With the existence of excitation functions for ^{12}C + α leading to 4α unbound final states as well as bound states (Ames, 1982), there is in principle sufficient data to perform a complete

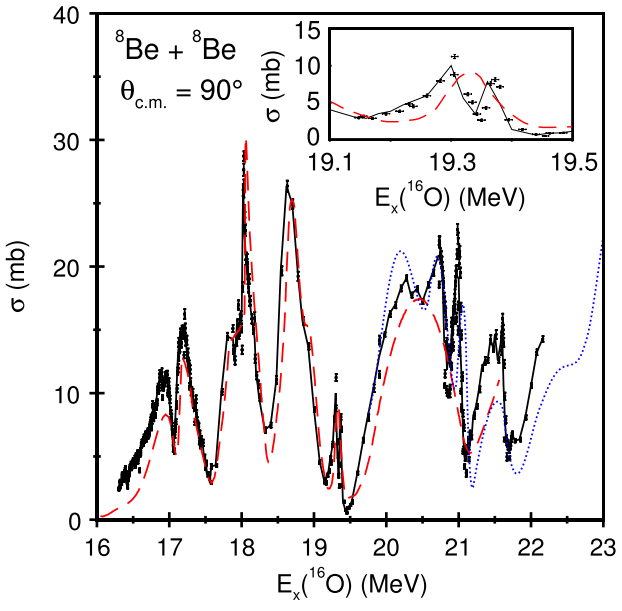

FIG. 6. Measurements of the ^{12}C(^{4}He, ^{8}Be)^{8}Be reaction for $\theta_{\text{c.m.}} = 90°$ (Curtis *et al.*, 2013) data points. The dashed and dotted lines correspond to the measurements of Chevallier *et al.* (1967) and Brochard *et al.* (1976). See Curtis *et al.* (2013) for more details.

R-matrix analysis of the data to constrain states with enhanced 4α reduced decay widths. This is likely to be a key component in constraining the structure of ^{16}O above the 4α-decay threshold. Recent measurements of α inelastic scattering populating 0^+ states in this region also indicate the spectrum of states may be more complicated than was previously concluded (Li *et al.*, 2017).

2. Molecular structures in neutron-rich nuclei

The idea that light nuclei might have a molecular structure where typically the valence neutron is exchanged between α-particle cores was explored extensively (Seya, Kohno, and Nagata, 1981; von Oertzen, 1996, 1997a, 1997b; Itagaki and Okabe, 2000). In essence, it is possible to form linear combinations of the neutron wave function around the α-particle cores and obtain, for example, two-centered molecules with delocalized neutrons in π and σ orbitals (von Oertzen, Freer, and Kanada-En'yo, 2006; Freer, 2007). Here the single-center orbitals both have p-type character. It is also possible to build more complex molecular structures with nonidentical cores, for example, in nuclei such as ^{21,22}Ne (von Oertzen, Freer, and Kanada-En'yo, 2006). This is illustrated in Fig. 7 (Kimura and Horiuchi, 2004).

The simplest example of this molecular behavior is found in the rotational bands of ^{9}Be. The ground-state band ($K^\pi = 3/2^-$) is well understood in terms of its π-type characteristics. The $1/2^+$ excited state at 1.68 MeV has a sequence of positive parity states $(3/2^+, 5/2^+, 7/2^+, \ldots)$ which may be connected to σ-type molecular structures as shown in Fig. 8. These two bands have spin and parity values consistent with molecular structures. Furthermore, as indicated in the figure, the moments of inertia extracted from the gradients of the bands are similar to the moment of inertia found for ^{8}Be, i.e., indicating the α-α core structure is largely preserved. There are few ways to directly observe the ground-state structure of the nucleus ^{9}Be; however, measurements of the decay correlations of ^{7}Be and ^{6}Li nuclei following the interaction with a ^{9}Be target showed strong and unexpected alignment. This was concluded to be evidence for the π-type molecular structure of the ^{9}Be ground state (Charity *et al.*, 2015). The right-hand panel of Fig. 8 shows the systematics of a negative parity band in ^{10}Be. Here this would correspond to a mixed π-σ configuration for the valence neutrons. Again the deformation is found to be consistent with the molecular

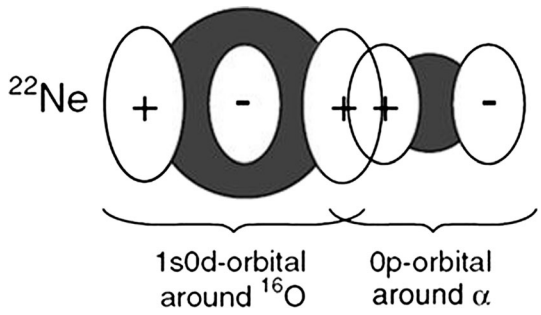

FIG. 7. The formation of molecular orbitals for neon isotopes from the valence orbitals of neutrons around the cores of ^{16}O and ^{4}He. From Kimura, 2007.

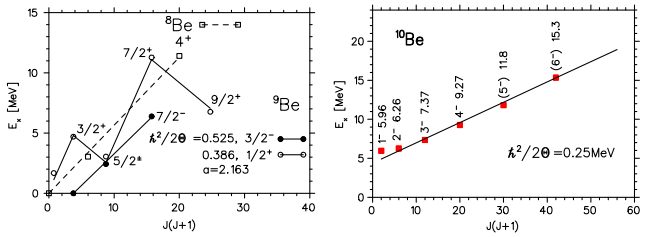

FIG. 8. Rotational bands of ^{8}Be, ^{9}Be, (left panel) and ^{10}Be (right panel). The excitation energies are plotted as a function of angular momentum $J(J+1)$. The Coriolis decoupling parameter a for the $K = 1/2$ band is indicated. From Freer, 2007.

picture, although it is apparent the moment of inertia has increased. Part of the origin of this effect is the proximity of this band to the α-decay threshold such that, as in the case of ^{12}C, the cluster structure is enhanced.

The most pronounced example of molecular behavior studied to date is that associated with a series of states close to the α- and neutron-decay thresholds in ^{10}Be. The 6.179 MeV, 0_2^+ state has a suppressed gamma decay, with a lifetime of the order of 1 ps. This isomeric behavior does not arise due to the lack of possible decay paths, but may be understood in terms of the small overlap of its structure and that of the more compact lower energy 3.36 MeV, 2_1^+ state. This already signals an unusual structure in analogy to the Hoyle state in ^{12}C. The excited state at 7.542 MeV, 2_2^+ is believed to be a collective excitation of this state. This state lies above, but very close to, the α-decay threshold (7.409 MeV), and thus its decay to this channel is strongly suppressed by the Coulomb and centrifugal barriers. Nevertheless, the α decay has been found to correspond to a very large reduced width (Liendo *et al.*, 2002), representative of the large degree of clusterization, although there is disagreement in the absolute value (Milin *et al.*, 2005). The 4^+ member of the band has been identified to lie at 10.15 MeV (Milin *et al.*, 2005). An unambiguous measurement of the spin and parity of the state was found in the resonant scattering of ^{6}He + ^{4}He (Freer *et al.*, 2006). This result has also been confirmed through a second resonant scattering measurement performed at Notre Dame (Suzuki *et al.*, 2013). If a collective model is applied, the moment of inertia associated with the rotational band would indicate that the state has a rather extreme deformation associated with the two valence neutrons occupying σ-like orbitals, with a density maximum between the two α particles which, via the Pauli exclusion principle, forces an increased separation of the two α particles. There are also indications from as yet unpublished measurements of a possible 6^+ state at higher energy.[4] Such a structure would be the analog of the 3α-chain state, but with two proton holes.

Valence neutrons in π and σ orbitals play an important role also in structure change of the ground states along Be isotopes. Because of the lowering mechanism of the $\sigma_{1/2}$ orbital in a well-clusterized 2α system, the $N = 8$ shell gap vanishes in neutron-rich Be. As a result, the ground states of ^{11}Be and ^{12}Be have σ-type molecular structures characterized by intruder configurations with large deformation (enhanced clustering), as supported by experimental observations such as Gamov-Teller and $E2$ transitions as well as the low-lying energy spectra (Suzuki and Otsuka, 1997; Iwasaki *et al.*, 2000a, 2000b; Navin *et al.*, 2000; Shimoura *et al.*, 2003; Pain *et al.*, 2006; Imai *et al.*, 2009; Meharchand *et al.*, 2012). Contrary to the enhanced clustering in ^{11}Be and ^{12}Be, the ground state of ^{10}Be has the weak clustering because of the attractive role of the π-orbital neutrons. The systematic change of cluster structures along the Be isotope chain is reflected in the N dependence of charge radii, which have been precisely determined by isotope shift measurements (Nörtershäuser *et al.*, 2009; Krieger *et al.*, 2012). The charge radius is smallest at $N = 6$ for ^{10}Be indicating a possible new magic number at $N = 6$ instead of $N = 8$. This trend is described well by the weakening and enhancement of the cluster structures in AMD and FMD calculations (Krieger *et al.*, 2012; Kanada-En'yo, 2015).

The experimental efforts to extend the systematics from dimers to trimers has seen a focus on trying to understand the systematics of three-centered molecules. Milin and von Oertzen had performed some pioneering work which established a set of candidate bands in ^{13}C (Milin and von Oertzen, 2002) and ^{14}C (von Oertzen *et al.*, 2004). In the case of ^{13}C the experimental situation remains unclear as the rotational systematics proposed by Milin and von Oertzen (2002) are inconsistent with measurements of ^{9}Be + α resonant scattering (Freer *et al.*, 2012b).[5] There are other studies of the ^{13}C system [see, e.g., Soic *et al.* (2003) and Rodrigues *et al.* (2010)], but these are inconclusive in terms of the molecular structure of this nucleus. There have been a number of studies of ^{10}Be + α resonant scattering which populate resonances above the α-decay threshold (12 MeV) (Freer *et al.*, 2014; Fritsch *et al.*, 2016; Yamaguchi *et al.*, 2017). This is higher energy than the 0^+ bandhead identified by von Oertzen *et al.* (2004), 9.75 MeV, and as such resonances may be associated with higher nodal cluster structures. Nevertheless, these latest measurements provide some tentative evidence for linear-chain structures in ^{14}C, as the level spacing and relative energies to the ^{10}Be + α threshold of the observed states agree well with the AMD prediction (Suhara and Kanada-En'yo, 2010a). However, it is clear that a definitive conclusion has yet to be reached here.

3. Key measurements that constrain *ab initio* theory

Clustering reveals much about the nature of the force through which the constituent components of the nucleus interact and the symmetries that result. This provides a crucial connection with *ab initio* theory. The nuclear strong interaction is clearly complex and this is revealed in the details of the unbound and bound light nuclei. The α particle is one of the most highly bound light nuclei with a very high-lying, ~20 MeV first excited state. And here the array of correlations includes not only $n - n$ and $p - p$ but also $n - p$ to maximize the binding energy. The tendency of other nuclei to optimize their own binding by generating spatial and momentum

[4] G. Rogachev, private communication.

[5] Also measurements from the Naples group, yet unpublished.

correlations induces the formation of clusters. This is responsible for clustering in α-conjugate nuclei, Borromean, and molecular systems alike.

Nuclei that display extreme or exotic behavior where the effects of the correlations are maximal are an excellent test of theory. Good examples of this are the ground and excited states of ^{8}Be and the Hoyle state in ^{12}C, which have both been described. To be useful in constraining theory and providing discrimination between approaches, high precision measurements are often required. One of the best examples of this is the study of the $T = 1$ analog states in ^{10}Be, ^{10}C, and ^{10}B*.

Precision measurements of the lifetime of the first 2^{+} state in ^{10}C using the Doppler shift attenuation method deduced a lifetime of $\tau = 219 \pm (7)\text{stat} \pm (10)\text{sys}$ fs, corresponding to a $B(E2)$ of $8.8(3)$ e^2 fm^4 (McCutchan *et al.*, 2012a). Similar measurements of the same transition in ^{10}Be found a $B(E2)$ of $9.2(3)$ e^2 fm^4 (McCutchan *et al.*, 2009). The ground and 2^{+} states of these nuclei are believed to possess a molecular structure where two valence particles (two neutrons or two protons) orbit the 2α-particle cores. These measurements were compared with both the Green's function Monte Carlo and NCSM calculations. The reproduction of the experimental results, especially the GFMC calculations, was not satisfactory and showed significant sensitivity to the details of the two- and three-body forces employed. A subsequent measurement of the $B(E2)$ for the transition from the $J = 2$, $T = 1$ state at 5.164 MeV to the $J = 0$, $T = 1$ state at 1.740 MeV in ^{10}B found a value of $6.1(22)$ e^2 fm^4 (McCutchan *et al.*, 2012b). This is much lower than the simple average of the ^{10}Be and ^{10}C measurement, which may not simply be understood and stands as an important test of *ab initio* theory. See Fig. 9 for a comparison of the experimental and theoretical results.

This set of measurements is an example of the need for precision experimental data to properly understand the nature of the strong interactions in light nuclei and the ability of first principles approaches to reproduce experimental properties. This must be a significant area of effort for experiment and theory over the next decade.

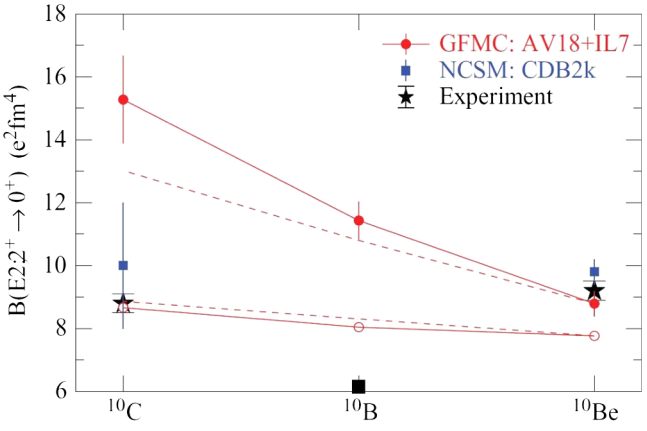

FIG. 9. Comparison between experimental $B(E2)$ values and GFMC and NCSM calculations using the AV18 potential with the IL7 three-nucleon interactions. The dashed lines show the corresponding isospin-symmetric results; see McCutchan *et al.* (2012a) for the full details. The black square at ^{10}B illustrates the experimental value of 6.1 e^2 fm^4. From McCutchan *et al.*, 2012b.

III. STRENGTHS AND CHALLENGES OF CURRENT THEORETICAL METHODS

It is useful to briefly summarize the strengths and challenges of the various theoretical approaches considered in this review. Many of the techniques we discuss are variational methods using some prescribed ansatz for the nuclear wave function. These include antisymmetrized molecular dynamics, fermionic molecular dynamics, the Tohsaki-Horiuchi-Schuck-Röpke wave function and container model, and microscopic cluster models using the resonating group or generator coordinate methods. These variational approaches often yield good agreement with experimental data as well as an intuitive picture of the underlying nuclear wave functions. The main challenges are to incorporate first principles nuclear forces and remove systematic errors associated with the choice of variational basis states.

Some variational methods have also been combined with Monte Carlo techniques. Variational Monte Carlo techniques use stochastic sampling to compute overlap integrals. It is also often used as a starting point for diffusion or Green's function Monte Carlo simulations. These calculations have used first principles nuclear forces, and the systematic errors can be estimated by allowing unrestricted evolution of the quantum wave function. The major challenge for these calculations is that the computational effort increases exponentially with the number of particles. Another method called the Monte Carlo shell model uses auxiliary-field Monte Carlo to select optimized variational basis states. As with other variational methods, the challenges are systematic errors due to the choice of basis states.

No-core shell models with continuum calculations start from first principles nuclear forces described by chiral effective field theory and have shown impressive agreement for the continuum properties of light nuclei. Similar to Green's function Monte Carlo techniques, the challenge for this method is the exponential scaling of effort when treating larger systems. The symmetry-adapted no-core shell model provides some promising ideas for mobilizing computational resources in an efficient manner based on symmetries. Nevertheless difficulties remain in accurately reaching larger systems with first principles nuclear forces.

Nuclear lattice effective field theory uses chiral effective field theory and lattice Monte Carlo techniques in determining nuclear structure, scattering, and reactions. It has the advantage of relatively mild scaling with system size and a common platform in which to treat few-body and many-body systems at zero and nonzero temperatures. However, there is the added difficulty of working on a lattice with broken rotational symmetry, and the lattice spacing must be decreased to reduce systematic errors.

We also mention several other recent studies. In one recent work, the states of ^{12}C are considered in a Skyrme model (Lau and Manton, 2014). While the calculations produce good agreement with the measured experimental spectrum, the detailed connection to the underlying nuclear forces is not yet fully realized. While the inadequacies of the shell model in describing cluster structures have been known since the early years, the explanation of nuclear clustering as an emergent collective phenomenon near open thresholds was provided by Okolowicz, Nazarewicz, and Ploszajczak (2013) by treating

the nucleus as an open quantum system coupling through nearby continuum states.

IV. MICROSCOPIC CLUSTER MODELS AND ANTISYMMETRIZED MOLECULAR DYNAMICS

Various cluster phenomena in stable nuclei have been theoretically investigated by using microscopic cluster models such as resonating group methods and generator coordinate methods. In the progress of understanding the physics of unstable nuclei, cluster models have been extended to deal with cluster structures with valence neutrons. Moreover, more flexible methods such as antisymmetrized molecular dynamics (Ono *et al.*, 1992a, 1992b; Kanada-En'yo, Horiuchi, and Ono, 1995; Kanada-En'yo and Horiuchi, 2001; Ono and Horiuchi, 2004; Kanada-En'yo, Kimura, and Ono, 2012) and fermionic molecular dynamics (Feldmeier, 1990; Feldmeier, Bieler, and Schnack, 1995; Feldmeier and Schnack, 2000; Neff and Feldmeier, 2003, 2004) have been developed which do not rely on the *a priori* assumption of the existence of clusters. The AMD and FMD wave functions are based not on cluster degrees of freedom but on nucleon degrees of freedom. In this sense, these models are not cluster models. Nevertheless, since they can express various kinds of cluster structures as well as shell-model features, they are powerful approaches for the study of cluster features in general nuclei.

In this section we give a brief overview of cluster models, the AMD method, and their extensions. Then we discuss some topics focusing on how these models describe the coexistence of cluster and mean-field aspects. It should be commented that the AMD and FMD methods were originally developed in the time-dependent form for nuclear reaction studies. However, we here explain the models for structure studies. For details of the AMD method for nuclear structure and reaction studies, see Kanada-En'yo and Horiuchi (2001), Kanada-En'yo, Kimura, and Ono (2012), and Kimura, Suhara, and Kanada-En'yo (2016) and references therein.

A. Overview of microscopic cluster models

Since the 1960s, microscopic cluster models have been applied to investigate cluster phenomena such as nuclear scattering and cluster structures. In the early history, scattering between light nuclei such as $\alpha+\alpha$ scattering has been intensively studied with the RGM (Wheeler, 1937a, 1937b; Wildermuth and Kanellopoulos, 1958; Tang, Lemere, and Thompson, 1978).

Despite the success of the RGM in microscopic description of relative motion between composite particles, practical application of the RGM is limited in the light mass region because of the computational costs of antisymmetrization in the treatment of the norm and Hamiltonian kernels. We discuss some recent developments in Sec. VI.B in *ab initio* no-core shell-model calculations.

Since the 1970s, owing to application of the GCM (Hill and Wheeler, 1953; Griffin and Wheeler, 1957) using the Bloch-Brink cluster wave function (Brink, 1966), further progress of microscopic studies of cluster phenomena has been made for heavy mass and many-cluster systems as well as unstable nuclei (Fujiwara *et al.*, 1980). The RGM and GCM are microscopic cluster models, in which antisymmetrization of all nucleons composing clusters are fully taken into account, and the Hamiltonian is composed of nucleon kinetic energies and nucleon-nucleon interactions based on nucleon degrees of freedom. Clusters are usually written in terms of simple shell-model configurations with or without excitation, and the intercluster motion is solved within the model wave functions.

The model wave function of the RGM for a single-channel case of two clusters C_1 and C_2 is given as

$$\Psi_{\rm RGM}=\mathcal{A}\{\phi(C_1)\phi(C_2)\chi(\boldsymbol{\xi})\}, \tag{4.1}$$

where $\mathcal{A}$ is the nucleon antisymmetrizer, $\phi(C_i)$ is the internal wave function of the C_i cluster, and $\boldsymbol{\xi}$ is the relative coordinate between the centers of mass of the clusters. The intercluster wave function $\chi(\boldsymbol{\xi})$ is determined by solving the RGM equation derived from the projection of the Schrödinger equation onto the RGM model space. Distortion of clusters and multichannel systems can be taken into account in the RGM by extending the single-channel to coupled-channel problems.

To describe the intercluster motion with the GCM approach, Brink adopted the following multicenter cluster wave function (called the Bloch-Brink cluster wave function) as a basis wave function (Brink, 1966):

$$\Phi_{\rm BB}(\boldsymbol{S}_1,\ldots,\boldsymbol{S}_k)=n_0\mathcal{A}\{\psi(C_1;\boldsymbol{S}_1)\cdots\psi(C_k;\boldsymbol{S}_k)\}, \tag{4.2}$$

where the ith cluster (C_i) is localized around $\boldsymbol{S}_i$, and n_0 is a normalization constant. The wave function $\psi(C_i;\boldsymbol{S}_i)$ for the ith cluster is written in terms of the harmonic oscillator shell-model wave function located at $\boldsymbol{S}_i$. When the clusters are far from each other and feel weak antisymmetrization effects between clusters, the parameter $\boldsymbol{S}_i$ indicates the mean center position of the cluster, and hence, the spatial configuration of the parameters $\{\boldsymbol{S}_1,\ldots,\boldsymbol{S}_k\}$ specifies the geometry of cluster structures. It means that the single Bloch-Brink cluster wave function expresses a cluster wave function, in which centers of clusters are localized around certain positions. In the small distance ($|\boldsymbol{S}_i|$) case that clusters largely overlap with each other, the Bloch-Brink cluster wave function becomes a specific shell-model wave function of the SU(3) shell model because of antisymmetrization of nucleons between clusters.

For the detailed description of intercluster motion, the superposition of the Bloch-Brink wave functions is considered by adopting the cluster center parameters $\{\boldsymbol{S}_1,\ldots,\boldsymbol{S}_k\}$ as generator coordinates in the GCM approach,

$$\Psi_{\rm GCM}=\int d\boldsymbol{S}_1,\ldots,d\boldsymbol{S}_k f(\boldsymbol{S}_1,\ldots,\boldsymbol{S}_k) \times P^{J\pi}_{MK}\Phi_{\rm BB}(\boldsymbol{S}_1,\ldots,\boldsymbol{S}_k), \tag{4.3}$$

where $P^{J\pi}_{MK}$ is the total-angular momentum and parity projection operator, and coefficients $f(\boldsymbol{S}_1,\ldots,\boldsymbol{S}_k)$ are determined by solving the Hill-Wheeler equation (Hill and Wheeler, 1953). In principle, the GCM with full model space of the basis Bloch-Brink wave functions is equivalent to the RGM (Horiuchi, 1970). With the GCM approach it became possible

to practically calculate heavy mass systems and also many-cluster systems microscopically.

For scattering problems, the RGM can be applied rather straightforwardly because the intercluster wave function is explicitly treated. On the other hand, in the application of the GCM to scattering problems, it is necessary to connect the basis wave functions in the internal region with continuum states in the asymptotic region at a chosen channel radius (Kamimura, 1977; Descouvemont and Baye, 2010).

Based on the GCM, Descouvemont and Baye (2010) studied various low-energy reactions of astrophysical interest. Following the progress in the physics of unstable nuclei, the microscopic cluster approaches have been extended and applied to study cluster structures of unstable nuclei. One of the main interests in the study of unstable nuclei is properties of valence neutrons surrounding one core or two clusters in neutron-rich nuclei. Microscopic three-body calculations for two valence neutrons around a core nucleus have been achieved by many groups to investigate the neutron halo and two-neutron correlation in drip-line nuclei such as ^{6}He, ^{11}Li, and ^{14}Be (Varga, Suzuki, and Lovas, 1994; Descouvemont, 1995, 1997; Arai, Suzuki, and Lovas, 1999). Baye and Descouvemont studied cluster features of the Be isotopes using a GCM approach with the Bloch-Brink wave functions of two α clusters and valence neutrons (Descouvemont, 2002). They also applied the coupled-channel GCM of $^{6}\mathrm{He}+{}^{6}\mathrm{He}$ and $^{8}\mathrm{He}+\alpha$ channels to study cluster structures of ^{12}Be (Descouvemont and Baye, 2001; Dufour, Descouvemont, and Nowacki, 2010).

Ito *et al.* applied a more generalized approach of the coupled-channel GCM to ^{10}Be and ^{12}Be (Ito, Kato, and Ikeda, 2004; Ito *et al.*, 2008; Ito and Ikeda, 2014). The method is successful in describing gradual changes of valence-neutron configurations from strong-coupling clustering with a molecular orbital structure to weak-coupling clustering in the asymptotic region with the increase of the α-α distance. Varga and his collaborators performed accurate calculations for many cluster systems in unstable p-shell nuclei with the stochastic variational method (SVM) (Varga, Suzuki, and Lovas, 1994; Varga and Suzuki, 1995; Varga, Suzuki, and Tanihata, 1995; Arai *et al.*, 2001). The SVM is a microscopic cluster model with the RGM-type cluster wave function written as a linear combination of stochastically chosen basis wave functions. Because of the stochastic procedure in choosing the basis wave functions, it is a powerful approach to treat many cluster systems. For instance, it has been applied to accurately solve four-cluster problems in the study of unstable p-shell nuclei such as the $2\alpha+2n$ system of ^{10}Be (Varga, Suzuki, and Tanihata, 1995; Ogawa *et al.*, 2000; Arai *et al.*, 2001; Arai, 2004).

To understand cluster structures of low-lying states of neutron-rich Be isotopes, molecular orbitals (MO) for surrounding neutrons around the 2α core were proposed (Seya, Kohno, and Nagata, 1981; von Oertzen, 1996; Itagaki and Okabe, 2000; von Oertzen, Freer, and Kanada-En'yo, 2006; Ito and Ikeda, 2014). Microscopic MO models (Okabe, Abe, and Tanaka, 1977, 1978) have been developed and applied to ^{10}Be by Itagaki and Okabe (2000). The model is based on the GCM for $2\alpha+2n$ using a truncated model space. Neutron configurations are restricted to the MOs, which are covalent bond orbitals written as linear combinations of p orbits around each α cluster, whereas the α-α distance is treated as the generator coordinate. The molecular orbital models have also been applied to neutron-rich C isotopes with the 3α core and valence neutrons (Itagaki *et al.*, 2001).

The relation of the cluster wave functions with shell-model ones was described based on the harmonic oscillator basis expansion and discussed from the SU(3) group symmetry (Bayman and Bohr, 1958; Elliott, 1958a, 1958b; Wildermuth and Kanellopoulos, 1958). The concept has been followed by symmetry adopted models such as symplectic (no-core) shell models (Rowe and Rosensteel, 1980; Draayer and Rosensteel, 1983; Dytrych *et al.*, 2007; Rowe and Wood, 2010) and algebraic cluster models (Cseh, 1992, 2014; Bijker and Iachello, 2002).

To describe competition between the cluster and jj-coupling shell-model states, Itagaki *et al.* extended the Bloch-Brink alpha cluster model wave function by adding spin-dependent imaginary parts to the cluster center parameters. This is essential for spin-orbit interactions in the jj-coupling shell model (Itagaki *et al.*, 2005; Suhara *et al.*, 2013). The model called the antisymmetrized quasicluster model (AQCM) can efficiently describe the smooth transition from the α-cluster wave function to the jj-coupling shell-model wave function in ^{12}C with the cluster breaking parameter Λ from $\Lambda=0$ to 1 as shown in Fig. 10.

B. Antisymmetrized molecular dynamics method

The AMD method is an approach which treats nucleon degrees of freedom independently without assuming any clusters. Nevertheless, the AMD can describe various cluster structures because the Bloch-Brink cluster wave functions for any cluster channels are contained in the AMD model space.

An AMD wave function is given by a Slater determinant of single-nucleon Gaussian wave functions,

$$\Phi_{\mathrm{AMD}}(\boldsymbol{Z})=\frac{1}{\sqrt{A!}}\mathcal{A}\{\varphi_1,\varphi_2,\ldots,\varphi_A\}, \tag{4.4}$$

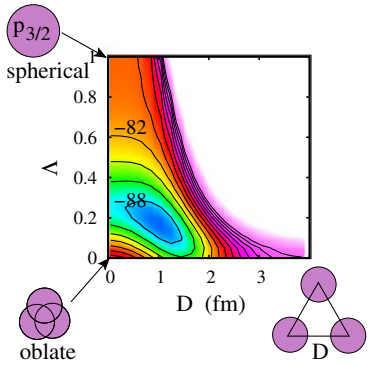

FIG. 10. 0^{+}-projected energy surface on the Λ-D plane for ^{12}C calculated by the AQCM. The interaction and width parameters are the same as those in Suhara *et al.* (2013).

where the ith single-particle wave function φ_i is written by a product of spatial, spin, and isospin wave functions as

$$\varphi_i = \phi_{X_i}\chi_i\tau_i, \tag{4.5}$$

$$\phi_{X_i}(\boldsymbol{r}) = \left(\frac{2\nu}{\pi}\right)^{4/3} \exp\{-\nu(\boldsymbol{r}-\boldsymbol{X}_i)^2\}, \tag{4.6}$$

$$\chi_i = (\tfrac{1}{2}+\xi_i)\chi_\uparrow + (\tfrac{1}{2}-\xi_i)\chi_\downarrow. \tag{4.7}$$

ϕ_{X_i} and χ_i are the spatial and spin functions, respectively, and τ_i is the isospin function fixed to be up (proton) or down (neutron). The width parameter ν is fixed to be an optimized value for each nucleus.

In the AMD wave function, the ith single-particle wave function is expressed by the Gaussian wave packet localized around the position $\boldsymbol{X}_i$. The Gaussian center positions $\boldsymbol{X}_i$ and the intrinsic-spin orientations ξ_i for all nucleons are treated independently as variational parameters which are determined by energy variation. It should be noted that the AMD wave function can be interpreted as an extended version of the Bloch-Brink wave function in the sense that all clusters are resolved completely to single nucleons. The AMD model covers the Bloch-Brink cluster model space as well as the AQCM. Indeed, by choosing a specific configuration of the Gaussian center positions $\{\boldsymbol{X}_i\}$, the AMD wave function can express the Bloch-Brink and AQCM wave functions. If a system favors a specific cluster structure, that structure is automatically obtained in the AMD model space after energy variation. The AMD wave function can also describe shell-model configurations because of the antisymmetrization between nucleons. It means that formation and dissolution of clusters are taken into account owing to the flexibility of the model wave function. This is a great advantage superior to cluster models in the description of both cluster and mean-field features in the ground and excited states of exotic nuclei. As an extension of the AMD wave function, triaxially deformed Gaussian wave packets were proposed by Kimura (2004) instead of the spherical Gaussian wave packets. The deformed base AMD is efficient to describe the coexistence of deformed mean-field states and cluster states in sd- and pf-shell nuclei; see Kanada-En'yo, Kimura, and Ono (2012) and Kimura, Suhara, and Kanada-En'yo (2016) and references therein. It should be commented that deformed Gaussian wave packets were proposed by Bauhoff *et al.* (1985) for the time-dependent cluster model (TDCM) (Caurier, Grammaticos, and Sami, 1982; Drozdz, Okolowicz, and Ploszajczak, 1982).

For structure studies in the AMD framework, the energy variation is performed after parity projection. For the angular momentum projection, the variation before the projection is performed in the simple AMD (Kanada-En'yo, Horiuchi, and Ono, 1995), whereas the variation is performed after the projection (VAP) in the AMD + VAP method (Kanada-En'yo, 1998).

For the description of excited states, the AMD wave functions obtained by the energy variation are superposed. For instance, mixing of different basis AMD wave functions (multiconfiguration mixing) is usually done in the AMD + VAP method. In the AMD + GCM method, many AMD wave functions are superposed by means of the GCM with constraint parameters as generator coordinates. In the β- and $\beta\gamma$-constraint AMD (Kimura, 2004; Suhara and Kanada-En'yo, 2010b), the energy variation is done under the constraints on the deformation parameters β and (β,γ), respectively. In the d-constraint AMD (Taniguchi, Kimura, and Horiuchi, 2004), the constraint for the distance between two (or three) centers of subgroups is adopted. After the energy variation with the constraints, the obtained AMD wave functions are superposed with the GCM treatment. Namely, coefficients of wave functions are determined by solving the Hill-Wheeler equation, i.e., by diagonalizing the norm and Hamiltonian matrices with respect to the adopted basis AMD wave functions. In the AMD + GCM, large amplitude dynamics along the generator coordinates are microscopically taken into account.

Although the AMD + GCM is useful for large amplitude collective motion, it is not efficient to describe single-particle excitations on a mean-field state because the lowest state is chosen in the energy variation procedure. To overcome this problem, the shifted basis AMD (sAMD) (Chiba, Kimura, and Taniguchi, 2016; Kanada-En'yo, 2016a, 2016b) has been constructed to describe small amplitude modes on top of the ground state; a small shift of the Gaussian center position of each single-particle wave function is prepared on the ground-state AMD wave function and all the shifted basis wave functions are superposed to describe linear combinations of one-particle and one-hole ($1p$-$1h$) excitations. The method combined with the cluster GCM was applied to monopole and dipole excitations in light nuclei and described coexistence of low-energy cluster modes and high-energy giant resonances.

Since the basis AMD wave function is written by a Slater determinant of single-particle wave functions, the simplest case of the single AMD wave function without projections can be regarded as a Hartree-Fock approach simplified in the restricted model space. However, because of the linear superpositions as well as the parity and angular momentum projections of AMD wave functions, higher correlations beyond mean-field approaches are taken into account even in the ground state in the AMD framework. As mentioned previously, the AMD model contains mean-field states as well as various cluster states in its model space and therefore it is able to describe the coexistence of mean-field and cluster aspects in the ground and excited states of nuclear systems.

C. Time-dependent antisymmetrized molecular dynamics method

The AMD wave function was originally used for nuclear reaction studies in a time-dependent framework (Ono *et al.*, 1992a, 1992b; Ono and Horiuchi, 2004). In the time-dependent AMD, the spin functions χ_i are usually fixed to be $\chi_\uparrow$ or $\chi_\downarrow$, and time evolution of a system is described by the time-dependent Gaussian center positions $\boldsymbol{X}_i$ determined by the time-dependent variational principle as

$$i\hbar\sum_{j\rho}C_{i\sigma,j\rho}\frac{dX_{j\rho}}{dt}=\frac{\partial}{\partial X^*_{i\sigma}}\frac{\langle\Phi_{\rm AMD}(\mathbf{Z})|H|\Phi_{\rm AMD}(\mathbf{Z})\rangle}{\langle\Phi_{\rm AMD}(\mathbf{Z})|\Phi_{\rm AMD}(\mathbf{Z})\rangle},$$

$$C_{i\sigma,j\rho}\equiv\frac{\partial^2}{\partial X^*_{i\sigma}\partial X_{j\rho}}\log\langle\Phi_{\rm AMD}(\mathbf{Z})|\Phi_{\rm AMD}(\mathbf{Z})\rangle, \quad (4.8)$$

where σ, $\rho = x$, y, z. The time-dependent AMD can be regarded as an extended version of the TDCM (Caurier, Grammaticos, and Sami, 1982; Drozdz, Okolowicz, and Ploszajczak, 1982; Bauhoff *et al.*, 1985) in the sense that all clusters are resolved completely into single nucleons.

In applications of the AMD and extended versions to heavy-ion collisions, the stochastic two-nucleon collision term is added to the equation of motion. The model successfully described multifragmentations at intermediate energy. Feldmeier proposed a wave function quite similar to the AMD wave function for nuclear reactions and structure studies (Feldmeier, 1990; Feldmeier, Bieler, and Schnack, 1995; Feldmeier and Schnack, 2000) and named it fermionic molecular dynamics. The model wave function of the FMD is also given by a Slater determinant of single-nucleon Gaussian wave packets. The major difference in the wave function between the FMD and the AMD is that the width parameter ν can be independently chosen for each nucleon as ν_i and treated as variational parameters in the FMD, whereas it is common for all nucleons in the AMD. Instead, the diffusion and the deformation of wave packets are stochastically incorporated in an extended version (AMD + Vlasov) for reaction studies (Ono and Horiuchi, 1996).

In structure studies the flexible treatment of the width parameters in the FMD is efficient, for example, for the neutron-halo structure of neutron-rich nuclei. The variation of width parameters in the time-dependent FMD (TD-FMD) is also effective in description of the giant monopole resonance (Furuta *et al.*, 2010), whereas the giant resonances are described with superposition of shifted single-particle Gaussian wave packets in the sAMD framework.

D. Effective nuclear interactions

In the cluster model and the AMD calculations, phenomenological effective nuclear interactions composed of the two-body central and spin-orbit (ls) forces are usually used. The Hamiltonian consists of the kinetic energies, the effective nuclear interactions, and the Coulomb interaction as

$$H=\sum_i t_i - T_{\rm c.m.}+\sum_{i<j}v_{ij}^{\rm nuclear}+\sum_{i<j}v_{ij}^{\rm Coulomb},$$

$$v_{ij}^{\rm nuclear}=v_{ij}^{\rm central}+v_{ij}^{ls}, \quad (4.9)$$

where the center-of-mass kinetic energy $T_{\rm c.m.}$ is subtracted. Note that the center-of-mass motion can be easily separated from the wave functions in the cluster and AMD models when a common width parameter is used. For the central forces of the effective nuclear interactions, Gaussian finite-range interactions with and without the zero-range density-dependent term (or the zero-range three-body term) are adopted in most cases. The central forces are supplemented with the finite-range or zero-range ls forces.

For light mass nuclei, density-independent interactions such as the Minnesota (Thompson, Lemere, and Tang, 1977) and Volkov (Volkov, 1965) interactions are often used. The Minnesota force is originally adjusted to fit the S-wave nucleon-nucleon scattering as well as scattering between light nuclei. For the Volkov force, the standard parameter set reproduces α-α scattering. The Volkov force can be adjusted to fit the S-wave nucleon-nucleon scattering lengths by tuning parameters for the Bartlett and Heisenberg terms. In general, these density-independent effective interactions cannot describe the saturation properties of nuclear matter and have an overbinding problem in heavy mass nuclei. Therefore, interaction parameters are sometimes readjusted to reproduce energies for the mass number region of interest, although the original parameter sets reproduce the properties of nucleon-nucleon and α-α scattering.

To overcome the overbinding problem, the central forces with the zero-range density-dependent or zero-range three-body term are used for heavy mass nuclei. Examples are the Gogny forces (Berger, Girod, and Gogny, 1991) and the modified Volkov (MV) forces (Ando, Ikeda, and Tohsaki-Suzuki, 1980). The central force of the Gogny forces consists of finite-range two-body terms and a zero-range density-dependent term, whereas that of the MV forces contains a zero-range three-body term instead of a zero-range density-dependent term. These interactions systematically reproduce the binding energies over a wide mass number region. However, they cannot quantitatively reproduce the scattering and structure properties of very light systems such as the nucleon-nucleon and α-α scattering as well as the size of the α particle.

There are many cluster model calculations for light nuclei using the Minnesota and Volkov forces. In the AMD calculations for p-shell, sd-shell, and pf-shell nuclei, the Volkov, modified Volkov No. 1 (MV1), and Gogny forces are used. As already mentioned, these interactions used in the cluster model and AMD calculations are effective nuclear interactions that are phenomenologically adjusted to properties of nuclear structures and/or scattering.

In the FMD calculations, effective nuclear interactions derived from the realistic nuclear interactions are usually used with the unitary correlation operator method (UCOM), in which the short-range and tensor correlations are taken into account in the interaction operator of the Hamiltonian (Feldmeier *et al.*, 1998; Neff and Feldmeier, 2003; Roth, Neff, and Feldmeier, 2010). Therefore the FMD + UCOM calculation is a first principles method starting from realistic nuclear interactions.

E. Description of cluster and mean-field aspects in AMD models

1. Cluster breaking effects on 3α structures in ^{12}C

Despite the success of 3α-cluster models for many excited states ^{12}C, microscopic 3α-cluster models are not sufficient to describe the large level spacing between the 0^+_1 and 2^+_1 states because α-cluster breaking is not taken into account in the models. Moreover, it is difficult to confirm the 3α-cluster formation in the 12-nucleon dynamics because clusters are *a priori* assumed in the models. These problems have been

overcome by the AMD and FMD models. In the AMD and FMD calculations for ^{12}C (Kanada-En'yo, 1998, 2007; Neff and Feldmeier, 2004; Chernykh *et al.*, 2007), 3α-cluster structures are formed in the calculated results without assuming the existence of α clusters.

As mentioned previously, the model spaces of the AMD and FMD contain the Bloch-Brink cluster wave functions and also cluster breaking configurations. In the $^{12}\mathrm{C}(0_1^+)$, the cluster breaking component, i.e., the $p_{3/2}$ closed-shell component is significantly mixed in the dominant 3α-cluster structure as seen in the compact intrinsic density distribution in Fig. 1. Because of the mixing of the cluster breaking component, the bandhead $^{12}\mathrm{C}(0_1^+)$ gains extra energy of the spin-orbit attraction resulting in stretching of the 0^+-2^+ level spacing consistently with the experimental energy spectra. It is also the case in the FMD calculation (see Fig. 4). The significant mixing of the cluster breaking component in $^{12}\mathrm{C}(0_1^+)$ is clearly indicated in the AQCM calculation in Fig. 10 by the finite value of the cluster breaking parameter Λ at the energy minimum.

The cluster breaking component does not give drastic effects to excited 3α cluster states. However, excited 0^+ structures are more or less affected by the cluster breaking component mixed in the $^{12}\mathrm{C}(0_1^+)$ through the orthogonality, and therefore, quantitative differences can be seen between model calculations with and without the cluster breaking. For example, in the calculated energy spectra shown in Fig. 4, the AMD and FMD calculations show a trend of the larger 0_2^+-2_2^+ level spacing than that obtained by 3α calculations without the cluster breaking, because the cluster breaking in the $^{12}\mathrm{C}(0_1^+)$ induces the global energy gain of excited 0^+ states. Moreover, the AMD calculation shows the larger $E2$ strength for $2_2^+ \to 0_3^+$ than that for $2_2^+ \to 0_2^+$, differently from the 3α calculations that give dominant $E2$ strength for $2_2^+ \to 0_2^+$. Suhara and Kanada-En'yo (2015) investigated the cluster breaking effects on 3α cluster structures in ^{12}C by explicitly adding the $p_{3/2}$ closed-shell configuration (cluster breaking component) into the 3α model space. Comparison of the results with and without the $p_{3/2}$ configuration is shown in the right two columns in the upper panel of Fig. 4. The figure shows increasing of the 2_1^+ and 2_2^+ energies relative to the 0_1^+, 0_2^+, and 0_3^+ ones, and also the inversion of the dominant $E2$ strengths between $2_2^+ \to 0_2^+$ and $2_2^+ \to 0_3^+$. It may indicate that the cluster breaking should not be ignored for detailed discussions of band assignments in model calculations.

2. Cluster and mean-field modes in monopole excitations in ^{12}C

In experimental and theoretical studies of nuclear clustering, isoscalar monopole (ISM) and dipole transitions are good probes to pin down cluster states (Funaki *et al.*, 2006; Kawabata *et al.*, 2007; Yamada *et al.*, 2012; Chiba and Kimura, 2015; Kanada-En'yo, 2016b). Yamada *et al.* (2012) pointed out that two different modes of ISM excitations coexist in ^{16}O: one is the isoscalar giant monopole resonance (ISGMR) known to be the collective breathing mode, and the other is the low-energy ISM strengths for cluster states. The low-energy ISM strengths were experimentally observed also for ^{12}C (Youngblood, Lui, and Clark, 1998; John *et al.*, 2003). A hybrid model of the sAMD and 3α GCM was applied to the ISM excitations in ^{12}C and described the low-energy ISM strengths for cluster modes separating from high-energy ISGMR strengths (Kanada-En'yo, 2016b). The separation of the low-energy and high-energy parts of the ISM strengths qualitatively agrees to the experimental data [see Figs. 11(a) and 11(b)]. As explained in the previous section, the sAMD bases describe coherent $1p$-$1h$ excitations for the GMR, whereas the 3α GCM bases are essential for the large amplitude cluster modes which contribute to the low-energy strengths. Figure 11(e) shows the ISM strengths obtained only by the sAMD bases without 3α configurations, and Figs. 11(c) and 11(d) show the ISM strengths calculated using specific 3α configurations in addition to the sAMD bases. As clearly seen, the sAMD describes only the high-energy ISM strengths for

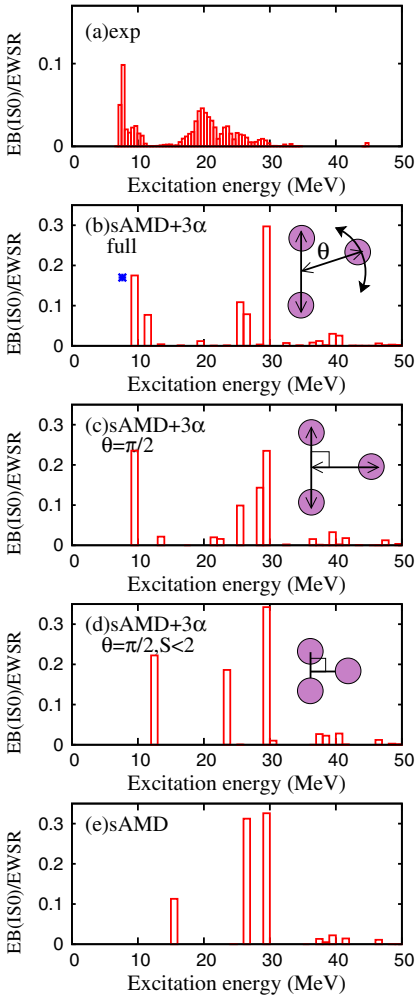

FIG. 11. The energy weighted ISM strength distributions obtained by the sAMD + 3α GCM and those measured by (α, α') scattering (John *et al.*, 2003). The experimental $E0$ strength for the 0_2^+ measured by electron scattering (Chernykh *et al.*, 2010) is also shown in (b). (c), (d) Those calculated with truncated model space of 3α configurations: (c) calculation using 3α configurations at $\theta = \pi/2$ and sAMD bases. (d) Same as (c) but only compact 3α configurations with $|\boldsymbol{S}_i| < 2$ fm. (e) Strengths obtained by the sAMD bases without the 3α configurations. (a), (b), and (e) From Kanada-En'yo, 2016b.

the ISGMR but fails to describe significant low-energy ISM strengths. As 3α configurations are added to the sAMD bases, a peak grows up and comes down to the low-energy region [see Fig. 11(c)]. Then the low-energy peak finally splits into the 0_2^+ and 0_3^+ in the full sAMD + 3α GCM calculation because of the coupling of the radial motion with the rotational motion of clusters. Namely, the large amplitude cluster motion is essential for the low-energy ISM strengths and the fragmentation of the ISM strengths occurs by the coupling of the radial and rotational motions in the 3α dynamics.

The lowering mechanism of the ISM strengths by the large amplitude cluster motion was also demonstrated in the time-dependent FMD calculation by Furuta *et al.* (2010). In applications of time-dependent approaches to nuclear excitations, the response functions are calculated by the Fourier transform (frequency) of the time evolution of the system. For the ISM excitations, the initial state is prepared by imposing an external field (operator) $\sum_i r_i^2$ to the ground state, and starting from the initial state the time evolution of the system is solved with the time-dependent FMD. In the FMD framework, the single-particle excitations are expressed by the time-dependent width parameters of single-nucleon Gaussian wave packets, whereas the radial cluster motion is described by the time-dependent Gaussian center positions. The Fourier transform of the root-mean-square radius shows two modes with different frequencies corresponding to the width oscillation mode and the radial cluster (intercluster) mode (see Fig. 12). They analyzed the dependence of frequencies of two modes on the oscillation amplitude and found that the higher frequency for the width mode, corresponding to the breathing mode, does not depend on the amplitude but the lower peak frequency for the cluster mode significantly comes down to lower energy as the amplitude becomes larger. This result is consistent with the sAMD + 3α GCM result discussed previously, although the GMR mode is expressed by a linear combination of shifted Gaussian wave packets with a fixed width in the sAMD instead of the variational width in the FMD wave function. Note that the quantization of excitation modes and spin-parity projections are performed in the sAMD + 3α GCM but not in the TD-FMD. It should be remarked that monopole vibration in ^{8}Be has been investigated with the TDCM of 2α which shows similar features of the width oscillation and radial cluster modes (Drozdz, Okolowicz, and Ploszajczak, 1982).

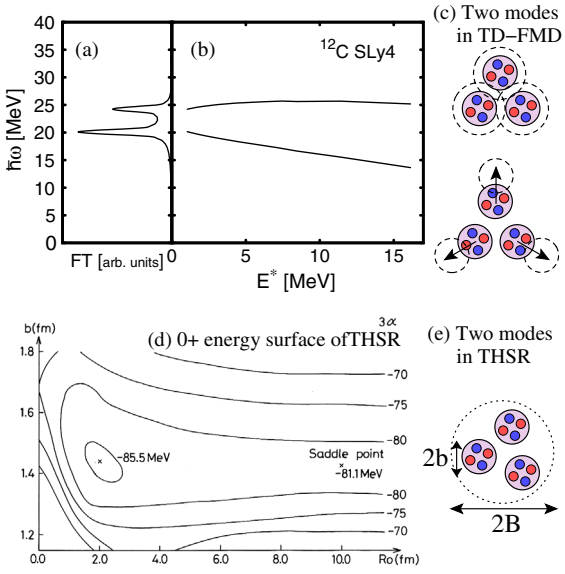

FIG. 12. (a), (b) Monopole excitations in ^{12}C calculated with the time-dependent FMD. From Furuta *et al.*, 2010. Oscillation frequencies of the root-mean-square radius are plotted against the Fourier component in the small amplitude limit in (a), and those are plotted as a function of the excitation energy given by the initial amplitude in (b). (c) Sketches for width oscillation and intercluster modes in the time-dependent FMD. (d) 0^+ energy surface of the 3α THSR wave function on the B-b plane (B is denoted by R_0). (e) Sketches for b and B modes in the THSR. (a), (b) From Kanada-En'yo, 2016b. (d) From Tohsaki *et al.*, 2001.

It is also valuable to consider a link to the THSR wave function for two kinds of monopole modes. In the THSR model, the width oscillation mode is expressed by the parameter b for the α-cluster size, and the radial cluster mode is described by the parameter B for the α distribution size as shown in Fig. 12(e). The 0^+ energy surface on the B-b plane in Fig. 12(d) shows the coexistence of two modes. The energy surface is very soft along the B mode and it is steep along the b mode. It indicates that the origin of the low-energy ISM strengths is the large amplitude cluster motion decoupled from the width (coherent single-particle excitation) mode for the ISGMR.

V. TOHSAKI-HORIUCHI-SCHUCK-RÖPKE WAVE FUNCTION AND CONTAINER MODEL

A. Introduction

Cluster model studies in the 1970s showed that the Hoyle state of ^{12}C has a gaslike structure of three α clusters which are weakly bound with predominantly S-wave correlations among the α particles (Horiuchi, 1974; Uegaki *et al.*, 1977; Kamimura, 1981). The gaslike structure of the Hoyle state was reconsidered in a new light by Tohsaki *et al.* (2001). In this paper it was proposed that the Hoyle state has a 3α-condensate-like structure, and the THSR wave function was presented to express the α-condensate-like structure. It was soon discovered (Funaki *et al.*, 2003) that the 3α THSR wave function was nearly identical to the 3α cluster model wave functions obtained in the 1970s, namely, the 3α Brink-GCM wave function of Uegaki *et al.* (1977) and the 3α RGM wave function of Kamimura (1981).

About 10 years later it was found that the THSR wave function for ^{16}O + α clustering in ^{20}Ne was nearly identical to the Brink-GCM wave function for ^{16}O + α clustering (Zhou *et al.*, 2013). This finding was striking since the ^{16}O + α Brink-GCM wave functions with spatially localized ^{16}O + α structures accurately describe the states of the so-called inversion-doublet bands of ^{20}Ne where the even parity and odd parity levels are split into two separate bands. The THSR wave function was found to describe well the spatially localized cluster structures even though it was originally designed to describe gaslike delocalized cluster wave functions. The fact that the THSR wave function can describe both localized and delocalized clustering led to the introduction of

the container model of cluster dynamics (Zhou, Funaki, Horiuchi *et al.*, 2014).

Here we discuss the THSR wave function and its history, starting from its initial introduction to the container model of cluster dynamics (Funaki, Horiuchi, and Tohsaki, 2015; Schuck *et al.*, 2016; Tohsaki *et al.*, 2017). We explain some characteristics of the THSR wave function that might appear contradictory, such as the nucleon density distribution showing localized clustering despite the nonlocalized character of the THSR wave function and the equivalence of prolate and oblate THSR wave functions after angular momentum projection. The container model is deeply connected to the evolution of the cluster structure, and we demonstrate this in ^{12}C and ^{16}O.

B. Alpha-condensate-like character of the Hoyle state

1. *S*-wave dominance of α-cluster motion in the Hoyle state

The Hoyle state, the second 0^+ state of ^{12}C, is located slightly above the 3α and $^8\mathrm{Be}(0_1^+)+\alpha$ thresholds. The small excitation energy of this state, 7.66 MeV, is difficult to explain by the shell model. The decay width Γ of the Hoyle state is very small (8.7 eV) because the energy is well below the Coulomb barrier. Assuming for the moment two subsystems in a relative S wave, the R-matrix calculation of the width gives

$$\Gamma = 2P_{L=0}(a)\gamma^2(a), \tag{5.1}$$

where $\gamma^2(a)$ is the reduced width,

$$P_{L=0}(a) = ka/[F_{L=0}^2(ka) + G_{L=0}^2(ka)] \tag{5.2}$$

is the Coulomb barrier penetrability, a is the channel radius, F_L and G_L are the regular and irregular Coulomb functions, respectively, and k is the wave number; see Descouvemont and Baye (2010) for a review. The observed value $\gamma^2_{\mathrm{obs}}(a)$ for the Hoyle state is very large. It is comparable to or larger than the Wigner-limit value $\gamma^2_W(a) = 3\hbar^2/(2\mu a^2)$ that corresponds to an α cluster with uniform density at radial distances less than a. The very large value of $\gamma^2_{\mathrm{obs}}(a)$ suggests that the structure of the Hoyle state is composed of an $^8\mathrm{Be}(0_1^+)$ core and loosely attached α cluster in an S wave. This conclusion does not support the idea of the 3α linear-chain structure proposed by Morinaga (1956, 1966), since the 3α linear-chain structure would produce a reduced width $\gamma^2(a)$ that is significantly smaller than $\gamma^2_W(a)$ (Suzuki, Horiuchi, and Ikeda, 1972).

The S-wave dominance of the $^8\mathrm{Be}(0_1^+)$-α relative wave function indicated by the observed α width was confirmed theoretically by solving the 3α problem by use of the 3α orthogonality condition model (OCM) (Horiuchi, 1974). Since $^8\mathrm{Be}(0_1^+)$ consists of two α clusters weakly coupled in a relative S wave, the Hoyle state was concluded to have a weakly coupled 3α structure in relative S waves with large spatial extent. It was therefore described as a gaslike state of α clusters. A few years later, the results of the 3α OCM study were confirmed by fully microscopic 3α calculations by two groups, namely, the 3α GCM calculation of Uegaki *et al.* (1977), and the 3α RGM calculation of Kamimura (1981). These calculations reproduced not only the excitation energy of the Hoyle state but also other experimental properties including the α-decay width, the inelastic electron-scattering charge form factor, and $E0$ and $E2$ transition properties.

2. Equivalence of the 3α RGM or GCM wave function to a single 3α THSR wave function

More than 20 years after the 3α OCM, GCM, and RGM studies mentioned, the Hoyle state was reconsidered in a new light by Tohsaki *et al.* (2001). They proposed, for the description of the Hoyle state, the following new model wave function $\Psi^{\mathrm{THSR}}_{3\alpha}$ called the THSR wave function. Let $\Phi(3\alpha)$ be a simple product of three α-cluster wave functions,

$$\Phi(3\alpha) = \phi(\alpha_1)\phi(\alpha_2)\phi(\alpha_3). \tag{5.3}$$

The THSR wave function has the form

$$\Psi^{\mathrm{THSR}}_{3\alpha}(B) = \mathcal{A}\left\{\exp\left[-\frac{2}{B^2}(\vec{X}_1^2+\vec{X}_2^2+\vec{X}_3^2)\right]\Phi(3\alpha)\right\} \tag{5.4}$$

$$= \exp\left(-\frac{6\vec{\xi}_3^2}{B^2}\right)\mathcal{A}\left\{\exp\left(-\frac{4\vec{\xi}_1^2}{3B^2}-\frac{\vec{\xi}_2^2}{B^2}\right)\Phi(3\alpha)\right\}, \tag{5.5}$$

where $\vec{X}_i$ is the center of mass of cluster i and $\vec{\xi}_k$ are Jacobi coordinates defined as

$$\vec{\xi}_1 = \vec{X}_1 - \tfrac{1}{2}(\vec{X}_2+\vec{X}_3), \tag{5.6}$$

$$\vec{\xi}_2 = \vec{X}_2 - \vec{X}_3, \tag{5.7}$$

$$\vec{\xi}_3 = \tfrac{1}{3}(\vec{X}_1+\vec{X}_2+\vec{X}_3). \tag{5.8}$$

With the center-of-mass dependence removed, the wave function has the form

$$\Phi(3\alpha\mathrm{THSR}) = C\Psi^{\mathrm{THSR}}_{3\alpha}(B)/\exp\left(-\frac{6\xi_3^2}{B^2}\right), \tag{5.9}$$

where C is a normalization constant. As shown in Eq. (5.5), the THSR wave function can be regarded as expressing the $^8\mathrm{Be}(0_1^+)+\alpha$ cluster structure, where a $^8\mathrm{Be}(0_1^+)$-like cluster $\mathcal{A}\{\exp(-\vec{\xi}_2^2/B^2)\phi(\alpha_2)\phi(\alpha_3)\}$ and the α_1 cluster couple via the S wave with intercluster wave function $\exp[-4\vec{\xi}_1^2/(3B^2)]$. On the other hand, Eq. (5.4) shows that the THSR wave function represents the state where three α clusters occupy the same single $0S$ orbit $\exp(-2\vec{X}^2/B^2)$, namely, a 3α condensate state which is a finite-size counterpart of the macroscopic α-particle condensation in infinite nuclear matter at low density (Röpke *et al.*, 1998). Tohsaki *et al.* (2001) proposed that the $^8\mathrm{Be}(0_1^+)+\alpha$ structure of the Hoyle state can be regarded as being a 3α condensate-like state. Furthermore, one can in general expect the existence of an $n\alpha$ condensate-like state in the vicinity of the $n\alpha$ threshold in α-conjugate nuclei.

An important and striking fact is that both the 3α GCM wave function of Uegaki *et al.* (1977) and the 3α RGM wave function of Kamimura (1981) are each nearly equivalent to a single 3α THSR wave function (Funaki *et al.*, 2003):

$$|\langle\Phi(3\alpha\ \mathrm{THSR})|\Phi(3\alpha\ \mathrm{GCM/RCM})\rangle|^2 \approx 100\%. \quad (5.10)$$

Hence the 3α THSR wave functions reproduce the same Hoyle state experimental data well described by the 3α RGM and GCM wave functions. See Tohsaki *et al.* (2017) for applications of the THSR wave function to the Hoyle state and discussions of electric transitions, α-condensation probabilities, and comparisons with quantum Monte Carlo calculations.

C. Localized versus nonlocalized clustering

1. Shell-model limit of THSR wave function

Let b be the single-nucleon oscillator size parameter with which the $0s$ harmonic oscillator (HO) orbit is expressed as

$$\phi_{0s}(\vec{r}) = (\pi b^2)^{-3/4}\exp\left(-\frac{\vec{r}^2}{2b^2}\right). \quad (5.11)$$

When $B = b$, we have

$$\exp\left(-\frac{2\vec{X}^2}{B^2}\right)\phi(\alpha) \propto \det|(0s)^4|. \quad (5.12)$$

Therefore $\Psi^{\mathrm{THSR}}_{3\alpha}(B=b)=0$ by the Pauli exclusion principle. By expressing the normalization constant of $\Psi^{\mathrm{THSR}}_{3\alpha}(B)$ with $B > b$ as $n^{\mathrm{THSR}}_{3\alpha}(B)$, one can prove that

$$\lim_{B\to b} n^{\mathrm{THSR}}_{3\alpha}(B)\Psi^{\mathrm{THSR}}_{3\alpha}(B) = |(0s)^4(0p)^8;[444]L=0\rangle, \quad (5.13)$$

where [444] refers to the spatial-symmetry Young diagram (Hutzelmeyer and Hackenbroich, 1970). Equation (5.13) means that $\Psi^{\mathrm{THSR}}_{3\alpha}(B)$ for B close to b is close to the shell-model wave function of the ^{12}C ground state. So while the THSR wave function for large B is a gaslike state of clusters, the THSR wave function with small B is a shell-model-like state.

Tohsaki *et al.* (2001) obtained the ground and Hoyle states of ^{12}C as the lowest and second lowest energy states of the GCM equation with the basis function $\Psi^{\mathrm{THSR}}_{3\alpha}(B)$,

$$\sum_B \langle\Psi^{\mathrm{THSR}}_{3\alpha}(B')|(H-E_k)|\Psi^{\mathrm{THSR}}_{3\alpha}(B)\rangle f_k(B) = 0. \quad (5.14)$$

The GCM wave functions of the ground and Hoyle states were found to have about 93% and 98% squared overlaps with single THSR wave functions.

2. Inversion-doublet bands of ^{20}Ne and THSR wave function

In ^{20}Ne the even-parity $K^\pi = 0^+$ rotational band upon the ground state and odd-parity $K^\pi = 0^-$ rotational band upon the $J^\pi = 1^-$ state at 5.80 MeV constitute inversion-doublet bands having the same intrinsic $^{16}\mathrm{O}+\alpha$ cluster structure (Horiuchi and Ikeda, 1968). The splitting between the even-parity and odd-parity bands can be understood as arising from tunneling of the α through the ^{16}O core to form the corresponding mirror configuration. The empirical success of this description constitutes evidence of spatial localization of the clusters. Much later it was discovered that the GCM and RGM wave functions describing the inversion-doublet bands were found to be almost equivalent to a single $^{16}\mathrm{O}+\alpha$ THSR wave function (Zhou *et al.*, 2012, 2013),

$$|\langle\Phi(^{16}\mathrm{O}+\alpha\mathrm{THSR})|\Phi(^{16}\mathrm{O}+\alpha\mathrm{GCM/RGM})\rangle|^2 \approx 100\%, \quad (5.15)$$

where the $^{16}\mathrm{O}+\alpha$ THSR wave function has the form

$$\Phi_L(^{16}\mathrm{O}+\alpha\mathrm{THSR}) = \lim_{|\vec{D}|\to 0} P_L\mathcal{A}\{e^{-8(\vec{r}-\vec{D})^2/5B^2}\phi(^{16}\mathrm{O})\phi(\alpha)\}, \quad (5.16)$$

where

$$\vec{r} = \vec{X}_{\mathrm{c.m.}}(^{16}\mathrm{O}) - \vec{X}_{\mathrm{c.m.}}(\alpha), \quad (5.17)$$

and P_L is the projection operator for angular momentum L.

The relation in Eq. (5.16) casts doubt on the use of the energy curve for the Brink wave function in determining the spatial localization of clusters. The $^{16}\mathrm{O}+\alpha$ Brink wave function $\mathcal{A}\{\exp[-8(\vec{r}-\vec{D})^2/(5b^2)]\phi(^{16}\mathrm{O})\phi(\alpha)\}$ has the intercluster separation parameter $\vec{D}$. The optimum value of $D = |\vec{D}|$ is obtained from the minimum energy point of the energy expectation value as a function of D. Zhou *et al.* (2013) showed that this way of determining the intercluster distance is misleading. If one uses a much smaller size parameter of $8/(5B^2)$ for the intercluster motion, rather than the $8/(5b^2)$ value given by the Brink wave function, then the energy minimum point resides at $D = 0$.

3. Localized clustering from intercluster Pauli repulsion

The limit $D \to 0$ appearing in Eq. (5.16) would seem to suggest that the distributions of the ^{16}O and α clusters are overlapping and therefore not localized. The resolution of this apparent contradiction becomes clear after calculating the nucleon density distribution of the $^{16}\mathrm{O}+\alpha$ THSR wave function as was performed by Zhou, Funaki, Horiuchi *et al.* (2014). In Fig. 13 we show the nucleon density distribution of the $^{16}\mathrm{O}+\alpha$ intrinsic THSR wave function of Eq. (5.16) for the small value $D = 0.6$ fm. We do not directly set $D = 0$ as this would force the intrinsic THSR wave function to be symmetric under parity. We see in Fig. 13 that there exists a large separation of about 3.6 fm between the ^{16}O and α clusters. This spatial localization of clusters is due to the nucleon antisymmetrizer $\mathcal{A}$. The antisymmetrizer $\mathcal{A}$ generates Pauli-forbidden states $\chi^F(\vec{r})$ for the ^{16}O-α relative motion which have the property

$$\mathcal{A}\{\chi^F(\vec{r})\phi(^{16}\mathrm{O})\phi(\alpha)\} = 0, \quad (5.18)$$

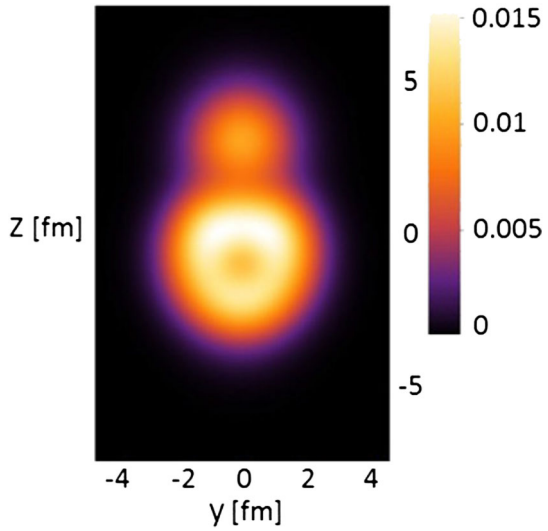

FIG. 13. Nucleon density distribution of the $^{16}\mathrm{O}+\alpha$ intrinsic THSR wave function of Eq. (5.16) for $D=0.6$ fm. A large distance of about 3.6 fm between $^{16}\mathrm{O}$ and α clusters is seen.

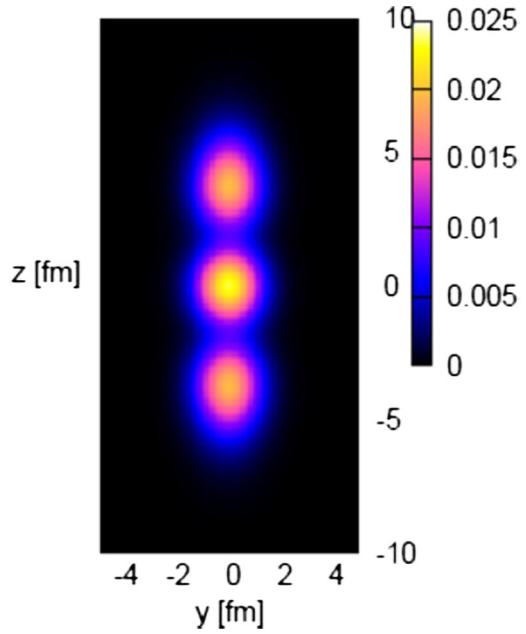

FIG. 14. Nucleon density distribution for a strongly prolate THSR wave function of 3αs.

where $\chi^F(\vec{r})$ are HO eigenstates with Gaussian factor $\exp[-8\vec{r}^2/(5b^2)]$ and oscillator quanta $2n+L$ smaller than 8. Thus the probability for two clusters $^{16}\mathrm{O}$ and α to be very close together is small. This is nothing more than Pauli repulsion.

We can say that the dynamics favors nonlocalized clustering but the constraints of antisymmetrization make the system exhibit localized clustering in the intrinsic frame. While this conclusion holds for two-cluster systems in general, the pairwise Pauli repulsion between clusters generally does not produce static localization in the intrinsic frame for more than two clusters. This is why a nonlocalized gaslike structure of three α clusters arises in the Hoyle state even though a localized dumbbell-like structure appears in the 2α system.

If there are additional constraints, however, there can be localized clustering even in systems with three or more clusters. An excited state can be viewed as the minimum energy state under the requirement of orthogonality to all energy eigenstates at lower energies. This requirement of orthogonality can constrain the possible deformations of the excited state. Consider, for example, an excited state of the 3α system that is orthogonal to the ground state, the Hoyle state, and also the next excited state above the Hoyle state. Suppose furthermore that these constraints energetically favor a strongly prolate THSR wave function of the form

$$\mathcal{A}\left\{\exp\left[-\sum_{k=1}^{3}\left(\frac{2(X_k^2+Y_k^2)}{b^2}+\frac{2Z_k^2}{B^2}\right)\right]\Phi(3\alpha)\right\}, \qquad (5.19)$$

where $B \gg b$. The nucleon density distribution for this THSR wave function is shown in Fig. 14 (Zhou, Funaki, Horiuchi *et al.*, 2014). We see three localized α clusters forming a linear-chain structure.

4. Equivalence of prolate and oblate THSR wave functions after angular momentum projection

One unusual feature of THSR wave functions is that prolate and oblate wave functions can become equivalent after angular momentum projection. Figure 15 shows a contour map of the squared overlaps between a prolate 0^+ THSR wave function with 0^+ THSR wave functions with various deformations in $^{20}\mathrm{Ne}$ (Zhou, Funaki, Horiuchi *et al.*, 2014). The deformed THSR wave function Φ_{Ne} of $^{20}\mathrm{Ne}$ has the form $\mathcal{A}[\chi(\vec{r})\phi(\alpha)\phi(^{16}\mathrm{O})]$, where $\chi(\vec{r})$ is $\exp[-\sum_{k=x,y,z}(8/5B_k^2)r_k^2]$

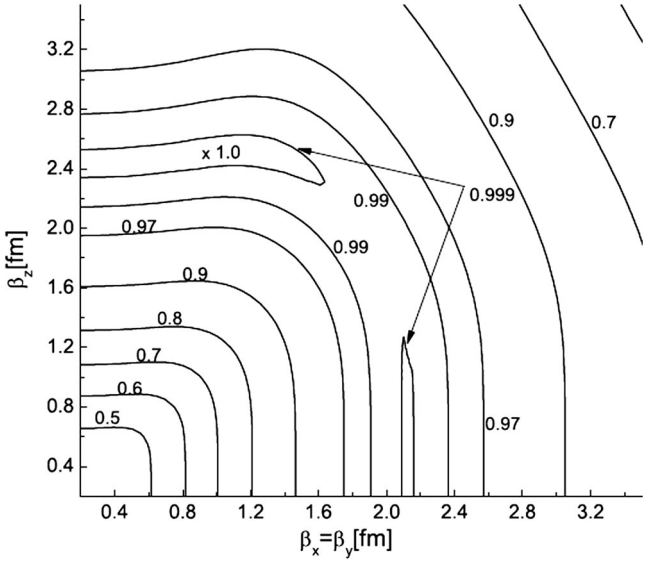

FIG. 15. Contour map of the squared overlap between a 0^+ wave function with $\beta_x=\beta_y=0.9$ fm, $\beta_z=2.5$ fm and 0^+ wave functions with various deformations $\beta_x=\beta_y$ and β_z. Numbers attached to the contour curves are squared overlap values. From Zhou, Funaki, Horiuchi *et al.*, 2014.

and $B_k^2 = b^2 + 2\beta_k^2$. We see in this figure that the prolate THSR wave function with $\beta_x = \beta_y = 0.9$ fm, $\beta_z = 2.5$ fm is almost 100% equivalent to oblate THSR wave functions with $\beta_x = \beta_y \approx 2.1$ fm and β_z between 0 and 1.2 fm after angular momentum projection onto 0^+. The equivalence of prolate and oblate THSR wave functions after angular momentum projection is true for all the spin-parity states of ^{20}Ne.

Despite this equivalence of prolate and oblate wave functions after angular momentum projection, we can say that the ^{20}Ne states expressed by the THSR wave functions all have prolate deformation as the actual deformation. This conclusion is obtained from the fact that the expectation values of the quadrupole moments of all the ^{20}Ne states expressed by THSR wave functions have negative sign. From the well-known formula

$$Q(J) = -\frac{J}{2J+3} Q(\text{intrinsic}), \tag{5.20}$$

we know that when the expectation value $Q(J)$ of the quadrupole moment of the wave function with good spin J is negative, the quadrupole moment of the intrinsic state $Q(\text{intrinsic})$ is positive and therefore prolate. The THSR wave function after angular momentum projection has the form $\Phi^J_{\text{Ne}} = \mathcal{A}[\chi_J(\vec{r})\phi(\alpha)\phi(^{16}\text{O})]$ and we can prove that this type of wave function Φ^J_{Ne} gives us the following formula for $Q(J)$ (Zhou, Funaki, Horiuchi *et al.*, 2014):

$$Q(J) = -\frac{J}{2J+3}\frac{16}{5}\langle r^2\rangle, \tag{5.21}$$

where

$$\frac{16}{5}\langle r^2\rangle = \langle \Phi^J_{\text{Ne}}| \sum_{j=1}^{20} (\vec{r}_j - \vec{X}_{\text{c.m.}})^2 |\Phi^J_{\text{Ne}}\rangle - R^2(^{16}\text{O}) - R^2(\alpha), \tag{5.22}$$

and

$$R^2(C_k) = \langle \phi(C_k)| \sum_{j\in C_k} [\vec{r}_j - \vec{X}_{\text{c.m.}}(C_k)]^2 |\phi(C_k)\rangle. \tag{5.23}$$

This shows that $Q(J)$ has negative value and explains why the calculated values of $Q(J)$ by THSR wave functions have all negative sign. Of course the negative sign of $Q(J)$ by THSR wave functions is in accordance with the prolate distribution of nucleon density shown in Fig. 13.

The reason why prolate and oblate THSR wave functions are almost equivalent after angular momentum projection is explained by the fact that the rotation average of a prolate THSR wave function is almost equivalent to an oblate THSR wave function. The rotation-averaged wave function $\Phi^{\text{ave}}(\beta_x = \beta_y, \beta_z)$ generated from a prolate THSR wave function $\Phi^{\text{prolate}}(\beta_x = \beta_y, \beta_z)$ is defined as

$$\Phi^{\text{ave}}(\beta_x = \beta_y, \beta_z) = \left(\frac{1}{2\pi}\int_0^{2\pi} d\theta e^{i\theta J_x}\right) \Phi^{\text{prolate}}(\beta_x = \beta_y, \beta_z). \tag{5.24}$$

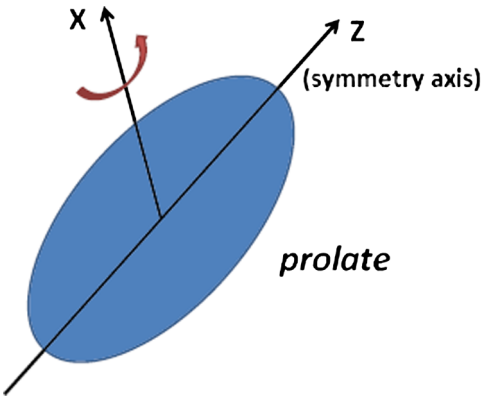

FIG. 16. Rotation average of a prolate THSR wave function around an axis (x axis) perpendicular to the symmetry axis (z axis) of the prolate deformation.

If we rotate a prolate THSR wave function around an axis (x axis) perpendicular to the symmetry axis (z axis) of the prolate deformation and construct a wave function by taking an average over this rotation, the density distribution of the rotation-average wave function will be oblate (see Fig. 16). In the case of the 0^+ state, when we construct the rotation-average wave function from the prolate THSR wave function with $(\beta_x, \beta_y, \beta_z) = (0.9, 0.9, 2.5\text{ fm})$ which gives the minimum energy for 0^+, it is almost 100% equivalent to the oblate THSR wave function with $(\beta_x, \beta_y, \beta_z) = (0.9, 2.1, 2.1\text{ fm})$.

$$\Phi^{\text{oblate}}(\beta_x = 0.9\text{ fm}, \beta_y = \beta_z = 2.1\text{ fm}) \approx \Phi^{\text{ave}}(\beta_x = \beta_y = 0.9\text{ fm}, \beta_z = 2.5\text{ fm}). \tag{5.25}$$

D. Container picture of cluster dynamics

The ground and Hoyle states in ^{12}C are obtained as the eigenstates with lowest and second lowest energies of Eq. (5.14). This equation is the GCM equation with respect to the size parameter B of the THSR wave function. The excitation of the system is described by the dynamics of the system size. This description is very different from the traditional description of the system excitation by the RGM or GCM equation, which treats the dynamics of intercluster motion. Zhou, Funaki, Horiuchi *et al.* (2014) called this new description of the cluster dynamics the container model of cluster dynamics. The container refers to the self-consistent field with size B in which clusters are accommodated and make nonlocalized motion.

The GCM equation with respect to the container size parameter B was also solved in the 4α system (Funaki *et al.*, 2010). Table I shows the energy spectra of 0^+ states obtained by 4α THSR-GCM. In this table, we show the energy spectra of 0^+ states obtained by 4α OCM (Funaki *et al.*, 2008) together with experimental spectra. This 4α OCM study confirmed the assignments by former $^{12}\text{C} + \alpha$ cluster model studies that the observed 0_2^+ and 0_3^+ states are dominantly $^{12}\text{C}(0_1^+) + \alpha$ (S wave) and $^{12}\text{C}(2_1^+) + \alpha$ (D wave) configurations, respectively. On the other hand, the 4α OCM study newly assigned the dominant configurations for the 0_4^+ and 0_5^+ states to be $^{12}\text{C}(0_1^+) + \alpha$ (higher nodal S wave) and

TABLE I. Comparison of the 0^+ energy spectra from experiments, 4α OCM calculation (Funaki *et al.*, 2008), and 4α THSR calculation (Funaki *et al.*, 2010). Energies E are measured in MeV from the 4α threshold, and rms radii $R_{\rm rms}$ are in fm.

	4α THSR			4α OCM		Expt.
	E	$R_{\rm rms}$		E	$R_{\rm rms}$	E
0_1^+	−15.05	2.5	0_1^+	−14.37	2.7	−14.44
0_2^+	−4.7	3.1	0_2^+	−8.0	3.0	−8.39
			0_3^+	−4.41	3.1	−2.39
0_3^+	1.03	4.2	0_4^+	−1.81	4.0	−0.84
			0_5^+	−0.25	3.1	−0.43
0_4^+	3.04	6.1	0_6^+	2.08	5.6	0.66

$^{12}\mathrm{C}(1_1^-)+\alpha$ (P wave), respectively. What is interesting about this 4α OCM study is the assignment of the 4α condensate-like structure to the observed 0_6^+ state at 15.1 MeV excitation. The reason for this assignment is that the reduced-width amplitude of the calculated 0_6^+ state is large only in the $^{12}\mathrm{C}(\mathrm{Hoyle})+\alpha$ (S wave) channel (Funaki *et al.*, 2008). The good accordance of the calculated decay width $\Gamma_{\rm cal}=136$ keV with the observed width $\Gamma_{\rm exp}=166$ keV for this 0_6^+ state gives high reliability to this OCM assignment. Yamada *et al.* (2012) reported that the fine structures of the observed isoscalar monopole strength function up to about 16 MeV in ^{16}O are well reproduced by this 4α OCM. Compared to the OCM calculation, the THSR-GCM calculation gives us only four 0^+ states in the excitation-energy region of observed six 0^+ states. However the fourth 0^+ state of the THSR-GCM calculation can be considered to correspond to the 0_6^+ state of 4α OCM and hence to the observed 0_6^+ state at 15.1 MeV excitation. It is because the reduced-width amplitude of the 0_4^+ state of the THSR-GCM calculation is markedly large only in the channel of $^{12}\mathrm{C}(\mathrm{Hoyle})+\alpha$ (S wave) (Funaki *et al.*, 2010). Thus also in the case of the 4α system the THSR-GCM calculation describes the excitation of the system from the ground state to the 4α gaslike excited state, although the description of the excitation to other states is incomplete. In order to remedy the incompleteness of the description of Funaki *et al.* (2010) we have to extend the 4α THSR wave function so that the THSR wave function includes not the single size parameter B but two or more B parameters. In the case of two B parameters, one B is for the container containing three α clusters and the other B is for the container for the relative motion between the 3α system and the fourth α cluster. In the next section we discuss the extension of the THSR wave function so that it includes two or more B parameters.

The GCM wave functions $\Phi_\lambda^{\text{THSR-GCM}}$ of the obtained four 0^+ states with $\lambda=1$, 2, 3, and 4 are found to have almost 100% squared overlaps with single orthogonalized THSR wave functions $\hat{\Phi}_\lambda(\beta_0)$ for a certain value of β_0 satisfying $B^2=b^2+2\beta_0^2$. $\hat{\Phi}_\lambda(\beta_0)$ is defined by

$$\hat{\Phi}_\lambda(\beta_0)=N_\lambda P_{\lambda-1}\Phi_{4\alpha}^{\text{THSR}}(\beta_0), \tag{5.26}$$

where

$$P_{\lambda-1}=1-\sum_{k=1}^{\lambda-1}|\Phi_k^{\text{THSR-GCM}}\rangle\langle\Phi_k^{\text{THSR-GCM}}|, \tag{5.27}$$

for $\lambda=2$, 3, and 4. Here N_λ is a normalization constant and $P_0=1$. Since the orthogonalization operator $P_{\lambda-1}$ expresses the necessary property which any excited state should satisfy, the essential character of $\Phi_\lambda^{\text{THSR-GCM}}$ is expressed by $\Phi_{4\alpha}^{\text{THSR}}(\beta_0)$. Thus, although $\Phi_\lambda^{\text{THSR-GCM}}$ is constructed by a linear combination of many 4α THSR wave functions, its essential character is described by only a single 4α THSR wave function. The optimum values of β_0 for four 0_λ^+ states are 1.2, 2.5, 4.0, and 6.5 fm, for $\lambda=1$, 2, 3, and 4, respectively, which means that the system size becomes larger with increasing λ.

E. Extended THSR wave function and examples of its application

1. Breathing-like excitation of the Hoyle state

The container model of cluster dynamics uses the system size parameter as the generator coordinate for clustering motion. In the case of the 3α system, we can introduce size parameters B_1 and B_2 for 2α and 3α containers as shown in Fig. 17. The extended THSR wave function for this double container system is given as (Zhou, Funaki, Tohsaki *et al.*, 2014)

$$\Phi_{3\alpha}^{\text{exTHSR}}(B_1,B_2)=\mathcal{A}\left\{\exp\left(-\frac{\vec{\xi}_1^2}{B_2^2}-\frac{\vec{\xi}_2^2}{B_1^2}\right)\Phi(3\alpha)\right\}. \tag{5.28}$$

When $B_2^2=(3/4)B_1^2$, $\Phi_{3\alpha}^{\text{exTHSR}}(B_1,B_2)=\Phi_{3\alpha}^{\text{THSR}}(B_1)$. As has been done in the traditional THSR wave function, we can use deformed containers. In this case, we replace $\vec{\xi}_1^2/B_2^2$ by $\sum_{i=x}^{z}\xi_{1i}^2/B_{2i}^2$ and also $\vec{\xi}_2^2/B_1^2$ by $\sum_{i=x}^{z}\xi_{2i}^2/B_{1i}^2$.

The extended THSR wave function for the 3α system has been applied to the studies of the ground state (Zhou, Funaki, Tohsaki *et al.*, 2014) and the positive-parity excited states in ^{12}C (Funaki, 2015; Zhou *et al.*, 2016). Funaki (2015) and Zhou *et al.* (2016) supported the existence of two 0^+ states (0_3^+ and 0_4^+) around 10 MeV excitation energy above the Hoyle state (0_2^+) which was proposed by the 3α OCM studies combined with the complex scaling method (CSM) in Kurokawa and Katō (2005) and Ohtsubo *et al.* (2013).

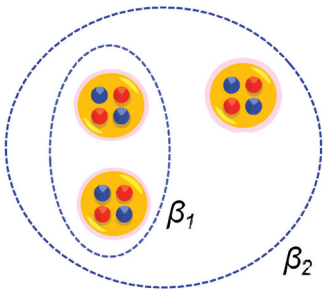

FIG. 17. Size parameters B_1 and B_2 for 2α and 3α containers, respectively, where $B_1^2=b^2+\beta_1^2$ and $B_2^2=(3/4)\,b^2+\beta_2^2$.

The 0_4^+ state is the state whose existence had long been known since the 1970s and this state is considered to have a bent-chain structure of 3α which has a large component of $^8\mathrm{Be}(2_1^+) + \alpha$ (D wave) (Uegaki *et al.*, 1977; Kanada-En'yo, 1998; Neff and Feldmeier, 2004). On the other hand, the 0_3^+ state is the state whose existence was newly proposed and which was suggested to be a breathing excitation of the Hoyle state in Kurokawa and Katō (2005, 2007). The theoretical proposal of the existence of two 0^+ states (0_3^+ and 0_4^+) around 10 MeV excitation energy was soon supported experimentally by Itoh *et al.* (2013). Itoh *et al.* (2013) reported that the observed broad 0^+ state at 10 MeV consists of two components. The lower 0^+ state to α decay to the ground state of ^{8}Be only while the higher 0^+ state has a distinct peak at 10.8 MeV with a width of 0.4 MeV in the coincidence spectrum for the first excited state of ^{8}Be channel. These two 0^+ states were considered to have consistent properties predicted for a higher nodal state of the Hoyle state and a linearlike 3α state, respectively.

Table II shows energies and rms radii of 0_2^+, 0_3^+, and 0_4^+ states of ^{12}C and monopole transition values $M(E0)$ between three 0^+ states which are calculated by extended 3α THSR wave functions (Funaki, 2015; Zhou *et al.*, 2016). We see that the Hoyle state (0_2^+) and two other 0^+ states have very large rms radii. The very large value of the calculated $E0$ strength $M(E0; 0_3^+ \to 0_2^+) = 35$ or 47 $e\,\mathrm{fm}^2$ supports the idea to regard the 0_3^+ state as a breathing-like excited state of the Hoyle state 0_2^+. Funaki (2015) calculated the total width of the 0_4^+ state to be 0.7 MeV which is to be compared with the observed width 1.42 MeV. As for the 0_3^+ state the calculated α width is 1.1 MeV which is rather close to the observed width 1.45 MeV (Itoh *et al.*, 2011).

Zhou *et al.* (2016) analyzed two kinds of intercluster relative wave functions which are contained in the four 0^+ states (0_1^+–0_4^+) obtained by the extended 3α container model. The first one is the S-wave relative wave function between $^8\mathrm{Be}(0_1^+)$ and the remaining α cluster and the second one is the S-wave relative wave function between two α clusters after the integration over the $\vec{\xi}_1$ Jacobi coordinate by using single Gaussian weight. It was found that both kinds of relative wave functions have one more node in the 0_3^+ state than in the Hoyle state. This result implies that the 0_3^+ state is the breathing-like excited state of the Hoyle state. It is because the generating operator for the breathing excitation

$$O_B = \sum_{i=1}^{12} (\vec{r}_i - \vec{r}_{\mathrm{c.m.}})^2 \tag{5.29}$$

can be rewritten as

$$O_B = \sum_{k=1}^{3} \sum_{i \in \alpha_k} (\vec{r}_i - \vec{X}_k)^2 + \frac{8}{3}\vec{\xi}_1^2 + 2\vec{\xi}_2^2. \tag{5.30}$$

TABLE II. Energies and rms radii of 0_2^+, 0_3^+, and 0_4^+ states of ^{12}C and monopole transition values $M(E0)$ between three 0^+ states which are calculated by extended THSR wave functions. Energies (MeV) are measured from the 3α threshold, radii are in fm, and $M(E0)$ values are in $e\,\mathrm{fm}^2$. Calculation A and Calculation B denote the results of Funaki (2015) and Zhou *et al.* (2016), respectively.

	Calculation A	Calculation B
$E(0_2^+)$, $R_{\mathrm{rms}}(0_2^+)$	0.23, 3.7	0,22, 3.9
$E(0_3^+)$, $R_{\mathrm{rms}}(0_3^+)$	2.6, 4.7	1.7, 5.2
$E(0_4^+)$, $R_{\mathrm{rms}}(0_4^+)$	3.9, 4.2	2.7, 4.0
$M(E0, 0_2^+ \to 0_1^+)$	6.3–6.4	6.2
$M(E0, 0_2^+ \to 0_3^+)$	34–37	47
$M(E0, 0_2^+ \to 0_4^+)$	0.5–1.4	7.7

2. Container evolution in ^{16}O

The extended THSR wave function was applied recently to study the evolution of cluster structure in ^{16}O (Funaki, 2018). As in the 3α system in Sec. V.E.1, two deformed containers are adopted where the first container is for the 3α subsystem and the second container is for the relative motion between the 3α subsystem and the fourth α cluster. Figure 18 shows the energy spectrum obtained by the extended 4α THSR (denoted as eTHSR) compared with the 4α OCM and experiment (Funaki, 2018). The fifth 0^+ state (0_5^+) by eTHSR is just above the 4α threshold and the two size parameters of its eTHSR wave function are nearly the same. This means that 4α clusters in this state are accommodated approximately in a single container. Since the size parameters of this state are large, $\beta_x = \beta_y \approx 5.6$ fm, $\beta_z \approx 2.0$ fm, the 0_5^+ state represents a Hoyle-analog state in ^{16}O.

The ground state (0_1^+) has the smallest radius and its intrinsic shape is reported to be terahedral. It is based on the calculated result that while the 3α subcontainer has an oblate shape the container describing the relative motion between the 3α subsystem and the fourth α cluster is of a prolate shape. The calculated second 0^+ state (0_2^+) is reported

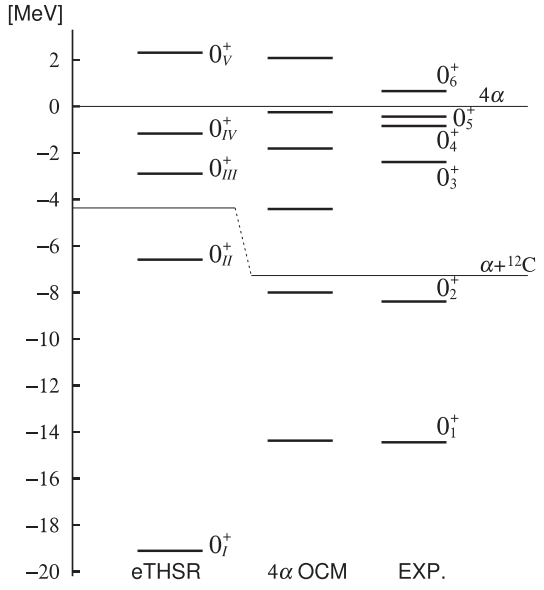

FIG. 18. Energy spectrum obtained by extended 4α THSR of Funaki (2018) which is compared with those by 4α OCM and experiment.

to have $^{12}\mathrm{C}(0_1^+)+\alpha$ (S wave) structure. The reason for this identification is that the size parameters of the 3α subcontainer are close to those of the 3α container of the ^{12}C ground state and are nearly spherical. Also, the container describing the relative motion between the 3α subsystem and the fourth α cluster is also nearly spherical but with a much larger radius. This structure of the second 0^+ state is in good accordance with previous cluster model studies (Suzuki, Horiuchi, and Ikeda, 1972; Funaki *et al.*, 2008). Similarly, the structure of the calculated third 0^+ state (0_3^+) is in good accordance with previous cluster model studies (Suzuki, Horiuchi, and Ikeda, 1972; Funaki *et al.*, 2008); namely, the 0_3^+ state is reported to have $^{12}\mathrm{C}(2_1^+)+\alpha$ (D wave) structure. The structure of the calculated fourth 0^+ state (0_{IV}^+) is reported to have $^{12}\mathrm{C}(0_1^+)+\alpha$ (S wave) where the container describing the relative motion between the 3α subsystem and the fourth α cluster is much larger than that of the second 0^+ state.

The container model and the extended THSR wave function describes the evolution of the cluster structure from the ground state up to the 4α condensate-like state (Hoyle-analog state) through the various $^{12}\mathrm{C}+\alpha$ structures and is therefore well suited for studying the evolution of the cluster structure. In describing this evolution, we go from a single container to several containers, a process called container evolution (Funaki, 2018).

3. Neutron-rich Be isotopes

Extended THSR wave functions have also been applied to neutron-rich nuclei. Since the container describing valence neutrons will have size parameters different from the container for the core part of the system, the use of the extended THSR wave function for neutron-rich nuclei is quite natural. Here we report the work of Lyu *et al.* (2015, 2016) which treats ^{9}Be and ^{10}Be, respectively.

In the case of ^{9}Be, the valence-neutron wave function $F(\vec{r})$ in the extended THSR wave function should have negative parity, and it is given by

$$F_n(\vec{r}) = \int d\vec{R} \exp\left(-\sum_{k=x}^{z}\frac{R_k^2}{\beta_k^2}\right)\exp(i\phi_R)\exp\left[-\frac{(\vec{r}-\vec{R})^2}{2b^2}\right]. \tag{5.31}$$

The phase factor $\exp(i\phi_R)$ makes the parity of $F_n(\vec{r})$ negative. Lyu *et al.* (2015) treated the ground rotational-band levels $3/2^-$, $5/2^-$, and $7/2^-$ and found that the extended THSR wave functions of these levels have about 95% squared overlaps with the wave functions obtained by the GCM calculation by using $2\alpha+n$ three-body Brink wave functions.

In the case of ^{10}Be, the energy spectra of two rotational bands upon the ground state and the 0_2^+ state were calculated using single extended THSR wave functions and were compared with those obtained by AMD calculations (Suhara and Kanada-En'yo, 2010; Kobayashi and Kanada-En'yo, 2012). For the ground band, the extended THSR wave functions where two valence neutrons occupy the orbit $F_n(\vec{r})$ were used. The modifications of these extended THSR wave functions were also made by introducing the distance parameter $\vec{R}_{\mathrm{pair}}$ between the c.m. of the 2α system and the c.m. of the $2n$ system. It was reported that both kinds of extended THSR wave functions give very similar energy spectra compared to that of the AMD calculation (Kobayashi and Kanada-En'yo, 2012). For the excited band, the extended THSR wave functions were constructed by accommodating two valence neutrons into the σ-orbit-type single-neutron orbit. The obtained energy spectrum is very similar to but a little higher than the AMD energy spectra (Suhara and Kanada-En'yo, 2010; Kobayashi and Kanada-En'yo, 2012). The extended THSR wave function of the 0_2^+ state is not orthogonalized to that of the ground state, but the squared overlap between them is as small as 1.4%. We see thus that the wave functions as simple as the single extended THSR wave functions give very good results quite similar to AMD calculations.

VI. NO-CORE SHELL MODEL

In contrast with the traditional shell-model approach which starts with an inert core of nucleons filling a closed shell, the no-core shell model treats all nucleons as active. The many-body basis states are the energy eigenstates of the spherical harmonic oscillator,

$$H_{\mathrm{osc}} = \sum_{i=1}^{A} H_i, \tag{6.1}$$

$$H_i = -\frac{\hbar^2}{2m}\nabla_i^2 + \frac{1}{2}m\Omega^2 r_i^2, \tag{6.2}$$

with some finite truncation imposed in the total oscillator excitation energy (Navrátil, Vary, and Barrett, 2000a, 2000b). Here m is the nucleon mass and Ω is the oscillator frequency. The truncation of the basis in terms of the total sum of oscillator excitation energies allows for an exact factorization of the wave function into separated center of mass and relative coordinate degrees of freedom.

In these no-core shell-model calculations the interactions among nucleons include a nucleon-nucleon potential fitted to experimental nucleon-nucleon scattering data as well as higher-nucleon interactions fitted to few-nucleon observables. Some take the approach of using a high-quality phenomenological potential (Wiringa, Stoks, and Schiavilla, 1995), while others apply the organizational principles of chiral effective field theory to produce effective chiral interactions for nucleons (Epelbaum, Hammer, and Meißner, 2009; Machleidt and Entem, 2011).

The method has had many remarkable successes in recent years in describing nuclear structure from first principles; see, e.g., Navrátil *et al.* (2007), Maris, Vary, and Shirokov (2009), Roth *et al.* (2011), and Barrett, Navrátil, and Vary (2013). For the study of nuclear clustering, however, the no-core shell model in its basic form is typically not efficient in describing spatial correlations among nucleons forming localized clusters.

A. Symmetry-adapted no-core shell-model approaches

The symmetry-adapted no-core shell model overcomes the problem of efficiently describing clustering by making use of exact and dynamical symmetries of the spherical harmonic oscillator Hamiltonian associated with collective mode excitations (Dytrych *et al.*, 2007, 2013; Draayer, Dytrych, and Launey, 2011; Dreyfuss *et al.*, 2013, 2016). We can rewrite the single-particle spherical harmonic oscillator Hamiltonian in terms of the usual ladder operators,

$$H_i = \hbar\Omega[c^\dagger_{x,i}c_{x,i} + c^\dagger_{y,i}c_{y,i} + c^\dagger_{z,i}c_{z,i} + \tfrac{3}{2}]. \tag{6.3}$$

We see there is a U(3) symmetry group associated with unitary 3×3 rotations of the x, y, and z quanta, and the component continuously connected to the identity forms an SU(3) symmetry group (Elliott, 1958a, 1958b). But the symmetry group can be expanded further by also allowing SU(1,1) transformations of the form

$$c_{x,i} \to \alpha c_{x,i} + \beta c^\dagger_{x,i}, \tag{6.4}$$

$$c^\dagger_{x,i} \to \alpha^* c^\dagger_{x,i} + \beta^* c_{x,i}, \tag{6.5}$$

$$|\alpha|^2 - |\beta|^2 = 1. \tag{6.6}$$

The transformation can also be applied to $c_{y,i}$, $c_{z,i}$, and any set of real orthogonal linear combinations of $c_{x,i}$, $c_{y,i}$, and $c_{z,i}$, and thus we also have an $\mathrm{SU}(1,1) \otimes \mathrm{O}(3)$ symmetry. It can be shown that the full dynamical group of the spherical harmonic oscillator is the real symplectic group $\mathrm{Sp}(6, \mathbf{R})$ for 6×6 matrices (Rowe and Wood, 2010).

The symmetry-adapted no-core shell model uses the real symplectic group $\mathrm{Sp}(6, \mathbf{R})$ and its subgroup SU(3) to generate linear combinations of spherical harmonic basis states which form complete representations of the SU(3) subgroup for some selected quantum numbers (λ, μ) of the Cartan subalgebra of SU(3). As the quantum numbers (λ, μ) correspond to different deformation geometries, the problem of capturing the collective behavior induced by clustering can be considerably more efficient in the symplectic basis. One of the future challenges for the symmetry-adapted no-core shell-model approach is to handle realistic nuclear forces with significant terms breaking symplectic or SU(3) symmetry.

A specific version of the symmetry-adapated no-core shell model called the no-core symplectic model was used to compute the low-lying even-parity states of ^{12}C (Dreyfuss *et al.*, 2013). The results for the rms matter radii and electric quadrupole moments are shown in Table III (Dreyfuss *et al.*, 2013). The NCSpM calculation gives a point matter rms radius for the ground state in agreement with experiment. The calculation yields a point matter radius of $r_{\mathrm{rms}} = 2.93$ fm for the Hoyle state, which is slightly larger than that of the ground state. While this result is smaller than the results typically obtained in cluster model calculations, it is close to a recent value deduced from experiment, 2.89(4) fm (Danilov *et al.*, 2009), and is similar to *ab initio* lattice EFT results at leading order, 2.4(2) fm (Epelbaum *et al.*, 2011).

TABLE III. NCSpM point rms matter radii and electric quadrupole moments for ^{12}C compared to experimental data.

	Matter radius (fm)		Q (e fm^2)	
	Expt.	NCSpM	Expt.	NCSpM
0^+_{gs}	2.43(2)[a]	2.43(1)		
0^+_2 (Hoyle)	2.89(4)[b,e]	2.93(5)		
0^+_3	⋯	2.78(4)		
2^+_1	2.36(4)[b,e]	2.42(1)	+6(3)[d]	+5.9(1)
2^+ above 0^+_2	3.07(13)[c,e]	2.93(5)	⋯	−21(1)
4^+_1	⋯	2.41(1)	⋯	+8.0(3)
4^+ above 0^+_2	⋯	2.93(5)	⋯	−26(1)

[a]Tanihata *et al.* (1985).
[b]Danilov *et al.* (2009).
[c]Ogloblin *et al.* (2013).
[d]Ajzenberg-Selove (1990).
[e]Experimentally deduced, based on model-dependent analyses of diffraction scattering.

The NCSpM calculations yield an electric quadrupole moment for the 2^+_1 state in agreement with the experimental value. Similarly, a positive quadrupole moment is found for the 4^+_1 state, and the 0^+_1, 2^+_1, and 4_1 are consistent with a rotational band with an oblate structure. On the other hand, a large negative result is found for the 2^+_2 state above the Hoyle state and the same for the 4^+ state above the Hoyle state. The results are consistent with a rotational band associated with the Hoyle state with a substantial prolate deformation. Such a prolate deformation has also been found in *ab initio* lattice EFT results (Epelbaum *et al.*, 2011, 2012).

We note that SU(3) symmetry has also been used to study clustering in shell-model calculations with a core. The cluster-nucleon configuration interaction model is one such approach (Volya and Tchuvil'sky, 2015). This method has recently been used to probe the cluster structure of ^{20}Ne resonances in elastic $^{16}\mathrm{O} + \alpha$ scattering (Nauruzbayev *et al.*, 2017).

B. Continuum no-core shell-model approaches

Another way to incorporate clustering in the no-core shell model is to consider spherical harmonic oscillator states corresponding to more than one center. This is done by combining the no-core shell-model formalism with the resonating group method (Friedrich and Langanke, 1975; Thompson, Lemere, and Tang, 1977; Fliessbach and Walliser, 1982). A review article summarizing recent developments can be found by Navrátil *et al.* (2016). In the following we discuss the case with two clusters.

Let the binary-cluster state of interest have total angular momentum J, parity π, and isospin T. We start with binary-channel basis states of the form (Quaglioni, Navrátil, and Roth, 2010)

$$|\Phi^{J^\pi T}_{\nu r}\rangle = [(|A - a\alpha_1 I^{\pi_1}_1 T_1\rangle |a\alpha_2 I^{\pi_2}_2 T_2\rangle)^{(sT)} \times Y_\ell(\hat{r}_{A-a,a})]^{(J^\pi T)} \frac{\delta(r - r_{A-a,a})}{r r_{A-a,a}}. \tag{6.7}$$

Here $|A-a\alpha_1 I_1^{\pi_1} T_1\rangle$ and $|a\alpha_2 I_2^{\pi_2} T_2\rangle$ are the internal wave functions of the first and second clusters, containing $A-a$ and a nucleons, respectively. They carry angular momentum quantum numbers I_1 and I_2 which are coupled together to form spin s, and the clusters have orbital angular momentum ℓ. Their parity, isospin, and additional quantum numbers are written as π_i, T_i, and α_i, respectively, with $i=1, 2$. The separation vector between the cluster centers is

$$\vec{r}_{A-a,a} = r_{A-a,a}\hat{r}_{A-a,a} = \frac{1}{A-a}\sum_{i=1}^{A-a}\vec{r}_i - \frac{1}{a}\sum_{j=A-a+1}^{A}\vec{r}_j, \tag{6.8}$$

where $\vec{r}_i$ are the single-particle coordinates for $i=1,\ldots,A$. It is convenient to group all relevant quantum numbers into a collective index $\nu=\{A-a\alpha_1 I_1^{\pi_1} T_1; a\alpha_2 I_2^{\pi_2} T_2; s\ell\}$. In order to enforce the correct fermionic statistics, one uses the intercluster antisymmetrizer,

$$\hat{\mathcal{A}}_\nu = \sqrt{\frac{(A-a)!a!}{A!}}\sum_P \mathrm{sgn}(P)P, \tag{6.9}$$

where the sum runs over all possible permutations P that can be carried out among nucleons, and $\mathrm{sgn}(P)$ is the sign of the permutation.

The antisymmetrized basis states can be used to expand the many-body wave function according to

$$|\Psi^{J^\pi T}\rangle = \sum_\nu \int dr r^2 \frac{g_\nu^{J^\pi T}(r)}{r}\hat{\mathcal{A}}_\nu|\Phi_{\nu r}^{J^\pi T}\rangle. \tag{6.10}$$

The coefficient functions $g_\nu^{J^\pi T}(r)$ correspond to the relative-motion radial wave functions between the clusters. These unknown coefficient functions are solved by the nonlocal integral-differential coupled-channel equations

$$\sum_\nu \int dr r^2 [\mathcal{H}_{\nu'\nu}^{J^\pi T}(r',r) - E\mathcal{N}_{\nu'\nu}^{J^\pi T}(r',r)]\frac{g_\nu^{J^\pi T}(r)}{r} = 0, \tag{6.11}$$

where E is the total energy in the center-of-mass frame, and the two integration kernels are the Hamiltonian kernel,

$$\mathcal{H}_{\nu'\nu}^{J^\pi T}(r',r) = \langle\Phi_{\nu' r'}^{J^\pi T}|\hat{\mathcal{A}}_{\nu'}H\hat{\mathcal{A}}_\nu|\Phi_{\nu r}^{J^\pi T}\rangle, \tag{6.12}$$

and the norm kernel,

$$\mathcal{N}_{\nu'\nu}^{J^\pi T}(r',r) = \langle\Phi_{\nu' r'}^{J^\pi T}|\hat{\mathcal{A}}_{\nu'}\hat{\mathcal{A}}_\nu|\Phi_{\nu r}^{J^\pi T}\rangle. \tag{6.13}$$

The nontrivial norm kernel is the result of the nonorthogonality of the basis states (6.7). Furthermore, the exchange terms in the antisymmetrizer give rise to nonlocal terms in the two kernels.

This no-core shell model with resonating group formalism has been used successfully to calculate many elastic scattering processes and inelastic reactions involving light nuclei (Quaglioni and Navrátil, 2008; Navrátil, Roth, and Quaglioni, 2010; Navrátil and Quaglioni, 2012). The method was recently improved further by also including basis states corresponding to the regular no-core shell basis with the full A-body space in one cluster. This has the advantage of encoding the short-range interactions between clusters more efficiently than the resonating group method would otherwise. This approach, known as the no-core shell model with continuum approach, has been used to describe two-body reactions (Dohet-Eraly *et al.*, 2016; Raimondi *et al.*, 2016), unbound states (Baroni, Navrátil, and Quaglioni, 2013), and even three-body reactions (Quaglioni, Romero-Redondo, and Navrtil, 2013). Quite recently there have also been no-core shell models with continuum studies of the cluster structure of ^{6}Li (Hupin, Quaglioni, and Navrtil, 2015) as an α cluster and deuteron and also of ^{6}He (Romero-Redondo *et al.*, 2014, 2016) in terms of an α cluster and two neutrons.

In Fig. 19 we show results for the ^{6}He wave function using the no-core shell model with continuum (Romero-Redondo *et al.*, 2016). The horizontal axis is the separation between the two halo neutrons r_{nn}, and the vertical axis is the separation between the alpha-particle core and the center of mass of the two halo neutrons $r_{\alpha,\mathrm{nn}}$. The plots show the dominance of a dineutron configuration where the two neutrons are about 2 fm apart and the α particle about 3 fm away. There is also a smaller contribution from a split configuration where the two neutrons are far from each other with the α particle situated in between.

The no-core shell model with continuum can be viewed as one of several continuum shell-model methods with a long history (Mahaux and Weidenmüller, 1969). Some other recent developments are the shell model embedded in the continuum (Okolowicz, Ploszajczak, and Rotter, 2003), the continuum shell model (Volya and Zelevinsky, 2005), and the no-core Gamow shell model (Papadimitriou *et al.*, 2013).

One recent work with particular relevance for nuclear clustering is Kravvaris and Volya (2017), which uses the

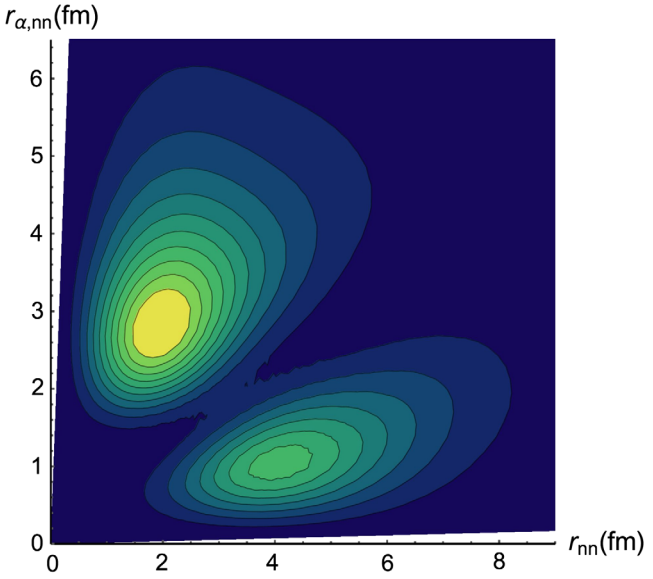

FIG. 19. Results for the ^{6}He wave function using a no-core shell model with continuum. The horizontal axis is the separation between the two halo neutrons r_{nn}, and the vertical axis is the separation between the α-particle core and the center of mass of the two halo neutrons $r_{\alpha,\mathrm{nn}}$. Adapted from Romero-Redondo *et al.*, 2016.

no-core shell model and resonating group method for clusters but also applies the harmonic oscillator expansion for the relative separation between clusters. In this work they compute spectroscopic amplitudes for the low-lying even-parity states of ^{8}Be, ^{10}Be, and ^{12}C into open α-separation thresholds.

VII. CONTINUUM QUANTUM MONTE CARLO METHODS

A recent review on continuum quantum Monte Carlo methods in nuclear physics was recently published (Carlson *et al.*, 2015). Here we give an overview of the methods and studies which have been used to investigate clustering in nuclei.

A. Variational Monte Carlo methods

Variational Monte Carlo methods rely on the variational principle that the energy of any trial wave function will be greater than or equal to the ground-state energy. We are of course assuming only physical states antisymmetrized with respect to the exchange of all identical fermions. The strategy is to start with some general functional form for the trial wave function $\Psi_T^{\{\alpha_i\}}$ which depends on some set of unknown parameters $\{\alpha_i\}$. One then computes the energy expectation $E_T^{\{\alpha_i\}}$ for the trial state

$$E_T^{\{\alpha_i\}} = \frac{\langle \Psi_T^{\{\alpha_i\}} | H | \Psi_T^{\{\alpha_i\}} \rangle}{\langle \Psi_T^{\{\alpha_i\}} | \Psi_T^{\{\alpha_i\}} \rangle}, \tag{7.1}$$

and minimizes with respect to $\{\alpha_i\}$. Instead of minimizing the energy, one can also minimize the expectation value of the variance operator $(H-\lambda I)^2$, which vanishes only when λ is an exact energy eigenvalue.

Since the trial wave function is typically a function with many degrees of freedom, the inner products in Eq. (7.1) are computed using Monte Carlo integration. If the interactions in H have a local structure in position space, then the required integration can be performed quite simply by selecting points in the space of the particle coordinates $\mathbf{r}_1, \mathbf{r}_2, \ldots$, chosen according to the squared absolute value of the trial wave function $|\Psi_T^{\{\alpha_i\}}(\mathbf{r}_1, \mathbf{r}_2, \ldots)|^2$ (McMillan, 1965; Ceperley, Chester, and Kalos, 1977). For each set of points, the expectation of H corresponds to the value of the function $\Psi_T^{\{\alpha_i\}} H \Psi_T^{\{\alpha_i\}}(\mathbf{r}_1, \mathbf{r}_2, \ldots)$. If one divides by the relative probability of selecting the points $\mathbf{r}_1, \mathbf{r}_2, \ldots$, then the value one records in the Monte Carlo integration of this observable is $H\Psi_T^{\{\alpha_i\}}(\mathbf{r}_1, \mathbf{r}_2, \ldots)/\Psi_T^{\{\alpha_i\}}(\mathbf{r}_1, \mathbf{r}_2, \ldots)$.

The quality of the variational Monte Carlo result depends entirely on the functional form used for the trial wave function. Therefore it is important to incorporate particle correlations into $\Psi_T^{\{\alpha_i\}}$. In variational Monte Carlo calculations of the structure of ^{16}O (Pieper, Wiringa, and Pandharipande, 1992), the trial wave function included noncentral two-body and three-body correlations acting on Slater determinants of S-wave and P-wave one-body wave functions. The expectation values of operators were calculated using a cluster expansion for the spin- and isospin-dependent terms up to four-body order. In many cases variational Monte Carlo methods are also used to optimize the trial wave function serving as a starting point for other Monte Carlo calculations such as diffusion or Green's function Monte Carlo methods.

B. Diffusion or Green's function Monte Carlo methods

Diffusion or GFMC starts with a trial wave function $|\Psi_T\rangle$ and uses Euclidean time evolution to extract the ground-state wave function (Kalos, 1962). Originally diffusion Monte Carlo and Green's function Monte Carlo methods referred to slightly different algorithms. However in today's usage, they refer to the same method. The ground-state wave function is obtained in the large time limit as

$$|\Psi_0\rangle \propto \lim_{\tau\to\infty} \exp[-(H-\lambda)\tau]|\Psi_T\rangle. \tag{7.2}$$

The parameter λ is used to stabilize the normalization of the wave function and gives an estimate of the ground-state energy E_0. A more direct calculation of the ground-state energy is given by

$$E_0 = \lim_{\tau\to\infty} \frac{\langle \Psi_T | H \exp[-(H-E_0)\tau] | \Psi_T \rangle}{\langle \Psi_T | \exp[-(H-E_0)\tau] | \Psi_T \rangle}. \tag{7.3}$$

When exponentiated over a short time step $\Delta\tau$, the kinetic energy term in H gives rise to a diffusion process which is modeled as a random walk in the space of all possible particle coordinates. Meanwhile, the particle interactions result in an exponential growth or decay for each possible spin and isospin channel.

One of the main computational challenges in GFMC is the sign oscillation problem associated with the exchange of identical fermions. These sign oscillations will render the numerator and denominator vanishingly small in the limit of large time τ. For real-valued wave functions the fixed-node approximation gives a remedy for this problem by restricting the random walk in the space of particle coordinates to a region where the trial wave function remains positive. For complex-valued wave functions as one finds in nuclear physics, a generalization of the approach called the constrained path approximation is used (Wiringa *et al.*, 2000). In the constrained path approximation one restricts the random walk to a region where the overlap of the propagated state with the trial wave function is positive (Carlson *et al.*, 2015).

GFMC has been used to compute the spectra of many light nuclei (Wiringa *et al.*, 2000; Pieper and Wiringa, 2001; Pieper, Varga, and Wiringa, 2002). This includes a well-known study of the α-cluster structure of the ^{8}Be ground state (Wiringa *et al.*, 2000). There have also been recent studies of the Hoyle state of ^{12}C (Carlson *et al.*, 2015) and its transitions to the ground state. These calculations found a radius for the Hoyle state of more than 3.1 fm, which is much larger than the ground-state radius 2.43 fm. Figure 20 shows that the density distributions $r^2\rho(r)$ of the ground state (0_1^+) and the Hoyle state (0_2^+) of ^{12}C (Carlson *et al.*, 2015). Similar results have been obtained using the THSR wave function (Tohsaki *et al.*, 2017).

In order to improve the computational scaling of the diffusion Monte Carlo simulations with the number of

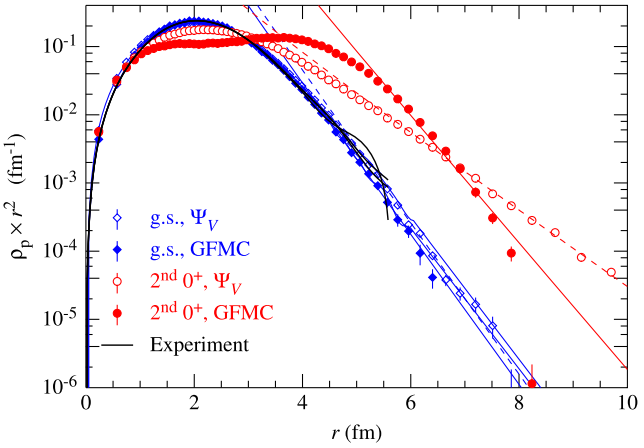

FIG. 20. The density distributions $r^2\rho(r)$ of the ground state (0_1^+) and the Hoyle state (0_2^+) of ^{12}C (Carlson *et al.*, 2015). The variational Monte Carlo results are indicated by Ψ_V while Green's function Monte Carlo results are labeled as GFMC. Adapted from Carlson *et al.*, 2015.

particles, one approach being pursued is introducing an auxiliary field to rewrite the spin-dependent interactions in terms of one-body spin operators. This method is called auxiliary-field diffusion Monte Carlo (Gandolfi *et al.*, 2007; Gezerlis *et al.*, 2013).

C. Monte Carlo shell model

The Monte Carlo shell-model (MCSM) approach is a variational method which uses auxiliary-field Monte Carlo simulations to determine a set of low-energy basis states $|\phi_n\rangle$ (Abe *et al.*, 2012). In this discussion we focus on the no-core version of MCSM where all nucleons are active. Each $|\phi_n\rangle$ is a Slater determinant of deformed single-particle shell-model states. The resulting states are given good angular momentum and parity quantum numbers by explicit projection. In order to remove residual errors due to the basis truncation, extrapolations are performed as a function of the energy variance (Shimizu *et al.*, 2010; Shimizu, Utsuno *et al.*, 2012). This method has been used to study the alpha-two-neutron cluster structure of ^{6}He, the two-alpha structure of ^{8}Be, and the two-alpha–two-neutron structure of ^{10}Be (Shimizu, Abe *et al.*, 2012; Yoshida *et al.*, 2013).

For the case with total angular momentum $J = 0$, the projected wave function is

$$|\Psi\rangle = P^{J=0}|\Phi\rangle, \qquad |\Phi\rangle = \sum_n f_n|\phi_n\rangle. \tag{7.4}$$

The linear combination of the unprojected basis states $|\Phi\rangle$ cannot be considered as an intrinsic state since the principal axis of each basis state $|\phi_n\rangle$ is not all aligned in the same direction. This is fixed by performing a rotation $R(\Omega_n)$ so that the quadrupole moment is diagonalized, and $Q_{zz} \geq Q_{yy} \geq Q_{xx}$ so that the principal axis is aligned with the z axis. The intrinsic wave function $|\Phi^{\text{intr}}\rangle$ is then defined as

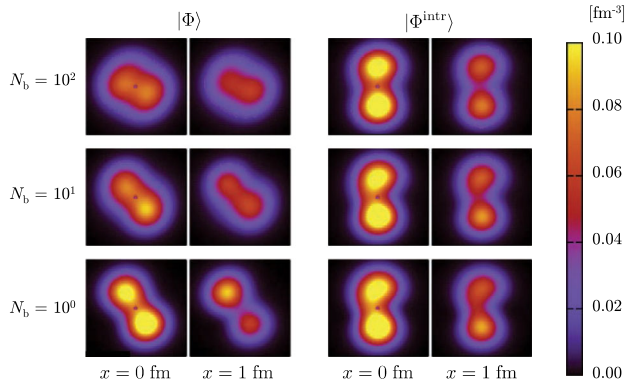

FIG. 21. The ^{8}Be proton densities for $|\Phi\rangle$ and $|\Phi^{\text{intr}}\rangle$ (Shimizu, Abe *et al.*, 2012; Yoshida *et al.*, 2013). Results are shown for $N_b = 10^0$, 10^1, and 10^2 basis states. Each density distribution shows the y-z plane for intercepts $x = 0$ and 1 fm. Adapted from Shimizu, Abe *et al.*, 2012.

$$|\Phi^{\text{intr}}\rangle \equiv \sum_n f_n R(\Omega_n)|\phi_n\rangle. \tag{7.5}$$

In Fig. 21 we show the ^{8}Be proton densities for $|\Phi\rangle$ and $|\Phi^{\text{intr}}\rangle$ (Shimizu, Abe *et al.*, 2012; Yoshida *et al.*, 2013). We show results for $N_b = 10^0$, 10^1, and 10^2 basis states. Each density distribution shows the y-z plane for intercepts $x = 0$ and 1 fm.

VIII. NUCLEAR LATTICE EFFECTIVE FIELD THEORY

A. Chiral effective field theory on a lattice

The basic idea of NLEFT is to merge the successful chiral EFT for nuclear forces pioneered by Weinberg (1990, 1991) with lattice Monte Carlo methods that allow for numerically exact solutions of the nuclear A-body problem. First, the ingredients to construct the chiral nuclear EFT are briefly discussed. The EFT is formulated in terms of the asymptotically observed states, the nucleons and the pions, the latter being the Goldstone bosons of the spontaneously broken chiral symmetry of QCD. The basic idea of the Weinberg approach is to use chiral perturbation theory to construct the potential between two, three, and four nucleons. The various contributions are organized according to the power counting based on the small parameter Q, with $Q \in \{p/\Lambda, M_\pi/\Lambda\}$. Here p denotes some soft external momentum, M_π the pion mass, and Λ the hard scale that accounts for all physics integrated out. Usually, this scale is set by the appearance of the first resonance, such as the $f_0(500)$ in pion-pion scattering or the $\Delta(1232)$ in pion-nucleon scattering. For the nuclear force problem, the leading-order (LO) contributions are of order $\mathcal{O}(Q^0)$, comprising the leading one-pion exchange and two local four-nucleon contact interactions without derivatives. At next-to-leading order (NLO) $\mathcal{O}(Q^2)$ one has the leading two-pion exchange (TPE) interactions and seven further four-nucleon terms with two derivatives (for on-shell scattering) as well as two isospin symmetry-breaking terms that account for the dominant strong interaction difference between the proton-proton, proton-neutron, and neutron-neutron systems. Finally, at next-to-next-lo-leading order

(NNLO) $\mathcal{O}(Q^3)$, that is the accuracy to which most NLEFT calculations have been carried out so far, one has further TPE corrections proportional to the dimension-two low-energy constants (LECs) c_i of the effective pion-nucleon Lagrangian that can be precisely determined from the dispersive Roy-Steiner equation analysis of pion-nucleon scattering (Hoferichter *et al.*, 2015). At this order, three-nucleon forces (3NFs) start to contribute. These fall into three topologies. The two-pion exchange diagram is entirely given in terms of the LECs $c_{1,3,4}$. The one-pion exchange coupling to a four-nucleon term and the local six-nucleon contact term are parametrized by the LECs D and E, respectively. These are commonly determined from the triton binding energy and the axial-vector current contribution to triton decay (Gazit, Quaglioni, and Navrátil, 2009). For further details, see Epelbaum, Hammer, and Meißner (2009) and Machleidt and Entem (2011).

In the lattice formulation, Euclidean space-time is given by a finite hypercubic volume, with L the length in any of the spatial directions and L_t the extension in the temporal direction. Further, the lattice is defined by a minimal spatial distance a, the lattice spacing, and similarly by a_t in the temporal direction. In most calculations discussed in what follows, a coarse spatial lattice with $a = 1/(100\ \mathrm{MeV}) = 1.97$ fm was used, while a_t is chosen to be $a_t = 1/(150\mathrm{MeV}) = 1.32$fm. One important feature of the finite lattice spacing is the UV finiteness of the theory, as the largest possible momentum is given by $p_{\max} = \pi/a \simeq 314$ MeV. Thus, the interaction is very soft and therefore most higher-order corrections, including also the Coulomb effects, can be treated in perturbation theory. Another advantage of this approach is the fact that all possible configurations of nucleons are sampled as depicted in Fig. 22. This gives the first hint that the phenomenon of clustering indeed will arise quite naturally in this approach. In the actual calculations, the interactions between the nucleons are described in terms of auxiliary fields, which makes the approach particularly suited for highly parallel computation. In essence, each nucleon evolves in time from the starting at $t = t_i$ up to the final time t_f. The value of t_f has to be large enough so that the asymptotic behavior of any observable for the A-nucleon state can be extracted. For further details, we refer to the detailed description of the LO chiral EFT interactions on the lattice in Borasoy *et al.* (2007a). See also the review by Lee (2009). Another important aspect to be discussed shortly is the approximate Wigner SU(4) symmetry of the nuclear interactions (Wigner, 1937), which rests upon the observation that combined spin-isospin rotations of the nucleon four-vector $(p\uparrow, p\downarrow, n\uparrow, n\downarrow)$ leave the nuclear forces in the S wave approximately invariant. This symmetry is broken by the one-pion exchange and the Coulomb interactions, but rather well respected by the four-nucleon short-range operators (Mehen, Stewart, and Wise, 1999). Most importantly, in the case of an exact Wigner symmetry, nuclei with spin and isospin zero do not show any sign oscillations (Chen, Lee, and Schäfer, 2004) removing the problem that makes finite density lattice quantum chromodynamics (QCD) simulations so difficult. This approximate symmetry can therefore be used as an inexpensive filter in the actual simulations. For further work on understanding the Wigner symmetry within QCD and its consequences, see, e.g., Lee (2004), Calle Cordon and Arriola (2008), and Beane *et al.* (2013). We will return to this issue in Sec. VIII.B. Before continuing, let us define what we mean by *ab initio* calculations in this context. The various parameters appearing in the lattice approach, such as the LECs and the smearing parameters as defined later, are determined in fits to properties of few-particle systems such as phase shifts and binding energies. Here few means less than or equal to 4. The properties of larger nuclei are then predicted with an accuracy determined by the quality of the underlying chiral EFT Hamiltonian. Note that recently it was found that also fitting to the low-energy α-α S-wave phase shifts for determining the pertinent LECs provides some advantage in controlling higher-body interactions in larger systems.

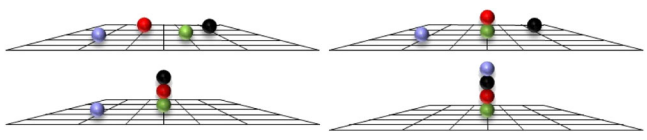

FIG. 22. Possible configurations of four nucleons on the lattice (shown here in a two-dimensional sketch).

B. Lattice formalism

To calculate the energy or any other static observable, we need an initial wave function for the nucleus under consideration $|\Psi_A^{\mathrm{in}}(t_i)\rangle$. Such a state can, on the one hand, be chosen as a Slater-determinant state composed of delocalized standing waves in the periodic cube with A nucleons, and, on the other hand, as localized α-cluster trial states (or any other type of cluster state). Such localized states have been used in the investigations of ^{12}C and ^{16}O (Epelbaum *et al.*, 2011, 2012, 2014). These can be used to check the calculations with the delocalized initial states, but also allow one to assess the spatial structure of the nuclei. It has to be understood that these states are always prepared with a given total angular momentum J and parity π that is a fixed J^π. The rotational symmetry breaking due to the lattice will be discussed later. The central object of NLEFT is the Euclidean time projection amplitude

$$Z_A(t) \equiv \langle \Psi_A(t')| \exp(-H_{\mathrm{LO}} t)|\Psi_A(t')\rangle \tag{8.1}$$

that allows one to compute the "transient energy" $E_A(t) = -\partial[\ln Z_A(t)]/\partial t$. Here H_{LO} is the leading-order Hamiltonian. In the infinite time limit, this gives the ground-state energy as all excited states have a larger energy and thus fall off faster. Note that a filter based on Wigner's SU(4) symmetry is used to suppress the sign oscillations, as detailed by Borasoy *et al.* (2007a). In fact, by now this method has been considerably improved by the so-called "triangulation" procedure introduced by Lähde *et al.* (2014) which allows one to significantly reduce the error related with the Euclidean time extrapolation. For example, using this method, the ground-state energies of ^{12}C and ^{16}O can be calculated with an absolute uncertainty of ± 200 keV. A more detailed discussion of this method and the associated uncertainties was given by Lähde *et al.* (2015).

In order to compute the low-lying excited states of a given nucleus, the Euclidean time projection method is extended to a multichannel calculation. Take the ^{12}C nucleus as an example (Epelbaum *et al.*, 2011). Here one applies the exponential operator $\exp(-Ht)$ to 24 single-nucleon standing waves in the periodic cube. From these standing waves one then builds initial states consisting of six protons and six neutrons each and extracts four orthogonal energy levels with the desired quantum properties. All four have even parity and total momentum equal to zero. As is well known, the lattice discretization of space and periodic boundaries reduce the full rotational group to a cubic subgroup, so that only 90-degree rotations along axes are exact symmetries. This complicates the identification of spin states. However, the degeneracy or nondegeneracy of energy levels for $J_z = 0$ and 2 allows one to distinguish between spin-0 and spin-2 states. This method can be refined by not only using delocalized standing waves but also initial cluster states, which can be generated either from four nucleons that after some time self-assemble to give α clusters or with α clusters that are formed by Gaussian wave packets and can be arranged in certain geometrical configurations (Epelbaum *et al.*, 2012). As shown in Fig. 23, various configurations that correspond to $J^\pi = 0^+$ indeed lead to the ground state (left panel) or the first excited 0^+ Hoyle state about 7 MeV above the ground state.

We have already noted that the proximity of the Hoyle state energy to the triple-α threshold is important for the production of carbon in the Universe. As with any near-threshold state, this very low-energy scale is well separated from other energy scales, and this separation of scales forms the basis for halo effective field theory (Bertulani, Hammer, and Van Kolck, 2002; Bedaque, Hammer, and van Kolck, 2003; Higa, Hammer, and van Kolck, 2008).

One interesting theoretical question is whether this proximity of the Hoyle state to the triple-α threshold is a generic feature of quantum chromodynamics or is this something that needs to be fine-tuned. The quark mass dependence of the

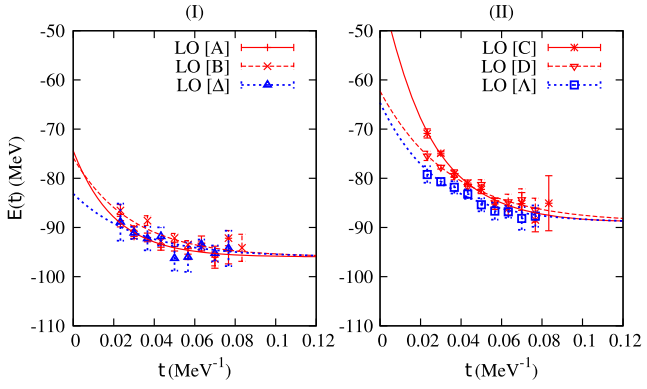

FIG. 23. Lattice results for the ^{12}C spectrum at leading order (LO). Panel I shows the results using initial states A, B, and Δ, each of which approaches the ground-state energy. Panel II shows the results using initial states C, D, and Λ. These trace out an intermediate plateau at an energy $\simeq$7 MeV above the ground state. Here $A - D$ are configurations that start with delocalized nucleons, where as Δ refers to a compact triangle, while Λ denotes an obtuse triangular configuration. For details, see Epelbaum *et al.* (2012).

Hoyle state energy has also been studied using lattice simulations (Epelbaum *et al.*, 2013a, 2013b) in connection with the anthropic principle, the production of carbon and oxygen, and the fine-tuning of the parameters of nature (Epelbaum, Meißner, and Glöckle, 2002, 2003; Beane and Savage, 2003a, 2003b; Bedaque, Luu, and Platter, 2011; Berengut *et al.*, 2013; Meißner, 2015).

Next, two-particle scattering has to be discussed. It is not only an important ingredient to fix the LECs of the effective Lagrangian but can also be used to investigate the nuclear dynamics encoded in nuclear reactions. The most well known and used method is due to Lüscher, who showed that the energy shift of an interacting two-particle system in a finite volume can be related to the continuum phase shift at the same energy (Lüscher, 1986, 1991). This method has by now been extended to cope with higher partial waves, partial-wave mixing, multichannel scattering, boosted frames, and all possible types of boundary conditions (He, Feng, and Liu, 2005; Liu, Feng, and He, 2006; Bernard *et al.*, 2008; Lage, Meißner, and Rusetsky, 2009; Bour *et al.*, 2011; König, Lee, and Hammer, 2011, 2012; Luu and Savage, 2011; Göckeler *et al.*, 2012; Briceno *et al.*, 2013; Li and Liu, 2013; Li, Li, and Liu, 2014; Li and Wu, 2015). However, for the case of nucleon-nucleon scattering, which involves higher energies, spin-orbit coupling, and partial-wave mixing, the method is less accurate than at low momenta. A more robust approach that makes use of the nonrelativistic character of the nuclear problem is the so-called spherical wall approach, formulated as early as in Carlson, Pandharipande, and Wiringa (1984) but reinvented for the lattice formulation used here in Borasoy *et al.* (2007b). Here one imposes a hard spherical wall boundary on the relative separation between the two particles at some radius R_W. In that way, copies of the interactions produced by the periodic lattice are removed and, from the solution of the Schrödinger equation for spherical standing waves at $r = R_W$, one can easily recover the phase shift for a given partial wave. Mixing of the partial waves caused by spin-orbit coupling is also easily dealt with. This method was improved significantly by Lu *et al.* (2016). First, so-called radial position states for a given partial wave are constructed according to

$$|r\rangle^{\ell,\ell_z} = \sum_{\vec{r}'} Y_{\ell,\ell_z}(\hat{r}')\delta_{r,|\vec{r}'|}|\vec{r}'\rangle, \tag{8.2}$$

with Y_{ℓ,ℓ_z} spherical harmonics with angular momentum quantum numbers ℓ, ℓ_z, and r to be restricted to less than half the box size $L/2$. Angular momentum is not conserved on the lattice. However, the amount of rotational invariance breaking decreases with increasing radial distance, and we can use spherical harmonics to determine the corresponding partial waves. This projection allows one to construct the so-called radial lattice Hamiltonian. Second, one introduces auxiliary potentials in the region before the spherical wall. By tuning the depth of this potential, one can dial the scattering energy. In the case of partial-wave mixing, this potential has to be chosen such that time-reversal symmetry is broken. This allows one to extract phase shifts and scattering angles with superior precision to what could be done before. For details, see Lu *et al.* (2016).

The aforementioned SU(4) symmetry can be further utilized to suppress the sign oscillations in the auxiliary-field Monte Carlo calculations. The underlying idea is to smoothly connect the LO lattice Hamiltonian with an SU(4)-symmetric counterpart that does not suffer from any sign oscillations. In that way, one can construct a one-parameter family of Hamiltonians $H(d) = dH_{\mathrm{LO}} + (1-d)H_{\mathrm{SU(4)}}$. For $d = 1$, one obviously recovers the microscopic chiral Hamiltonian. One can then perform simulations for various values of d and thus $H(d)$ and extrapolate to the limit $d = 1$. This method is called symmetry-sign extrapolation (SSE) and is discussed in detail by Lähde, Luu *et al.* (2015). In contrast to techniques introduced earlier in shell-model Monte Carlo calculations (Alhassid *et al.*, 1994; Koonin, Dean, and Langanke, 1997), the sign oscillations in the lattice approach are quadratic in the interfering interaction effects and thus the growth of the sign problem is weaker. Therefore, it is believed that the SSE will become a valuable tool in studying the physics of neutron-rich and proton-rich nuclei.

Another important issue in such a lattice approach is smearing, which means that the interactions are not strictly pointlike but distributed over some lattice sites. This method is very common in lattice QCD to enhance the strength of a given quark source; see, e.g., Güsken (1990), Daniel *et al.* (1992), Allton *et al.* (1993), Morningstar and Peardon (2004), Hasenfratz, Hoffmann, and Schaefer (2007), and Edwards, Joo, and Lin (2008) for some ground-breaking work. In NLEFT, smearing is done for various reasons. First, the four-nucleon interaction terms are smeared with a Gaussian-type function, whose parameter is fixed from the averaged nucleon-nucleon S-wave effective ranges. As discussed in detail by Borasoy *et al.* (2007a), this type of smearing is required to avoid overbinding due to the configurations with four nucleons on one lattice site; cf. Fig. 22. This has the added value that the important effective range corrections are treated nonperturbatively rather than perturbatively, i.e., some important higher-order corrections are also resummed. Second, a novel type of nonlocal smearing was introduced by Elhatisari *et al.* (2016). For that, one considers nonlocal nucleon annihilation (creation) operators and two-nucleon densities, such as

$$\begin{aligned} a_{\mathrm{NL}}(\mathbf{n}) &= a(\mathbf{n}) + s_{\mathrm{NL}} \sum_{\langle \mathbf{n}'\mathbf{n}\rangle} a(\mathbf{n}'), \\ a^{\dagger}_{\mathrm{NL}}(\mathbf{n}) &= a^{\dagger}(\mathbf{n}) + s_{\mathrm{NL}} \sum_{\langle \mathbf{n}'\mathbf{n}\rangle} a^{\dagger}(\mathbf{n}'), \\ \rho_{\mathrm{NL}}(\mathbf{n}) &= a^{\dagger}_{\mathrm{NL}}(\mathbf{n}) a_{\mathrm{NL}}(\mathbf{n}), \end{aligned} \tag{8.3}$$

where the three-vector $\mathbf{n}$ denotes a lattice site, and $\sum_{\langle \mathbf{n}'\mathbf{n}\rangle}$ denotes the sum over nearest-neighbor lattice sites of $\mathbf{n}$, so that $|\mathbf{n}' - \mathbf{n}| = a$. The smearing parameter s_{NL} is to be determined together with the other parameters and LECs as discussed later. This nonlocal smearing offers the possibility of considering nonlocal interactions on the lattice, besides the pion exchanges, as discussed in Sec. VIII.D.3.

Another issue to be addressed is the lattice spacing dependence. In contrast to lattice QCD, in NLEFT one does not perform the continuum limit $a \to 0$ as we are dealing with an effective field theory that only makes sense below some hard (breakdown) scale Λ. Physically, one can understand this intuitively, the EFT is not appropriate to resolve the inner structure of the nucleon, given by the proton charge radius of about 0.85 fm. Therefore, one expects that the calculations within NLEFT are invariant under variations of a between 1 and 2 fm, provided that the LECs are properly readjusted. This expectation is indeed borne out by explicit calculations. Klein *et al.* (2015) showed that within the pionless as well as the pionful LO EFT the S-wave phase shifts and the deuteron binding energy can be reproduced for $0.5 \lesssim a \lesssim 2.0$ fm. This was recently sharpened by studying the neutron-proton interactions to NNLO for lattice spacings from 1 to 2 fm (Alarcón *et al.*, 2017). Presently, larger systems are systematically investigated to establish this a independence in general.

Finally, we mention that simple α-cluster models were used by Lu *et al.* (2014, 2015) to gain a deeper understanding of the effects of the rotational symmetry breaking on the lattice and to develop methods to overcome this. Lu *et al.* (2014) demonstrated that lattice spacing errors are closely related to the commensurability of the lattice with the intrinsic length scales of the system and that rotational symmetry-breaking effects can be significantly reduced by using improved lattice actions. In particular, the physical energy levels are accurately reproduced by the weighted average of a given spin multiplets. Further, Lu *et al.* (2015) studied the matrix elements of multipole moment operators. It could be shown that the physical reduced matrix element is well reproduced by averaging over all possible orientations of the quantum state, and this is expressed as a sum of matrix elements weighted by the corresponding Clebsch-Gordan coefficients. These methods will become important when more detailed investigations of the electromagnetic structure of nuclei within NLEFT will be performed.

C. Adiabatic projection method

To study reactions and inelastic processes on the lattice, one makes use of the so-called "adiabatic projection method" (APM). The APM was developed by Pine, Lee, and Rupak (2013) and Rupak and Lee (2013) and further refined by Elhatisari and Lee (2014), Rokash *et al.* (2015), and Elhatisari, Lee, Meißner, and Rupak (2016). From the setup, it is similar to the recent studies combining the resonating group method with the no-core shell model; see, e.g., Quaglioni and Navrátil (2008), Navrátil, Roth, and Quaglioni (2010), Navrátil and Quaglioni (2012), and Romero-Redondo *et al.* (2014). Within the APM, the cluster-cluster scattering problem on the lattice is evaluated in a two-step procedure. First, one uses Euclidean time projection to determine an adiabatic Hamiltonian for the participating clusters. Strictly speaking, for finite temporal lattice spacing, an adiabatic transfer matrix rather than the Hamiltonian is constructed, but the method is essentially the same, and for simplicity, the Hamiltonian formulation is discussed here. In the second step, this adiabatic Hamiltonian is then used to calculate the pertinent phase shifts. The biggest advantage of the APM is that the computational time appears to scale as $t_{\mathrm{CPU}} \sim (A_1 + A_2)^2$ with A_i the number of nucleons

in cluster i, while more conventional approaches exhibit a factorial or even exponential scaling.

Consider an L^3 periodic lattice and a set of two-cluster states $|\vec{R}\rangle$ labeled by their separation vector $\vec{R}$ as illustrated in Fig. 24. In general, there are spin and flavor indices for these states, but we suppress writing the indices for notational simplicity. Also, it is favorable to perform a radial projection as given in Eq. (8.2). However, the exact form of these two-cluster states is not important except that they are localized so that for large separations they factorize as a tensor product of two individual clusters $|\vec{R}\rangle = \sum_{\vec{r}} |\vec{r}+\vec{R}\rangle_1 \otimes |\vec{r}\rangle_2$. These states are propagated in Euclidean time to form dressed cluster states $|\vec{R}\rangle_\tau = \exp(-H\tau)|\vec{R}\rangle$. An important consequence of this evolution in Euclidean time with the microscopic Hamiltonian is the fact that deformations and polarizations of the interacting clusters are incorporated automatically. Also, in this way one projects onto the space of low-energy scattering states in the finite volume, so that in the limit of large Euclidean time, these dressed cluster states span the low-energy subspace of two-cluster continuum states. Next, matrix elements of the microscopic Hamiltonian with respect to the dressed cluster states are formed, $[H_\tau]_{\vec{R},\vec{R}'} = {}_\tau\langle\vec{R}|H|\vec{R}'\rangle_\tau$. However, since the dressed cluster states $|\vec{R}\rangle_\tau$ are, in general, not orthogonal, one needs to construct the norm matrix N_τ, $[N_\tau]_{\vec{R},\vec{R}'} = {}_\tau\langle\vec{R}|\vec{R}'\rangle_\tau$, so that the Hermitian adiabatic Hamiltonian can be readily calculated as

$$[H^a_\tau]_{\vec{R},\vec{R}'} = \sum_{\vec{R}'',\vec{R}'''} [N_\tau^{-1/2}]_{\vec{R},\vec{R}''}[H_\tau]_{\vec{R}'',\vec{R}'''}[N_\tau^{-1/2}]_{\vec{R}''',\vec{R}'}. \quad (8.4)$$

In the limit of large τ, the spectrum of H^a_τ exactly reproduces the low-energy finite volume spectrum of the microscopic Hamiltonian H. From this adiabatic Hamiltonian, elastic phase shifts can be calculated using the methods discussed. Inelastic processes can also be dealt within this scheme by just adding additional channels; see Pine, Lee, and Rupak (2013) for details. One remark is in order. Since one is working in Euclidean time, the time evolution operator indeed acts as a diffusion operator. The precise definition of the asymptotic states must therefore account for this, and in fact one can define an asymptotic radius R_ϵ as the radius such that for $|\vec{R}| > R_\epsilon$ the amount of overlap between the cluster wave packets is less than any small positive parameter ϵ (Rokash *et al.*, 2015). Consequently, in the asymptotic region $|\vec{R}| > R_\epsilon$, the dressed clusters are widely separated and interact only through long-range forces such as the Coulomb interaction. This is schematically shown in Fig. 25. For cases where there are no long-range interactions, the scattering states of the adiabatic Hamiltonian are given by a superposition of Bessel functions in the asymptotic region. For the case with Coulomb interactions, the scattering states of the adiabatic Hamiltonian in the asymptotic region correspond to a superposition of Coulomb wave functions. A much refined version of the adiabatic Hamiltonian based on an improved radial "binning" was given by Elhatisari, Lee, Meißner, and Rupak (2016). Thus, large-scale numerical computations of nucleus-nucleus scattering and reactions using Monte Carlo methods are possible. We will discuss the archetypical process of elastic α-α scattering in Sec. VIII.D.2.

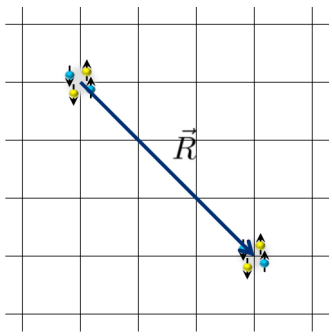

FIG. 24. An initial state formed of two clusters $|\vec{R}\rangle$. The two clusters are separated by the displacement vector $\vec{R}$.

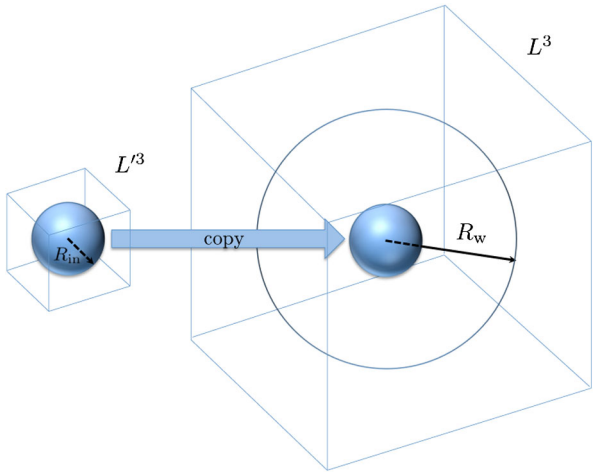

FIG. 25. A sketch of the lattices for the cluster-cluster calculations in the overlapping and the noninteracting regions. $R_{\rm in}$ is the largest radial distance that is free of systematic errors due to the periodic boundary in the cubic box with volume L'^3, where $L'^3 \ll L^3$. $R_{\rm w}$ indicates the radius of the spherical wall discussed in Sec. VIII.B.

D. Results

1. Alpha-cluster nuclei

Epelbaum *et al.* (2011, 2012) calculated the even-parity spectrum and structure of ^{12}C. The underlying Hamiltonian was given at NNLO precision, which includes the first contributions of the 3NF. The 11 LECs related to the

TABLE IV. Ground-state energies for α-cluster nuclei above ^{12}C. Shown are the results at LO and NNLO. NNLO* denotes the force supplemented with a four-nucleon interaction. The experimental values are also given. Units are MeV.

	^{16}O	^{20}Ne	^{24}Mg	^{28}Si
LO	−147.3(5)	−199.7(9)	−255(2)	−330(3)
NNLO	−138.8(5)	−184.3(9)	−232(2)	−308(3)
NNLO*	−131.3(5)	−165.9(9)	−198(2)	−233(3)
Expt.	−127.62	−160.64	−198.26	−236.54

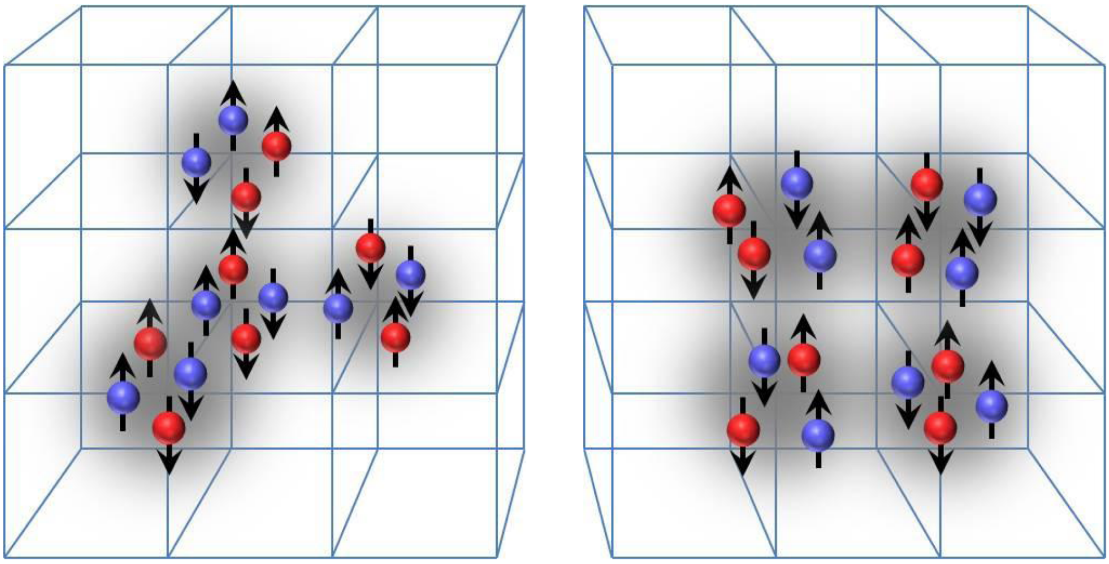

FIG. 26. Schematic illustration of the α-cluster initial states in ^{16}O with tetrahedral and planar configurations.

nucleon-nucleon interactions were fixed from the S- and P-wave np phase shifts as well from the pp and nn scattering lengths. The two LECs related to the 3NF were fixed from the triton binding energy and the weak axial-vector current. With that, the binding energy of ^{4}He is $-28.3(6)$ MeV in agreement with the empirical value. The next α-type nucleus ^{8}Be is bound with $-55(2)$ MeV, compared to the empirical value of -56.5 MeV, which is above the 2α threshold, i.e., ^{8}Be is unbound in nature. Nevertheless, ^{8}Be is long lived, so given the accuracy of the NNLO calculation, this agreement is satisfactory. The resulting even-parity spectrum of ^{12}C is shown in the NLEFT results presented in Fig. 4. The uncertainties on the energy levels have been considerably reduced to what was quoted in the original papers (Epelbaum *et al.*, 2011, 2012), the ground state can now be calculated with an uncertainty of about 200 keV, and similar errors are expected for the excited states. Most importantly, the clustering arises very naturally as already discussed in Sec. VIII.B. Also, by using initial cluster-type states, one can map out the most important contributions for a state of given energy, spin, and parity. It was found that the ground and the first excited 2^+ state of ^{12}C are mostly given by a compact triangular configuration of three alpha particles, while the Hoyle state and the second 2^+ state receive a large contribution from the so-called "bent-arm" configuration (obtuse triangle). This is an indication that the second 2^+ state is indeed a rotational excitation of the Hoyle state. However, one has to be aware that such "pictorials" of the wave function are resolution dependent; that means for a finer lattice spacing one will be able to resolve these structures in more detail. The charge radii, quadrupole moments, and electromagnetic transitions among the low-lying even-parity states of ^{12}C have also been calculated at LO. These results tend to be on the low side of the experimental values. This can be traced back to the fact that at LO, the charge radius comes out about 10% too small. If one scales the corresponding moments and transition elements with appropriate powers of $r(0_1^+)^{\mathrm{exp}}/r(0_1^+)^{\mathrm{LO}}$, the agreement is quite satisfactory. Of course, this needs to be backed up in the future by higher-order calculations of these observables.

Before elaborating on the structure of heavier nuclei, it is important to scrutinize the NNLO forces. This was done by Lähde *et al.* (2014), where it was shown that for α-cluster nuclei beyond $A = 12$ an overbinding appears that grows with the atomic number; cf. Table IV. This was also observed in other *ab initio* approaches using soft interactions (Roth *et al.*, 2011; Hagen *et al.*, 2012; Jurgenson *et al.*, 2013).[6] Lähde *et al.* (2014) overcame this problem by adding an effective repulsive four-nucleon force, whose strength was determined from the ground-state energy of ^{24}Mg. As one can see from Table IV, including this, one achieves a good description of the ground-state energies of all α-cluster nuclei up to ^{28}Si. Another method to overcome this deficiency is discussed in Sec. VIII.D.3.

The even-parity spectrum and structure of ^{16}O was discussed by Epelbaum *et al.* (2014). The ground state has $J^\pi = 0^+$ and its energy is within 3% of the empirical value; cf. Table IV. One finds a second 0^+ state at $-123(2)$ MeV and the first 2^+ state at the same energy. This is consistent with the empirical values $E(0_2^+) = -121.57$ and $E(2_1^+) = -120.70$ MeV. By measuring four-nucleon correlations, one finds that the dominant cluster configuration on the lattice is the tetrahedron [see Fig. 26 (left)], while the excited states have a strong overlap with the planar-type configurations also shown in Fig. 26 (right).

This implies that the first 2^+ state is a rotational excitation of the first excited 0^+. As in the case of ^{12}C, the charge radius of the ground state comes out too small, we get $r(0_1^+)^{\mathrm{LO}} = 2.3(1)$ fm, while the empirical value is 2.710(15) fm. This again is due to the overbinding at LO. If one rescales as described, one finds that the predictions for the $E2$ and

[6]We note that the NNLO$_{\mathrm{sat}}$ interaction in Ekström *et al.* (2015) is a soft interaction that does not overbind medium-mass nuclei, and thus there are other aspects of the interactions that also come into play.

$E0$ transitions are in good agreement with the experimental values. In particular, NLEFT is able to explain the empirical value of $B(E2, 2_1^+ \to 0_2^+)$, which is ≃30 times larger than the Weisskopf single-particle shell-model estimate. This provides further confirmation of the interpretation of the 2_1^+ state as a rotational excitation of the 0_2^+ state. Again, more detailed higher calculations of the electromagnetic response of ^{16}O within NLEFT are needed.

2. *Ab initio* alpha-alpha scattering

Although there has been impressive progress in *ab initio* calculations of nuclear scattering and reactions in the last years (Nollett *et al.*, 2007; Navrátil, Roth, and Quaglioni, 2010; Hagen and Michel, 2012; Navrátil and Quaglioni, 2012; Orlandini *et al.*, 2014), the aforementioned computational limits did so far not allow one to consider astrophysically relevant reactions such elastic α-α, α-^{12}C, or ^{12}C-^{12}C scattering. A major step forward in this direction was reported by Elhatisari *et al.* (2015). There the first *ab initio* calculation of α-α scattering based on chiral EFT and using the lattice formulation was discussed. It is based on the same NNLO chiral Hamiltonian that was used for the analysis of ^{12}C and ^{16}O that means all parameters were determined before. Using the APM, the S- and D-wave scattering phase shifts could be calculated as shown in Fig. 27. For more details on the actual computations, see Elhatisari *et al.* (2015). In the chiral counting employed, the Coulomb interactions appear only at NLO, and therefore the LO curves deviate significantly from the data. However, already at NLO one finds a good description of the S wave and a fair description for the D wave. While the NNLO corrections in the S wave are very small, these corrections bring the D wave close to the data, although there is still some room for improvement. The observed energy of the S-wave resonance is 0.091 84 MeV above threshold. For the lattice results, the ground state is found at 0.79(9) MeV below threshold at LO, and 0.11(1) MeV below threshold at both NLO and NNLO. The D-wave resonance is located at $E_R = 2.92(18)$ MeV and $\Gamma = 1.34(50)$ MeV (Afzal, Ahmad, and Ali, 1969), but there is some model dependence as discussed by Elhatisari *et al.* (2015). In NLEFT, one finds at NNLO $E_R = 3.27(12)$ MeV and $\Gamma = 2.09(16)$ MeV. This calculation can be considered a benchmark for *ab initio* calculations of nuclear scattering processes. Clearly, it needs to be refined by going to higher orders and also working with finer lattices. However, arguably the most significant finding of this investigation is the fact that the computing time scales approximately quadratically with the number of nucleons involved. Therefore, the computation of the "holy grail" of nuclear astrophysics (Fowler, 1984), namely, the reaction $\alpha + ^{12}\mathrm{C} \to ^{16}\mathrm{O} + \gamma$ at stellar energies, is in reach.

3. Nuclear binding near a quantum phase transition

We had already seen that the NNLO forces overbind in larger nuclei, so higher-order calculations will be needed and eventually higher-body forces might be required. Elhatisari *et al.* (2016) combined two ideas to give further insight into how nuclei are formed and what role α clustering plays. First, the nonlocal smearing already discussed in Sec. VIII.B was utilized to construct two new LO interactions, motivated by the hope that the smearing would further suppress the sign oscillations. Second, it was speculated that determining the LECs from also fitting to data from nucleus-nucleus scattering might make the troublesome higher-order corrections small. To quantify these ideas, two different LO interactions were constructed. More precisely, interaction A consists of nonlocal short-range interactions and one-pion exchange, supplemented by the Coulomb interaction. Interaction B has in addition local short-distance interactions. Second, while interaction A was entirely determined by a fit to np scattering data and the deuteron binding energy, interaction B was in addition tuned to the S-wave α-α phase shifts. The resulting ground-state energies for ^{3}H, ^{3}He, ^{4}He, and α-cluster nuclei are given in Table V. While the results up to ^{8}Be are similar,

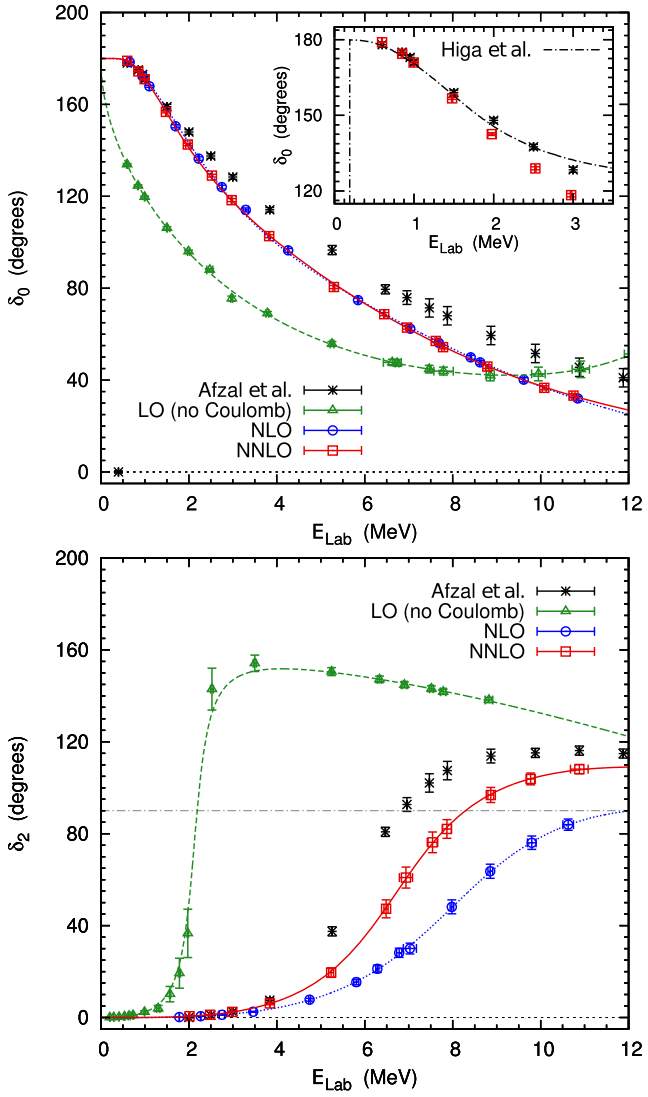

FIG. 27. Top panel: S-wave phase shifts for α-α scattering at LO, NLO, and NNLO. Inset: The calculation based on an EFT with pointlike α particles is shown. From Higa, Hammer, and van Kolck, 2008. Bottom panel: D-wave phase shifts at LO, NLO, and NNLO. From Heydenburg and Temmer, 1956, Nilson *et al.*, 1958, and Afzal, Ahmad, and Ali, 1969).

TABLE V. Ground-state energies of various nuclei for interactions A and B. Shown are results for LO and LO + C(oulomb). All energies are in units of MeV.

Nucleus	A (LO)	B (LO)	A (LO + C)	B (LO + C)
^{3}H	−7.82(5)	−7.78(12)	−7.82(5)	−7.78(12)
^{3}He	−7.82(5)	−7.78(12)	−7.08(5)	−7.09(12)
^{4}He	−29.36(4)	−29.19(6)	−28.62(4)	−28.45(6)
^{8}Be	−58.61(14)	−59.73(6)	−56.51(14)	−57.29(7)
^{12}C	−88.2(3)	−95.0(5)	−84.0(3)	−89.9(5)
^{16}O	−117.5(6)	−135.4(7)	−110.5(6)	−126.0(7)
^{20}Ne	−148(1)	−178(1)	−137(1)	−164(1)

interaction A fails to describe the heavier nuclei, quite in contrast to interaction B, which gives an amazingly good description. From this one concludes that α-α scattering is quite sensitive to the degree of locality of the nucleon-nucleon lattice interactions. This can be understood from the compactness of the α-particle wave function as explained in more detail by Elhatisari *et al.* (2016). From Table V one further reads off that in the absence of Coulomb interactions, the binding energy for a nucleus made of N α particles is almost exactly N times the α energy for interaction A, that is, it describes a Bose-condensed gas of particles. These observations allow one to draw interesting conclusions about the many-body limit with the Coulomb interactions switched off. Then, one can define a one-parameter family of interactions via $V_\lambda = (1-\lambda)V_{\rm A} + \lambda V_{\rm B}$. While the properties of the two-, three-, and four-nucleon systems vary only slightly with λ, the many-body ground state of V_λ undergoes a quantum phase transition from a Bose-condensed gas to a nuclear liquid. The corresponding zero-temperature phase diagram is sketched in Fig. 28. The phase transition occurs when the α-α S-wave scattering length $a_{\alpha\alpha}$ crosses zero, and the Bose gas collapses due to the attractive interactions (Stoof, 1994; Kagan, Muryshev, and Shlyapnikov, 1998). At slightly larger λ, finite α-type nuclei also become bound, starting with the largest nuclei first. The last α-like nucleus to be bound is ^{8}Be in the so-called unitarity limit $|a_{\alpha\alpha}| = \infty$. Superimposed on the phase diagram, the α-like nuclear ground-state energies E_A for A nucleons up to $A = 20$ relative to the corresponding multi-alpha threshold $E_\alpha A/4$ are also depicted. This shows that varying λ, one can move any α-cluster state up and down with respect to the α separation thresholds. This can be used as a new window to view the structure of these exotic nuclear states. In particular, this allows one to continuously connect the Hoyle state wave function without Coulomb interactions

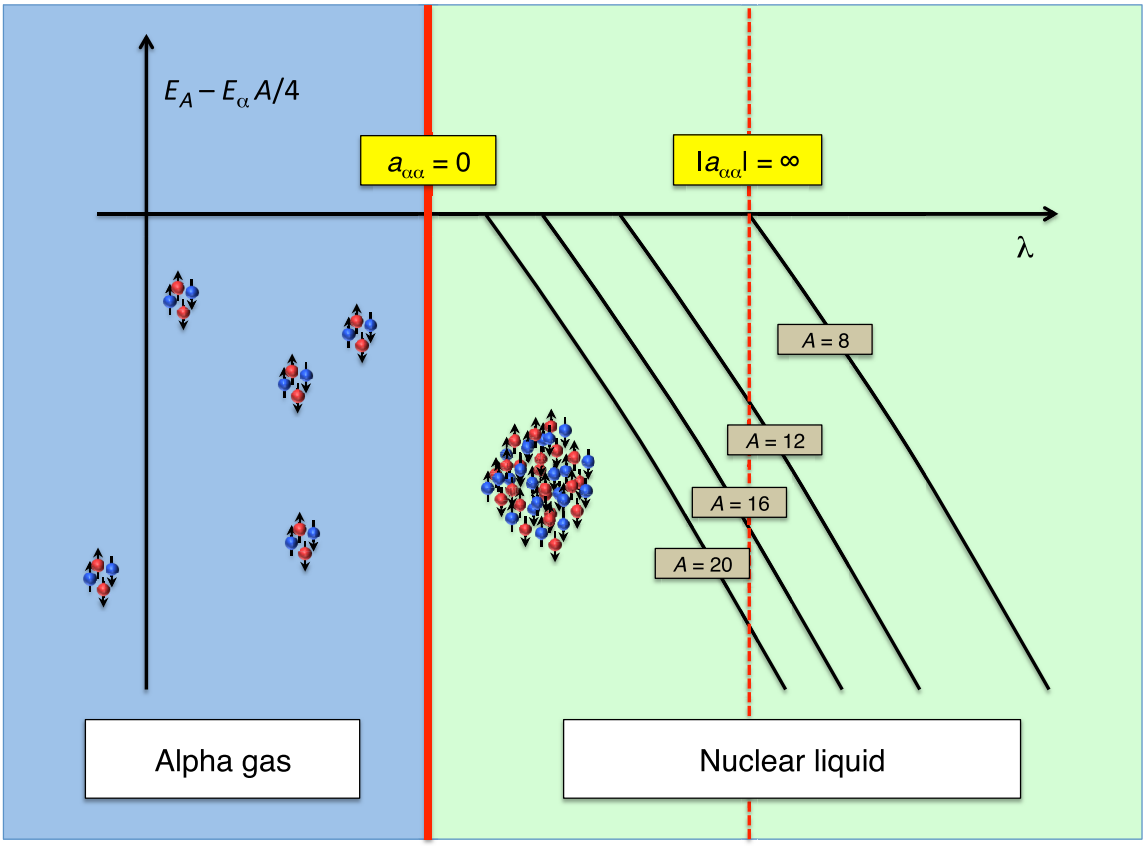

FIG. 28. Zero-temperature phase diagram as a function of the parameter λ in the strong interaction $V_\lambda = (1-\lambda)V_{\rm A} + \lambda V_{\rm B}$. A first-order quantum phase transition from a Bose gas to a nuclear liquid at the point appears where the scattering length $a_{\alpha\alpha}$ crosses zero. This is very close to the value $\lambda = 0$. Also shown are the α-like nuclear ground-state energies E_A for A nucleons up to $A = 20$ relative to the corresponding multi-alpha threshold $E_\alpha A/4$. The last α-like nucleus to be bound is ^{8}Be at the unitarity point where $|a_{\alpha\alpha}| = \infty$. This unitarity point is very close to the value $\lambda = 1$.

to a universal Efimov trimer (Efimov, 1971; Braaten and Hammer, 2006; Kraemer *et al.*, 2006).

Another interesting system is the second 0^+ state of ^{16}O, which should be continuously connected to a universal Efimov tetramer (Kraemer *et al.*, 2006; Hammer and Platter, 2007; von Stecher, D'Incao, and Greene, 2009). In summary, the main findings of this work are that the α-α interaction is a key control parameter which determines whether the ground state of a many-nucleon system is a Bose-condensed gas of α particles or a nuclear liquid. The proximity of this first-order quantum phase transition may explain why seemingly similar nuclear interactions can produce very different results in *ab initio* nuclear structure calculations. These conclusions need to be solidified by more detailed higher-order calculations. Similar results were found by Ebran *et al.* (2012, 2013, 2014a, 2014b, 2015) using density functional methods.

One might ask what the dependence on λ means for future nuclear structure calculations for heavier systems using chiral effective field theory? It suggests that the order-by-order convergence of chiral effective field theory might benefit from some optimization of the forces and regulators used in the chiral interactions. This need for optimization may not be visible in few-nucleon observables until very high orders in chiral effective field theory. But the dependence on λ appears as a leading-order effect in the framework of cluster effective field theory for two low-energy α particles. This suggests that some acceleration of the convergence of chiral effective field theory in heavier systems might be possible by making links to cluster effective field theory.

4. Clustering in neutron-rich nuclei

In addition to the discussion of the quantum phase transition, another development by Elhatisari *et al.* (2016) was the use of nonlocal interactions to reduce sign oscillations in the lattice Monte Carlo simulations. This idea was utilized by Elhatisari *et al.* (2017) to perform lattice simulations of neutron-rich nuclei. While this work considered interactions only at leading order in chiral effective field theory, the ground-state energies of the hydrogen, helium, beryllium, carbon, and oxygen isotopes could be reproduced with an accuracy of 0.7 MeV per nucleon or less with only three adjustable parameters.

Elhatisari *et al.* (2017) introduced a new model-independent method for measuring clustering in nuclei using localized three- and four-nucleon operators. Let $\rho(\mathbf{n})$ be the total nucleon density operator on lattice site $\mathbf{n}$. ρ_3 is defined as the expectation value of $:\rho^3(\mathbf{n})/3!:$ summed over $\mathbf{n}$, where the $::$ symbols denote normal ordering where all annihilation operators are moved to the right and all creation operators are moved to the left. Similarly ρ_4 is defined as the expectation value of $:\rho^4(\mathbf{n})/4!:$ summed over $\mathbf{n}$.

Although the expectation values ρ_3 and ρ_4 depend on the manner in which short-distance physics is regularized, the leading part of this dependence is an overall factor which does not depend on the nucleus being considered. So if $\rho_{3,\alpha}$ and $\rho_{4,\alpha}$ are the corresponding values for the α particle, then the ratios $\rho_3/\rho_{3,\alpha}$ and $\rho_4/\rho_{4,\alpha}$ are free from short-distance divergences and are model-independent quantities up to contributions from higher-dimensional operators in an operator product expansion. Elhatisari *et al.* (2017) computed the quantities $\rho_3/\rho_{3,\alpha}$ and $\rho_4/\rho_{4,\alpha}$ and quantified the amount of α clustering in the helium, beryllium, carbon, and oxygen isotopes in a model-independent manner. It was observed that these ratios $\rho_3/\rho_{3,\alpha}$ and $\rho_4/\rho_{4,\alpha}$ could be used to probe the shape of the α clusters as well as the amount of quantum entanglement of nucleons from different α clusters.

Another development by Elhatisari *et al.* (2017) was the determination of α-cluster correlations in the carbon isotopes ^{12}C, ^{14}C, and ^{16}C by measuring density correlations among the three spin-up protons. This approach relies on the fact that, on average, there is only one spin-up proton within each α cluster. The similarities among the ^{12}C, ^{14}C, and ^{16}C α-cluster geometries suggest that there should be α-cluster states in ^{14}C and ^{16}C that are analogs of the α-cluster states in ^{12}C. For example, the bound 0_2^+ state at 6.59 MeV above the ground state of ^{14}C could be a bound-state analog to the Hoyle state resonance in ^{12}C.

IX. SUMMARY AND OUTLOOK

We have presented a review on the current status and understanding of microscopic clustering in nuclei. We began with a history of the field and then discussed recent experimental results on α-conjugate nuclei, molecular structures in neutron-rich nuclei, and constraints for *ab initio* theory. There has been impressive progress in recent years clarifying clustering phenomena in ^{8,9,10}Be, ^{10,12,13,14}C, ^{16}O, and several other nuclei. However, many more precision measurements are needed, and these will provide vital benchmarks for first principles calculations. In addition to rotational bands, form factors, electromagnetic transition strengths, decays, and reaction cross sections, model-independent assessments of clustering such as ANCs are also very useful in making connections to *ab initio* theory.

There are also new opportunities for discovery in exploring clustering phenomena over a wide range of nuclear systems, from light to heavy nuclei and from the proton drip line to the neutron drip line. One of the fundamental questions of the field is understanding how prevalent nuclear clustering is across the nuclear chart. This includes systems where clustering is more subtly expressed and mixed with other effects such as particle-hole excitations. Having a large empirical database of nuclear phenomena will shed light on the control parameters for nuclear cluster formation and stability.

On the theoretical side we discussed methods used to study microscopic clustering. We reviewed the resonating group and generator coordinate methods, antisymmetrized molecular dynamics, fermionic molecular dynamics, Tohsaki-Horiuchi-Schuck-Röpke wave function and container models, no-core shell model, continuum quantum Monte Carlo methods, and lattice effective field theory.

While there have been many significant advances in the past decade, the field of microscopic nuclear clustering theory is now just entering the era of precision calculations. The future holds many opportunities for improvement in theory, methods or algorithms, and analysis. With the rapid growth of *ab initio* nuclear theory in the past few years, one great challenge for the field is to describe nuclear clustering from first principles with controlled systematic errors. This is no easy task as

recent studies have found that the interactions between nuclear clusters are very sensitive to details of the nuclear forces.

One area where all theoretical groups may choose to invest time and effort is on error quantification and the systematic reduction of errors. One question relevant to all groups is how results on nuclear clustering depend on the microscopic nuclear forces utilized. The follow-up question is how this difference can be systematically reduced by including the relevant missing physics. For lattice calculations another important question is to estimate and reduce the size of lattice discretization errors. For methods based on finite basis truncation or variational parameter optimization, a key question is the residual dependence on the choice of truncated space or variational ansatz. For continuum quantum Monte Carlo methods, the analogous question is the dependence on wave-function constraints and the trial wave function.

In addition to reproducing observed experimental data, another challenge for theoretical calculations is to compute model-independent observables that provide a quantitative measure of clustering and also serve as standard benchmarks for all different theoretical approaches. We have already mentioned ANCs for shallow bound states, but other model-independent observables could also be computed and defined for resonances as well.

We hope that our review captures some of the excitement of the growing and vibrant field of nuclear clustering. With many open questions and challenges still remaining, we anticipate fascinating new chapters to be written in the coming years.

ACKNOWLEDGMENTS

We acknowledge the work of our collaborators J. Alarcón, D. Du, S. Elhatisari, E. Epelbaum, Y. Funaki, N. Klein, H. Krebs, T. Lähde, N. Li, B. Lu, T. Luu, M. Lyu, Z. Ren, A. Rokash, G. Röpke, P. Schuck, A. Tohsaki, C. Xu, T. Yamada, and B. Zhou. We also acknowledge helpful discussions with K. Launey, P. Navrátil, W. Nazarewicz, T. Neff, and S. Pieper. Partial financial support was provided by the JSPS KAKENHI Grants No. 26400270 and No. JP16K05351, the Deutsche Forschungsgemeinschaft (Sino-German CRC 110), the Helmholtz Association (Contract No. VH-VI-417), the BMBF (Grant No. 05P15PCFN1), the U.S. Department of Energy (No. DE-FG02-03ER41260), VolkswagenStiftung (Grant No. 93562), and the Chinese Academy of Sciences (CAS) President's International Fellowship Initiative (PIFI) Grant No. 2017VMA0025. Computing resources were provided by the Jülich Supercomputing Centre at Forschungszentrum Jülich and RWTH Aachen.

REFERENCES

Abe, T., P. Maris, T. Otsuka, N. Shimizu, Y. Utsuno, and J. P. Vary, 2012, "Benchmarks of the full configuration interaction, Monte Carlo shell model, and no-core full configuration methods," Phys. Rev. C **86**, 054301.

Afzal, S. A., A. A. Z. Ahmad, and S. Ali, 1969, "Systematic survey of the α-α interaction," Rev. Mod. Phys. **41**, 247–273.

Ajzenberg-Selove, F., 1990, "Energy levels of light nuclei A=11-12," Nucl. Phys. A **506**, 1–158.

Akaishi, Y., S. A. Chin, H. Horiuchi, and K. Ikeda, 1986, *Cluster Models and Other Topics, International Review of Nuclear Physics* (World Scientific, Singapore), Vol. 4.

Alarcón, Jose Manuel, Dechuan Du, Nico Klein, Timo A. Lähde, Dean Lee, Ning Li, Bing-Nan Lu, Thomas Luu, and Ulf-G. Meißner, 2017, "Neutron-proton scattering at next-to-next-to-leading order in Nuclear Lattice Effective Field Theory," Eur. Phys. J. A **53**, 83.

Alhassid, Y., D. J. Dean, S. E. Koonin, G. Lang, and W. E. Ormand, 1994, "Practical solution to the Monte Carlo sign problem: Realistic calculations of Fe-54," Phys. Rev. Lett. **72**, 613–616.

Ali, S., and A. R. Bodmer, 1966, "Phenomenological α-α potentials," Nucl. Phys. **80**, 99.

Allton, C. R., *et al.* (UKQCD Collaboration), 1993, "Gauge invariant smearing and matrix correlators using Wilson fermions at Beta=6.2," Phys. Rev. D **47**, 5128–5137.

Ames, Lawrence L., 1982, "Natural parity levels in O-16," Phys. Rev. C **25**, 729–755.

Ando, T., K. Ikeda, and A. Tohsaki-Suzuki, 1980, "Nucleus-Nucleus interaction and nuclear saturation property—Microscopic study of O-16 + O-16 interaction by new effective nuclear-force," Prog. Theor. Phys. **64**, 1608–1626.

Angeli, I., and K. P. Marinova, 2013, "Table of experimental nuclear ground state charge radii: An update," At. Data Nucl. Data Tables **99**, 69–95.

Arai, K., Y. Suzuki, and R. G. Lovas, 1999, "Structure of He-6 with an extended three-cluster model," Phys. Rev. C **59**, 1432–1439.

Arai, Koji, 2004, "Structure of the excited states of Be-10 in a microscopic cluster model," Phys. Rev. C **69**, 014309.

Arai, Koji, Yoko Ogawa, Yasuyuki Suzuki, and Klmn Varga, 2001, "Microscopic multicluster description of light exotic nuclei with stochastic variational method on correlated gaussians," Prog. Theor. Phys. Suppl. **142**, 97–156.

Artemenkov, D. A., K. Z. Mamatkulov, S. P. Kharlamov, A. A. Zaitsev, and P. I. Zarubin, 2017, "Recent Findings in Relativistic Dissociation of ^{10}B and ^{12}C Nuclei," Few-Body Syst. **58**, 89.

Avila, M. L., G. V. Rogachev, E. Koshchiy, L. T. Baby, J. Belarge, K. W. Kemper, A. N. Kuchera, A. M. Mukhamedzhanov, D. Santiago-Gonzalez, and E. Uberseder, 2015, "Constraining the 6.05 MeV 0^+ and 6.13 MeV 3^- cascade transitions in the $^{12}C(\alpha,\gamma)^{16}O$ reaction using the Asymptotic Normalization Coefficients," Phys. Rev. Lett. **114**, 071101.

Barker, F. C., and P. B. Treacy, 1962, "Nuclear levels near thresholds," Nucl. Phys. **38**, 33–49.

Baroni, Simone, Petr Navrátil, and Sofia Quaglioni, 2013, "Unified ab initio approach to bound and unbound states: no-core shell model with continuum and its application to ^{7}He," Phys. Rev. C **87**, 034326.

Barrett, Bruce R., Petr Navrátil, and James P. Vary, 2013, "Ab initio no core shell model," Prog. Part. Nucl. Phys. **69**, 131–181.

Bauhoff, W., E. Caurier, B. Grammaticos, and M. Ploszajczak, 1985, "Description of light-ion collisions in the time-dependent cluster model," Phys. Rev. C **32**, 1915–1926.

Bauhoff, W., H. Schultheis, and R. Schultheis, 1984, "Alpha cluster model and the spectrum of O-16," Phys. Rev. C **29**, 1046–1055.

Bayman, B. F., and A. Bohr, 1958, "On the connection between the cluster model and the su3 coupling scheme for particles in a harmonic oscillator potential," Nucl. Phys. **9**, 596–599.

Beane, S. R., *et al.* (NPLQCD Collaboration), 2013, "Nucleon-Nucleon Scattering Parameters in the Limit of SU(3) Flavor Symmetry," Phys. Rev. C **88**, 024003.

Beane, Silas R., and Martin J. Savage, 2003a, "The Quark mass dependence of two nucleon systems," Nucl. Phys. A **717**, 91–103.
Beane, Silas R., and Martin J. Savage, 2003b, "Variation of fundamental couplings and nuclear forces," Nucl. Phys. A **713**, 148–164.
Beck, C., 2010, Ed., *Clusters in Nuclei*, Lecture Notes in Physics, Vol. 1 (Springer-Verlag, Berlin).
Beck, C., 2012, Ed., *Clusters in Nuclei*, Lecture Notes in Physics, Vol. 2 (Springer-Verlag, Berlin).
Beck, C., 2014, Ed., *Clusters in Nuclei*, Lecture Notes in Physics, Vol. 3 (Springer-Verlag, Berlin).
Bedaque, P. F., H. W. Hammer, and U. van Kolck, 2003, "Narrow resonances in effective field theory," Phys. Lett. B **569**, 159–167.
Bedaque, Paulo F., Thomas Luu, and Lucas Platter, 2011, "Quark mass variation constraints from Big Bang nucleosynthesis," Phys. Rev. C **83**, 045803.
Berengut, J. C., E. Epelbaum, V. V. Flambaum, C. Hanhart, U.-G. Meißner, J. Nebreda, and J. R. Pelaez, 2013, "Varying the light quark mass: impact on the nuclear force and Big Bang nucleosynthesis," Phys. Rev. D **87**, 085018.
Berger, J. F., M. Girod, and D. Gogny, 1991, "Time-dependent quantum collective dynamics applied to nuclear fission," Comput. Phys. Commun. **63**, 365–374.
Bernard, Véronique, Michael Lage, Ulf-G. Meißner, and Akaki Rusetsky, **2008**, "Resonance properties from the finite-volume energy spectrum," J. High Energy Phys. 08, 024.
Bertulani, C. A., H. W. Hammer, and U. Van Kolck, 2002, "Effective field theory for halo nuclei," Nucl. Phys. A **712**, 37–58.
Bijker, R., 2015, Lectures notes from IX Escuela Mexicana de Fisica Nuclear, Mexico, Distrito Federal (unpublished).
Bijker, R., and F. Iachello, 2002, "The Algebraic cluster model: Three body clusters," Ann. Phys. (Amsterdam) **298**, 334–360.
Bijker, R., and F. Iachello, 2014, "Evidence for Tetrahedral Symmetry in O16," Phys. Rev. Lett. **112**, 152501.
Borasoy, Bugra, Evgeny Epelbaum, Hermann Krebs, Dean Lee, and Ulf-G. Meißner, 2007a, "Lattice simulations for light nuclei: Chiral effective field theory at leading order," Eur. Phys. J. A **31**, 105–123.
Borasoy, Bugra, Evgeny Epelbaum, Hermann Krebs, Dean Lee, and Ulf-G. Meißner, 2007b, "Two-particle scattering on the lattice: Phase shifts, spin- orbit coupling, and mixing angles," Eur. Phys. J. A **34**, 185–196.
Bour, Shahin, Sebastian König, Dean Lee, H.-W. Hammer, and Ulf-G. Meißner, 2011, "Topological phases for bound states moving in a finite volume," Phys. Rev. D **84**, 091503.
Braaten, Eric, and H. W. Hammer, 2006, "Universality in few-body systems with large scattering length," Phys. Rep. **428**, 259–390.
Briceno, Raul A., Zohreh Davoudi, Thomas Luu, and Martin J. Savage, 2013, "Two-nucleon systems in a finite volume. II. $^3S_1 - {}^3D_1$ coupled channels and the deuteron," Phys. Rev. D **88**, 114507.
Brink, D. M., 1966, "Alpha cluster model," in *Proceedings of the International School of Physics Enrico Fermi, Varenna Course 36* (Academic Press, New York), p. 247.
Brink, D. M., 2008, "History of cluster structure in nuclei," J. Phys. Conf. Ser. **111**, 012001.
Brink, D. M., and E. Boeker, 1967, "Effective interactions for Hartree-Fock calculations," Nucl. Phys. A **91**, 1–26.
Brochard, F., P. Chevallier, D. Disdier, V. Rauch, G. Rudolf, and F. Scheibling, 1976, "C-12 (alpha, Be-8) Be-8 reaction in the energy range Ealpha=17–33 MeV," Phys. Rev. C **13**, 967–975.
Broniowski, Wojciech, and Enrique Ruiz Arriola, 2014, "Signatures of α Clustering in Light Nuclei from Relativistic Nuclear Collisions," Phys. Rev. Lett. **112**, 112501.
Calle Cordon, A., and E. Ruiz Arriola, 2008, "Wigner symmetry, Large N(c) and Renormalized One Boson Exchange Potential," Phys. Rev. C **78**, 054002.
Carlson, J., S. Gandolfi, F. Pederiva, Steven C. Pieper, R. Schiavilla, K. E. Schmidt, and R. B. Wiringa, 2015, "Quantum Monte Carlo methods for nuclear physics," Rev. Mod. Phys. **87**, 1067.
Carlson, J., V. R. Pandharipande, and R. B. Wiringa, 1984, "Variational calculations of resonant states in 4He," Nucl. Phys. A **424**, 47–59.
Caurier, E., B. Grammaticos, and T. Sami, 1982, "The time dependent cluster model," Phys. Lett. B **109**, 150–154.
Ceperley, D., G. V. Chester, and M. H. Kalos, 1977, "Monte carlo simulation of a many-fermion study," Phys. Rev. B **16**, 3081–3099.
Cerny, J., 1974, *Nuclear Spectroscopy and Reactions. Part B*, Pure and Applied Physics, Vol. 40-B (Academic Press, New York).
Charity, R. J., *et al.*, 2015, "Spin alignment of excited projectiles due to target spin-flip interactions," Phys. Rev. C **91**, 024610.
Chen, Jiunn-Wei, Dean Lee, and Thomas Schäfer, 2004, "Inequalities for Light Nuclei in the Wigner Symmetry Limit," Phys. Rev. Lett. **93**, 242302.
Chernykh, M., H. Feldmeier, T. Neff, P. von Neumann-Cosel, and A. Richter, 2007, "Structure of the Hoyle State in C-12," Phys. Rev. Lett. **98**, 032501.
Chernykh, M., H. Feldmeier, T. Neff, P. von Neumann-Cosel, and A. Richter, 2010, "Pair decay width of the Hoyle state and carbon production in stars," Phys. Rev. Lett. **105**, 022501.
Chevallier, P., F. Scheibling, G. Goldring, I. Plesser, and M. W. Sachs, 1967, "Breakup of O-16 into Be-8 + Be-8," Phys. Rev. **160**, 827–834.
Chiba, Y., and M. Kimura, 2015, "Cluster states and isoscalar monopole transitions of ^{24}Mg," Phys. Rev. C **91**, 061302.
Chiba, Y., M. Kimura, and Y. Taniguchi, 2016, "Isoscalar dipole transition as a probe for asymmetric clustering," Phys. Rev. C **93**, 034319.
Clark, J. W., and T.-P. Wang, 1966, "Theory of alpha matter," Ann. Phys. (N.Y.) **40**, 127.
Cook, C., W. A. Fowler, C. C. Lauritsen, and T. Lauritsen, 1957, Phys. Rev. **107**, 508.
Cseh, J., 1992, "Semimicroscopic algebraic description of nuclear cluster states. Vibron model coupled to the SU(3) shell model," Phys. Lett. B **281**, 173–177.
Cseh, J., 2014, "On the intersection of the shell, collective and cluster models of atomic nuclei I: Multi-shell excitations," arXiv:1404.3500.
Curtis, N., *et al.*, 2013, "Investigation of the 4-alpha linear chain state in 16O," Phys. Rev. C **88**, 064309.
Curtis, N., *et al.*, 2016, "Be8+Be8 and C12+ breakup states in O16 populated via the C13(He4,4)n reaction," Phys. Rev. C **94**, 034313.
Daniel, David, Rajan Gupta, Gregory W. Kilcup, Apoorva Patel, and Stephen R. Sharpe, 1992, "Phenomenology with Wilson fermions using smeared sources," Phys. Rev. D **46**, 3130–3145.
Danilov, A. N., T. L. Belyaeva, A. S. Demyanova, S. A. Goncharov, and A. A Ogloblin, 2009, "Determination of nuclear radii for unstable states in C-12 with diffraction inelastic scattering," Phys. Rev. C **80**, 054603.
Datar, V. M., *et al.*, 2013, "Electromagnetic Transition from the 4+ to 2+ Resonance in Be8 Measured via the Radiative Capture in He4+He4," Phys. Rev. Lett. **111**, 062502.
Dell'Aquila, D., *et al.*, 2017, "High-precision probe of the fully sequential decay width of the Hoyle state in 12C," Phys. Rev. Lett. **119**, 132501.

Dennison, David M., 1940, "Excited States of the O-16 Nucleus," Phys. Rev. **57**, 454.
Dennison, David M., 1954, "Energy Levels of the O-16 Nucleus," Phys. Rev. **96**, 378–380.
Descouvemont, P., 1995, "Halo structure of Be-14 in a microscopic Be-12 + n+n cluster model," Phys. Rev. C **52**, 704–710.
Descouvemont, P., 1997, "Simultaneous study of the 11 Li and 10 Li nuclei in a microscopic cluster model," Nucl. Phys. A **626**, 647–668.
Descouvemont, P., 2002, "Microscopic study of α clustering in the 9,10,11 Be isotopes," Nucl. Phys. A **699**, 463–478.
Descouvemont, P., and D. Baye, 1987, "Microscopic theory of the Be-8 (alpha, gamma) C-12 reaction in a three-cluster model," Phys. Rev. C **36**, 54–59.
Descouvemont, P., and D. Baye, 2001, "12 Be molecular states in a microscopic cluster model," Phys. Lett. B **505**, 71–74.
Descouvemont, P., and D. Baye, 2010, "The R-matrix theory," Rep. Prog. Phys. **73**, 036301.
Dohet-Eraly, Jérémy, Petr Navrátil, Sofia Quaglioni, Wataru Horiuchi, Guillaume Hupin, and Francesco Raimondi, 2016, "^{3}He$(\alpha,\gamma)^7$Be and ^{3}H$(\alpha,\gamma)^7$Li astrophysical S factors from the no-core shell model with continuum," Phys. Lett. B **757**, 430–436.
Draayer, J. P., T. Dytrych, and K. D. Launey, 2011, "Ab initio symmetry-adapted no-core shell model," J. Phys. Conf. Ser. **322**, 012001.
Draayer, J. P., and G. Rosensteel, 1983, "Major shell centroids in the symplectic collective model," Phys. Lett. B **125**, 237–239.
Dreyfuss, A. C., K. D. Launey, T. Dytrych, J. P. Draayer, R. B. Baker, C. M. Deibel, and C. Bahri, 2016, "Understanding emergent collectivity and clustering in nuclei from a symmetry-based no-core shell-model perspective," arXiv:1611.00060.
Dreyfuss, Alison C., Kristina D. Launey, Tomas Dytrych, Jerry P. Draayer, and Chairul Bahri, 2013, "Hoyle state and rotational features in Carbon-12 within a no-core shell model framework," Phys. Lett. B **727**, 511–515.
Drozdz, S., J. Okolowicz, and M. Ploszajczak, 1982, "The time-dependent cluster theory application to the - collision," Phys. Lett. B **109**, 145–149.
Dufour, M., P. Descouvemont, and F. Nowacki, 2010, "Microscopic investigation of the 12 Be spectroscopy," Nucl. Phys. A **836**, 242–255.
Dytrych, T., K. D. Launey, J. P. Draayer, P. Maris, J. P. Vary, E. Saule, U. Catalyurek, M. Sosonkina, D. Langr, and M. A. Caprio, 2013, "Collective Modes in Light Nuclei from First Principles," Phys. Rev. Lett. **111**, 252501.
Dytrych, Tomas, Kristina D. Sviratcheva, Chairul Bahri, Jerry P. Draayer, and James P. Vary, 2007, "Evidence for symplectic symmetry in Ab initio no-core shell model results for light nuclei," Phys. Rev. Lett. **98**, 162503.
Ebran, J. P., E. Khan, T. Niksic, and D. Vretenar, 2012, "How atomic nuclei cluster," Nature (London) **487**, 341–344.
Ebran, J. P., E. Khan, T. Niksic, and D. Vretenar, 2013, "Localization and clustering in the nuclear Fermi liquid," Phys. Rev. C **87**, 044307.
Ebran, J.-P., E. Khan, T. Niksic, and D. Vretenar, 2014a, "Density Functional Theory studies of cluster states in nuclei," Phys. Rev. C **90**, 054329.
Ebran, J.-P., E. Khan, T. Niksic, and D. Vretenar, 2014b, "Cluster-liquid transition in finite saturated fermionic systems," Phys. Rev. C **89**, 031303(R).
Ebran, J. P., E. Khan, T. Niksic, and D. Vretenar, 2015, "Nuclear clustering in the energy density functional approach," AIP Conf. Proc. **1681**, 020005.
Edwards, Robert G., Balint Joo, and Huey-Wen Lin, 2008, "Tuning for Three-flavors of Anisotropic Clover Fermions with Stout-link Smearing," Phys. Rev. D **78**, 054501.
Efimov, V. N., 1971, "Weakly-bound states of 3 resonantly-interacting particles," Sov. J. Nucl. Phys. **12**, 589.
Ekström, A., G. R. Jansen, K. A. Wendt, G. Hagen, T. Papenbrock, B. D. Carlsson, C. Forssén, M. Hjorth-Jensen, P. Navrátil, and W. Nazarewicz, 2015, "Accurate nuclear radii and binding energies from a chiral interaction," Phys. Rev. C **91**, 051301.
Elhatisari, Serdar, Evgeny Epelbaum, Hermann Krebs, Timo A. Lähde, Dean Lee, Ning Li, Bing-nan Lu, Ulf-G. Meißner, and Gautam Rupak, 2017, "Ab initio calculations of the isotopic dependence of nuclear clustering," Phys. Rev. Lett. **119**, 222505.
Elhatisari, Serdar, and Dean Lee, 2014, "Fermion-dimer scattering using an impurity lattice Monte Carlo approach and the adiabatic projection method," Phys. Rev. C **90**, 064001.
Elhatisari, Serdar, Dean Lee, Ulf-G. Meißner, and Gautam Rupak, 2016, "Nucleon-deuteron scattering using the adiabatic projection method," Eur. Phys. J. A **52**, 174.
Elhatisari, Serdar, Dean Lee, Gautam Rupak, Evgeny Epelbaum, Hermann Krebs, Timo A. Lähde, Thomas Luu, and Ulf-G. Meißner, 2015, "Ab initio alpha-alpha scattering," Nature (London) **528**, 111.
Elhatisari, Serdar, *et al.*, 2016, "Nuclear binding near a quantum phase transition," Phys. Rev. Lett. **117**, 132501.
Elliott, J. P., 1958a, "Collective motion in the nuclear shell model. 1. Classification schemes for states of mixed configuration," Proc. R. Soc. A **245**, 128.
Elliott, J. P., 1958b, "Collective motion in the nuclear shell model. 2. The Introduction of instrinsic wave functions," Proc. R. Soc. A **245**, 562–581.
Epelbaum, Evgeny, Hans-Werner Hammer, and Ulf-G. Meißner, 2009, "Modern Theory of Nuclear Forces," Rev. Mod. Phys. **81**, 1773.
Epelbaum, Evgeny, Hermann Krebs, Timo A. Lähde, Dean Lee, and Ulf-G. Meissner, 2012, "Structure and rotations of the Hoyle state," Phys. Rev. Lett. **109**, 252501.
Epelbaum, Evgeny, Hermann Krebs, Timo A. Lähde, Dean Lee, and Ulf-G. Meißner, 2013a, "Dependence of the triple-alpha process on the fundamental constants of nature," Eur. Phys. J. A **49**, 82.
Epelbaum, Evgeny, Hermann Krebs, Timo A. Lähde, Dean Lee, and Ulf-G. Meißner, 2013b, "Viability of Carbon-Based Life as a Function of the Light Quark Mass," Phys. Rev. Lett. **110**, 112502.
Epelbaum, Evgeny, Hermann Krebs, Timo A. Lähde, Dean Lee, Ulf-G. Meißner, and Gautam Rupak, 2014, "Ab initio calculation of the spectrum and structure of ^{16}O," Phys. Rev. Lett. **112**, 102501.
Epelbaum, Evgeny, Hermann Krebs, Dean Lee, and Ulf-G. Meißner, 2011, "Ab initio calculation of the Hoyle state," Phys. Rev. Lett. **106**, 192501.
Epelbaum, Evgeny, Ulf-G. Meißner, and Walter Glöckle, 2002, "Further comments on nuclear forces in the chiral limit," arXiv:nucl-th/0208040.
Epelbaum, Evgeny, Ulf-G. Meißner, and Walter Glöckle, 2003, "Nuclear forces in the chiral limit," Nucl. Phys. A **714**, 535–574.
Feldmeier, H., 1990, "Fermionic molecular dynamics," Nucl. Phys. A **515**, 147–172.
Feldmeier, H., K. Bieler, and J. Schnack, 1995, "Fermionic molecular dynamics for ground states and collisions of nuclei," Nucl. Phys. A **586**, 493–532.
Feldmeier, H., T. Neff, R. Roth, and J. Schnack, 1998, "A Unitary correlation operator method," Nucl. Phys. A **632**, 61–95.
Feldmeier, Hans, and Jurgen Schnack, 2000, "Molecular dynamics for fermions," Rev. Mod. Phys. **72**, 655–688.

Fliessbach, T., and H. Walliser, 1982, "The structure of the resonating group equation," Nucl. Phys. A **377**, 84–104.
Fossez, K., W. Nazarewicz, Y. Jaganathen, N. Michel, and M. Poszajczak, 2016, "Nuclear rotation in the continuum," Phys. Rev. C **93**, 011305.
Fowler, William A., 1984, "Experimental and theoretical nuclear astrophysics: the quest for the origin of the elements," Rev. Mod. Phys. **56**, 149–179.
Freer, M., and H. O. U. Fynbo, 2014, "The Hoyle state in ^{12}C," Prog. Part. Nucl. Phys. **78**, 1–23.
Freer, M., and A. C. Merchant, 1997, "Developments in the study of nuclear clustering in light even—even nuclei," J. Phys. G **23**, 261.
Freer, M., *et al.*, 1994, "Limits for the 3 alpha branching ratio of the decay of the 7.65 MeV, 02+ state in C-12," Phys. Rev. C **49**, R1751–R1754.
Freer, M., *et al.*, 2006, "$\alpha:2n:\alpha$ Molecular Band in Be^{10}," Phys. Rev. Lett. **96**, 042501.
Freer, M., *et al.*, 2007, "Reexamination of the excited states of C12," Phys. Rev. C **76**, 034320.
Freer, M., *et al.*, 2009, "2+ excitation of the C-12 Hoyle state," Phys. Rev. C **80**, 041303.
Freer, M., *et al.*, 2011, "Evidence for a new C-12 state at 13.3 MeV," Phys. Rev. C **83**, 034314.
Freer, M., *et al.*, 2012a, "Consistent analysis of the 2+ excitation of the C-12 Hoyle state populated in proton and alpha-particle inelastic scattering," Phys. Rev. C **86**, 034320.
Freer, M., *et al.*, 2012b, "Resonances in C^{11} observed in the $He^4(Be^7,\alpha)Be^7$ and $He^4(Be^7,\rho)B^{10}$ reactions," Phys. Rev. C **85**, 014304.
Freer, M., *et al.*, 2014, "Resonances in C^{14} observed in the $He^4(^{10}Be,\alpha)Be^{10}$ reaction," Phys. Rev. C **90**, 054324.
Freer, Martin, 2007, "The clustered nucleuscluster structures in stable and unstable nuclei," Rep. Prog. Phys. **70**, 2149.
Friedrich, H., and K. Langanke, 1975, "Description of elastic - 40 Ca scattering by the resonating group method," Nucl. Phys. A **252**, 47–61.
Fritsch, A., *et al.*, 2016, "One-dimensionality in atomic nuclei: A candidate for linear-chain alpha clustering in ^{14}C," Phys. Rev. C **93**, 014321.
Fujiwara, Y., *et al.*, 1980, "Chapter II. Comprehensive Study of Alpha-Nuclei," Prog. Theor. Phys. Suppl. **68**, 29.
Funaki, Y., 2015, "Hoyle band and α condensation in 12C," Phys. Rev. C **92**, 021302(R).
Funaki, Y., 2018, "Container evolution for cluster structures in ^{16}O," Phys. Rev. C **97**, 021304.
Funaki, Y., H. Horiuchi, and A. Tohsaki, 2015, "Cluster models from RGM to alpha condensation and beyond," Prog. Part. Nucl. Phys. **82**, 78–132.
Funaki, Y., H. Horiuchi, W. von Oertzen, G. Röpke, P. Schuck, A. Tohsaki, and T. Yamada, 2009, "Concepts of nuclear alpha-particle condensation," Phys. Rev. C **80**, 064326.
Funaki, Y., A. Tohsaki, H. Horiuchi, P. Schuck, and G. Röpke, 2003, "Analysis of previous microscopic calculations for second 0+ state in C-12 in terms of three alpha particle Bose condensed state," Phys. Rev. C **67**, 051306.
Funaki, Y., A. Tohsaki, H. Horiuchi, P. Schuck, and G. Röpke, 2006, "Inelastic form-factors to alpha particle condensate states in C-12 and O-16: What can we learn?," Eur. Phys. J. A **28**, 259–263.
Funaki, Y., T. Yamada, H. Horiuchi, G. Röpke, P. Schuck, and A. Tohsaki, 2008, "α-Particle Condensation in O 16 Studied with a Full Four-Body Orthogonality Condition Model Calculation," Phys. Rev. Lett. **101**, 082502.
Funaki, Y., T. Yamada, A. Tohsaki, H. Horiuchi, G. Röpke, and P. Schuck, 2010, "Microscopic study of 4-alpha-particle condensation with proper treatment of resonances," Phys. Rev. C **82**, 024312.
Furuta, T., K. H. O. Hasnaoui, F. Gulminelli, C. Leclercq, and A. Ono, 2010, "Monopole oscillations in light nuclei with a molecular dynamics approach," Phys. Rev. C **82**, 034307.
Fynbo, H. O. U., and M. Freer, 2011, "Viewpoint: Rotations of the Hoyle State in Carbon-12," Physics **4**, 94.
Gamow, G., 1928, "Zur quantentheorie des atomkernes," Z. Phys. **51**, 204.
Gandolfi, S., F. Pederiva, S. Fantoni, and K. E. Schmidt, 2007, "Auxiliary Field Diffusion Monte Carlo calculation of nuclei with $A \leq 40$ with tensor interactions," Phys. Rev. Lett. **99**, 022507.
Garrido, E., A. S. Jensen, and D. V. Fedorov, 2013, "Rotational bands in the continuum illustrated by ^{8}Be results," Phys. Rev. C **88**, 024001.
Garrido, E., A. S. Jensen, and D. V. Fedorov, 2016, "Rotational character of the 12C spectrum investigated through inelastic cross sections via photon emission," Eur. Phys. J. Web Conf. **113**, 06005.
Gazit, Doron, Sofia Quaglioni, and Petr Navrátil, 2009, "Three-Nucleon Low-Energy Constants from the Consistency of Interactions and Currents in Chiral Effective Field Theory," Phys. Rev. Lett. **103**, 102502.
Gezerlis, A., I. Tews, E. Epelbaum, S. Gandolfi, K. Hebeler, A. Nogga, and A. Schwenk, 2013, "Quantum Monte Carlo Calculations with Chiral Effective Field Theory Interactions," Phys. Rev. Lett. **111**, 032501.
Göckeler, M., R. Horsley, M. Lage, U.-G. Meißner, P. E. L. Rakow, A. Rusetsky, G. Schierholz, and J. M. Zanotti, 2012, "Scattering phases for meson and baryon resonances on general moving-frame lattices," Phys. Rev. D **86**, 094513.
Griffin, James J., and John A. Wheeler, 1957, "Collective Motions in Nuclei by the Method of Generator Coordinates," Phys. Rev. **108**, 311–327.
Gurney, R. W., and E. U. Condon, 1928, "Quantum mechanics and radioactive disintegration," Nature (London) **122**, 439.
Güsken, S., 1990, "A Study of smearing techniques for hadron correlation functions," Nucl. Phys. B, Proc. Suppl. **17**, 361–364.
Hafstad, L. R., and E. Teller, 1938, "The alpha-particle model of the nucleus," Phys. Rev. **54**, 681.
Hagen, G., M. Hjorth-Jensen, G. R. Jansen, R. Machleidt, and T. Papenbrock, 2012, "Evolution of shell structure in neutron-rich calcium isotopes," Phys. Rev. Lett. **109**, 032502.
Hagen, G., and N. Michel, 2012, "Elastic proton scattering of medium mass nuclei from coupled-cluster theory," Phys. Rev. C **86**, 021602.
Hammer, H. W., and L. Platter, 2007, "Universal Properties of the Four-Body System with Large Scattering Length," Eur. Phys. J. A **32**, 113–120.
Hasenfratz, Anna, Roland Hoffmann, and Stefan Schaefer, **2007**, "Hypercubic smeared links for dynamical fermions," J. High Energy Phys. 05, 029.
He, Song, Xu Feng, and Chuan Liu, 2005, "Two particle states and the s-matrix elements in multi- channel scattering," J. High Energy Phys. 07, 011.
Heydenburg, N. P., and G. M. Temmer, 1956, "Alpha-Alpha Scattering at Low Energies," Phys. Rev. **104**, 123–134.
Higa, R., H.-W. Hammer, and U. van Kolck, 2008, "Alpha-Alpha Scattering in Halo Effective Field Theory," Nucl. Phys. A **809**, 171–188.

Hill, David Lawrence, and John Archibald Wheeler, 1953, "Nuclear constitution and the interpretation of fission phenomena," Phys. Rev. **89**, 1102–1145.

Hoferichter, Martin, Jacobo Ruiz de Elvira, Bastian Kubis, and Ulf-G. Meißner, 2015, "Matching pion-nucleon Roy-Steiner equations to chiral perturbation theory," Phys. Rev. Lett. **115**, 192301.

Horikawa, Y., Y. Torizuka, A. Nakada, S. Mitsunobu, Y. Kojima, and M. Kimura, 1971, "The deformations in 20 Ne, 24 Mg and 28 Si from electron scattering," Phys. Lett. B **36**, 9–11.

Horiuchi, H., 1970, "Generator coordinate treatment of composite particle reaction and molecule-like structures," Prog. Theor. Phys. **43**, 375.

Horiuchi, H., 1974, "Three-Alpha Model of 12C: Orthogonality Condition Model as an Approximation of Resonating Group Treatment," Prog. Theor. Phys. **51**, 1266.

Horiuchi, H., and K. Ikeda, 1968, "A Molecule-like Structure in Atomic Nuclei of 16O* and 20Ne," Prog. Theor. Phys. **40**, 277.

Horiuchi, H., K. Ikeda, and K. Kato, 2012, "Recent developments in nuclear cluster physics," Prog. Theor. Phys. Suppl. **192**, 1.

Hoyle, F., 1954, "On Nuclear Reactions Occuring in Very Hot Stars. 1. The Synthesis of Elements from Carbon to Nickel," Astrophys. J. Suppl. Ser. **1**, 121–146.

Hupin, Guillaume, Sofia Quaglioni, and Petr Navrtil, 2015, "Unified description of ^{6}Li structure and deuterium-^{4}He dynamics with chiral two- and three-nucleon forces," Phys. Rev. Lett. **114**, 212502.

Hutzelmeyer, H., and H. H. Hackenbroich, 1970, "Carbon 12 as a nucleus of symmetry [444]," Z. Phys. A **232**, 356–362.

Ikeda, K., N. Tagikawa, and H. Horiuchi, 1968, "The Systematic Structure-Change into the Molecule-like Structures in the Self-Conjugate 4n Nuclei," Prog. Theor. Phys. Suppl. **E68**, 464.

Imai, N., *et al.*, 2009, "First lifetime measurement of 2+(1) state in Be-12," Phys. Lett. B **673**, 179–182.

Itagaki, N., H. Masui, M. Ito, and S. Aoyama, 2005, "Simplified modeling of cluster-shell competition," Phys. Rev. C **71**, 064307.

Itagaki, N., and S. Okabe, 2000, "Molecular orbital structures in Be-10," Phys. Rev. C **61**, 044306.

Itagaki, N., S. Okabe, K. Ikeda, and I. Tanihata, 2001, "Molecular orbital structure in neutron rich C isotopes," Phys. Rev. C **64**, 014301.

Ito, M., N. Itagaki, H. Sakurai, and K. Ikeda, 2008, "Coexistence of Covalent Superdeformation and Molecular Resonances in an Unbound Region of Be-12," Phys. Rev. Lett. **100**, 182502.

Ito, M., K. Kato, and K. Ikeda, 2004, "Application of the generalized two center cluster model to Be-10," Phys. Lett. B **588**, 43–48.

Ito, Makoto, and Kiyomi Ikeda, 2014, "Unified studies of chemical bonding structures and resonant scattering in light neutron-excess systems, 10,12 be," Rep. Prog. Phys. **77**, 096301.

Itoh, M., *et al.*, 2011, "Candidate for the 2+ excited Hoyle state at $E_x \sim 10$ MeV in C-12," Phys. Rev. C **84**, 054308.

Itoh, M., *et al.*, 2013, "Nature of 10 MeV state in 12C," J. Phys. Conf. Ser. **436**, 012006.

Itoh, M., *et al.*, 2014, "Further Improvement of the Upper Limit on the Direct 3 Decay from the Hoyle State in C12," Phys. Rev. Lett. **113**, 102501.

Iwasaki, H., *et al.*, 2000a, "Low-lying intruder 1^- state in ^{12}Be and the melting of the $N = 8$ shell closure," Phys. Lett. B **491**, 8–14.

Iwasaki, H., *et al.*, 2000b, "Quadrupole deformation of ^{12}Be studied by proton inelastic scattering," Phys. Lett. B **481**, 7–13.

John, Bency, Y. Tokimoto, Y. W. Lui, H. L. Clark, X. Chen, and D. H. Youngblood, 2003, "Isoscalar electric multipole strength in C-12," Phys. Rev. C **68**, 014305.

Jurgenson, E. D., P. Maris, R. J. Furnstahl, P. Navrátil, W. E. Ormand, and J. P. Vary, 2013, "Structure of p-shell nuclei using three-nucleon interactions evolved with the similarity renormalization group," Phys. Rev. C **87**, 054312.

Jyväskylä, 2013, "Evidence for a new rotational band based on the Hoyle state in 12C," Jyväskylä Accelerator News **21**, 3.

Kagan, Y., A. E. Muryshev, and G. V. Shlyapnikov, 1998, "Collapse and Bose-Einstein Condensation in a Trapped Bose Gas with Negative Scattering Length," Phys. Rev. Lett. **81**, 933–937.

Kalos, M. H., 1962, "Monte carlo calculations of the ground state of three- and four-body nuclei," Phys. Rev. **128**, 1791–1795.

Kamimura, M., 1981, "Transition densities between the 0 1 +, 2 1 +, 4 1 +, 0 2 +, 2 2 +, 1 1 and 3 1 states in 12 C derived from the three-alpha resonating-group wave functions," Nucl. Phys. A **351**, 456–480.

Kamimura, Masayasu, 1977, "Chapter V. A Coupled Channel Variational Method for Microscopic Study of Reactions between Complex Nuclei," Prog. Theor. Phys. Suppl. **62**, 236–294.

Kanada-En'yo, Y., 1998, "Variation after angular momentum projection for the study of excited states based on antisymmetrized molecular dynamics," Phys. Rev. Lett. **81**, 5291.

Kanada-En'yo, Y., 2007, "Structure of ground and excited states of C-12," Prog. Theor. Phys. **117**, 655–680; **121**, 895(E) (2009).

Kanada-En'yo, Yoshiko, 2015, "Proton radii of Be, B, and C isotopes," Phys. Rev. C **91**, 014315.

Kanada-En'yo, Yoshiko, 2016a, "Isovector and isoscalar dipole excitations in ^{9}Be and ^{10}Be studied with antisymmetrized molecular dynamics," Phys. Rev. C **93**, 024322.

Kanada-En'yo, Yoshiko, 2016b, "Isoscalar monopole and dipole excitations of cluster states and giant resonances in ^{12}C," Phys. Rev. C **93**, 054307.

Kanada-En'yo, Yoshiko, and Hisashi Horiuchi, 2001, "Structure of light unstable nuclei studied with antisymmetrized molecular dynamics," Prog. Theor. Phys. Suppl. **142**, 205.

Kanada-En'yo, Yoshiko, Hisashi Horiuchi, and Akira Ono, 1995, "Structure of Li and Be isotopes studied with antisymmetrized molecular dynamics," Phys. Rev. C **52**, 628–646.

Kanada-En'yo, Yoshiko, Masaaki Kimura, and Akira Ono, 2012, "Antisymmetrized molecular dynamics and its applications to cluster phenomena," Prog. Theor. Exp. Phys. **2012**, 01A202.

Kawabata, T., *et al.*, 2007, "Indication of dilute 2 alpha + t cluster structure in B-11," Phys. Lett. B **646**, 6–11.

Kimura, M., T. Suhara, and Y. Kanada-En'yo, 2016, "Antisymmetrized molecular dynamics studies for exotic clustering phenomena in neutron-rich nuclei," Eur. Phys. J. A **52**, 373.

Kimura, Masaaki, 2004, "Deformed base antisymmetrized molecular dynamics and its application to Ne-20," Phys. Rev. C **69**, 044319.

Kimura, Masaaki, 2007, "Molecular orbitals and alpha + O-18 molecular bands of Ne-22," Phys. Rev. C **75**, 034312.

Kimura, Masaaki, and Hisashi Horiuchi, 2004, "O-16 + O-16 nature of the superdeformed band of S-32 and the evolution of the molecular structure," Phys. Rev. C **69**, 051304.

Kirsebom, O. S., H. O. U. Fynbo, A. M. Howard, and K. L. Laursen, 2014, "Applying new tools to old problems-experimental studies of resonances in (12)C," J. Phys. Conf. Ser. **569**, 012013.

Kirsebom, O. S., *et al.*, 2010, "Breakup of C-12 resonances into three alpha particles," Phys. Rev. C **81**, 064313.

Kirsebom, O. S., *et al.*, 2012, "Improved Limit on Direct alpha Decay of the Hoyle State," Phys. Rev. Lett. **108**, 202501.

Klein, Nico, Dean Lee, Weitao Liu, and Ulf-G. Meißner, 2015, "Regularization Methods for Nuclear Lattice Effective Field Theory," Phys. Lett. B **747**, 511–516.

Kobayashi, F., and Y. Kanada-En'yo, 2012, "Novel cluster states in 10Be," Phys. Rev. C **86**, 064303.
Kokalova, Tz, *et al.*, 2013, "Precision measurement of the 9.641 MeV, 3^- state in ^{12}C," Phys. Rev. C **87**, 057307.
König, Sebastian, Dean Lee, and H.-W. Hammer, 2011, "Volume Dependence of Bound States with Angular Momentum," Phys. Rev. Lett. **107**, 112001.
König, Sebastian, Dean Lee, and H.-W. Hammer, 2012, "Non-relativistic bound states in a finite volume," Ann. Phys. (Amsterdam) **327**, 1450–1471.
Koonin, S. E., D. J. Dean, and K. Langanke, 1997, "Shell Model Monte Carlo Methods," Phys. Rep. **278**, 1.
Kraemer, T., *et al.*, 2006, "Evidence for efimov quantum states in an ultracold gas of cesium atoms," Nature (London) **440**, 315.
Kravvaris, Konstantinos, and Alexander Volya, 2017, "Study of nuclear clustering from an ab initio perspective," Phys. Rev. Lett. **119**, 062501.
Krieger, A., *et al.*, 2012, "Nuclear Charge Radius of ^{12}Be," Phys. Rev. Lett. **108**, 142501.
Kurokawa, C., and K. Katō, 2007, Nucl. Phys. A **792**, 87.
Kurokawa, C., and K. Katō, 2005, "New broad 0+ state in 12C," Phys. Rev. C **71**, 021301.
Lage, Michael, Ulf-G. Meißner, and Akaki Rusetsky, 2009, "A Method to measure the antikaon-nucleon scattering length in lattice QCD," Phys. Lett. B **681**, 439–443.
Lähde, Timo A., Evgeny Epelbaum, Hermann Krebs, Dean Lee, Ulf-G. Meißner, and Gautam Rupak, 2014, "Lattice Effective Field Theory for Medium-Mass Nuclei," Phys. Lett. B **732**, 110–115.
Lähde, Timo A., Thomas Luu, Dean Lee, Ulf-G. Meißner, Evgeny Epelbaum, Hermann Krebs, and Gautam Rupak, 2015, Nuclear Lattice Simulations using Symmetry-Sign Extrapolation," Eur. Phys. J. A **51**, 92.
Lähde, Timo A., *et al.*, 2015, "Uncertainties of Euclidean Time Extrapolation in Lattice Effective Field Theory," J. Phys. G **42**, 034012.
Lau, P. H. C., and N. S. Manton, 2014, "States of Carbon-12 in the Skyrme Model," Phys. Rev. Lett. **113**, 232503.
Lee, Dean, 2004, "Inequalities for low-energy symmetric nuclear matter," Phys. Rev. C **70**, 064002.
Lee, Dean, 2009, "Lattice simulations for few- and many-body systems," Prog. Part. Nucl. Phys. **63**, 117–154.
Li, K. C. W., *et al.*, 2017, "Characterization of the proposed 4 cluster state candidate in o16," Phys. Rev. C **95**, 031302.
Li, Ning, Song-Yuan Li, and Chuan Liu, 2014, "Generalized Lüschers formula in multichannel baryon-baryon scattering," Phys. Rev. D **90**, 034509.
Li, Ning, and Chuan Liu, 2013, "Generalized Lüscher formula in multichannel baryon-meson scattering," Phys. Rev. D **87**, 014502.
Li, Ning, and Ya-Jie Wu, 2015, "Generalized Lüscher's formula in baryon-meson and baryon-baryon scattering with twisted boundary condition," Eur. Phys. J. A **51**, 4.
Liendo, J. A., N. Curtis, D. D. Caussyn, N. R. Fletcher, and T. Kurtukian-Nieto, 2002, "Near threshold three-body final states in Li-7 + Li-7 reactions at Elab=34-MeV," Phys. Rev. C **65**, 034317.
Liu, Chuan, Xu Feng, and Song He, 2006, "Two particle states in a box and the S-matrix in multi-channel scattering," Int. J. Mod. Phys. A **21**, 847–850.
Lu, Bing-Nan, Timo A. Lähde, Dean Lee, and Ulf-G. Meißner, 2014, "Breaking and restoration of rotational symmetry on the lattice for bound state multiplets," Phys. Rev. D **90**, 034507.
Lu, Bing-Nan, Timo A. Lähde, Dean Lee, and Ulf-G. Meißner, 2015, "Breaking and restoration of rotational symmetry for irreducible tensor operators on the lattice," Phys. Rev. D **92**, 014506.
Lu, Bing-Nan, Timo A. Lähde, Dean Lee, and Ulf-G. Meißner, 2016, "Precise determination of lattice phase shifts and mixing angles," Phys. Lett. B **760**, 309–313.
Lüscher, M., 1986, "Volume dependence of the energy spectrum in massive quantum field theories. 2. scattering states," Commun. Math. Phys. **105**, 153–188.
Lüscher, Martin, 1991, "Two particle states on a torus and their relation to the scattering matrix," Nucl. Phys. B **354**, 531–578.
Luu, Thomas, and Martin J. Savage, 2011, "Extracting Scattering Phase-Shifts in Higher Partial-Waves from Lattice QCD Calculations," Phys. Rev. D **83**, 114508.
Lyu, M., Z. Ren, B. Zhou, Y. Funaki, H. Horiuchi, G. Röpke, P. Schuck, A. Tohsaki, C. Xu, and T. Yamada, 2015, "Investigation of 9Be from a nonlocalized clustering concept," Phys. Rev. C **91**, 014313.
Lyu, M., Z. Ren, B. Zhou, Y. Funaki, H. Horiuchi, G. Röpke, P. Schuck, A. Tohsaki, C. Xu, and T. Yamada, 2016, "Investigation of 10Be and its cluster dynamics with the nonlocalized clustering approach," Phys. Rev. C **93**, 054308.
Mabiala, J., A. A. Cowley, S. V. Fortsch, E. Z. Buthelezi, R. Neveling, F. D. Smit, G. F. Steyn, and J. J. Van Zyl, 2009, "Analyzing power and cross section distributions of the C-12 (p, p alpha) Be-8 cluster knockout reaction at an incident energy of 100 MeV," Phys. Rev. C **79**, 054612.
Machleidt, R., and D. R. Entem, 2011, "Chiral effective field theory and nuclear forces," Phys. Rep. **503**, 1–75.
Mahaux, C., and H. A. Weidenmüller, 1969, *Shell-model approach to nuclear reactions* (North-Holland Publishing Co., Amsterdam).
Manfredi, J., R. J. Charity, K. Mercurio, R. Shane, L. G. Sobotka, A. H. Wuosmaa, A. Banu, L. Trache, and R. E. Tribble, 2012, "alpha decay of the excited states in C-12 at 7.65 and 9.64 MeV," Phys. Rev. C **85**, 037603.
Margenau, H., 1941, "Interaction of alpha-particles," Phys. Rev. **59**, 37.
Marin-Lambarri, D. J., R. Bijker, M. Freer, M. Gai, Tz. Kokalova, D. J. Parker, and C. Wheldon, 2014, "Evidence for Triangular D_{3h} Symmetry in ^{12}C," Phys. Rev. Lett. **113**, 012502.
Maris, P., J. P. Vary, and A. M. Shirokov, 2009, "Ab initio no-core full configuration calculations of light nuclei," Phys. Rev. C **79**, 014308.
McCutchan, E. A., *et al.*, 2009, "Precise electromagnetic tests of ab-initio calculations of light nuclei: States in Be-10," Phys. Rev. Lett. **103**, 192501.
McCutchan, E. A., *et al.*, 2012a, "On the lifetime of the 2+ state in 10C," Phys. Rev. C **86**, 014312.
McCutchan, E. A., *et al.*, 2012b, "Precise gamma-ray intensity measurements in B-10," Phys. Rev. C **86**, 057306.
McMillan, W. L., 1965, "Ground state of liquid he^4," Phys. Rev. **138**, A442–A451.
Meharchand, R., *et al.*, 2012, "Probing Configuration Mixing in Be-12 with Gamow-Teller Transition Strengths," Phys. Rev. Lett. **108**, 122501.
Mehen, Thomas, Iain W. Stewart, and Mark B. Wise, 1999, "Wigner symmetry in the limit of large scattering lengths," Phys. Rev. Lett. **83**, 931–934.
Meißner, Ulf-G., 2015, "Anthropic considerations in nuclear physics," Science Bulletin **60**, 43–54.
Milin, M., and W. von Oertzen, 2002, "Search for molecular bands in 13c," Eur. Phys. J. A **14**, 295–307.

Milin, M., *et al.*, 2005, "Sequential decay reactions induced by a 18 MeV 6 He beam on 6 Li and 7 Li," Nucl. Phys. A **753**, 263–287.
Morinaga, H., 1956, "Interpretation of Some of the Excited States of 4n Self-Conjugate Nuclei," Phys. Rev. **101**, 254–258.
Morinaga, H., 1966, "On the spin of a broad state around 10 MeV in ^{12}C," Phys. Lett. **21**, 78.
Morningstar, Colin, and Mike J. Peardon, 2004, "Analytic smearing of SU(3) link variables in lattice QCD," Phys. Rev. D **69**, 054501.
Nakada, A., Y. Torizuka, and Y. Horikawa, 1971, "Determination of the deformation in ^{12}C from electron scattering," Phys. Rev. Lett. **27**, 1102–1102.
Nauruzbayev, D. K., V. Z. Goldberg, A. K. Nurmukhanbetova, M. S. Golovkov, A. Volya, G. V. Rogachev, and R. E. Tribble, 2017, "Structure of ^{20}Ne states in the resonance $^{16}\mathrm{O}+\alpha$ elastic scattering," Phys. Rev. C **96**, 014322.
Navin, A., *et al.*, 2000, "Direct Evidence for the Breakdown of the N=8 Shell Closure in B-12e," Phys. Rev. Lett. **85**, 266–269.
Navrátil, P., V. G. Gueorguiev, J. P. Vary, W. E. Ormand, and A. Nogga, 2007, "Structure of A=10-13 nuclei with two- plus three-nucleon interactions from chiral effective field theory," Phys. Rev. Lett. **99**, 042501.
Navrátil, P., J. P. Vary, and B. R. Barrett, 2000a, "Large basis ab initio no-core shell model and its application to C-12," Phys. Rev. C **62**, 054311.
Navrátil, P., J. P. Vary, and B. R. Barrett, 2000b, "Properties of C-12 in the ab initio nuclear shell model," Phys. Rev. Lett. **84**, 5728–5731.
Navrátil, Petr, and Sofia Quaglioni, 2012, "Ab initio many-body calculations of the 3H(d,n)4He and 3He(d,p)4He fusion," Phys. Rev. Lett. **108**, 042503.
Navrátil, Petr, Sofia Quaglioni, Guillaume Hupin, Carolina Romero-Redondo, and Angelo Calci, 2016, "Unified ab initio approaches to nuclear structure and reactions," Phys. Scr. **91**, 053002.
Navrátil, Petr, Robert Roth, and Sofia Quaglioni, 2010, "Ab initio many-body calculations of nucleon scattering on ^{4}He, ^{7}Li, ^{7}Be, ^{12}C and ^{16}O," Phys. Rev. C **82**, 034609.
Neff, T., and H. Feldmeier, 2004, "Cluster structures within fermionic molecular dynamics," Nucl. Phys. A **738**, 357–361.
Neff, Thomas, and Hans Feldmeier, 2003, "Tensor correlations in the unitary correlation operator method," Nucl. Phys. A **713**, 311–371.
Neff, Thomas, and Hans Feldmeier, 2014, "The Hoyle state and its relatives," J. Phys. Conf. Ser. **569**, 012062.
Nilson, R., W. K. Jentschke, G. R. Briggs, R. O. Kerman, and J. N. Snyder, 1958, "Investigation of Excited States in Be^{8} by Alpha-Particle Scattering from He," Phys. Rev. **109**, 850–860.
Nollett, Kenneth M., Steven C. Pieper, Robert B. Wiringa, J. Carlson, and G. M. Hale, 2007, "Quantum Monte Carlo calculations of neutron-alpha scattering," Phys. Rev. Lett. **99**, 022502.
Nörtershäuser, W., *et al.*, 2009, "Nuclear Charge Radii of Be-7, Be-9, Be-10 and the one-neutron halo nucleus Be-11," Phys. Rev. Lett. **102**, 062503.
Ogawa, Y., K. Arai, Y. Suzuki, and K. Varga, 2000, "Microscopic four-cluster description of Be-10 and C-10 with the stochastic variational method," Nucl. Phys. A **673**, 122–142.
Ogloblin, A. A., T. L. Belyaeva, A. N. Danilov, A. S. Demyanova, and S. A. Goncharov, 2013, "Radius of ^{12}C in the excited 2_2^+ Hoyle state," Eur. Phys. J. A **49**, 46.
Ogloblin, A. A., *et al.*, 2014, "Rotational band in 12C based on the Hoyle state," Eur. Phys. J. Web Conf. **66**, 02074.
Ohtsubo, S., Y. Fukushima, M. Kamimura, and E. Hiyama, 2013, "Complex-scaling calculation of three-body resonances using complex-range Gaussian basis functions: Application to 3α resonances in ^{12}C," Prog. Theor. Exp. Phys. **2013**, 073D02.
Okabe, S., Y. Abe, and H. Tanaka, 1977, "The Structure of 9Be Nucleus by a Molecular Model. I," Prog. Theor. Phys. **57**, 866.
Okabe, S., Y. Abe, and H. Tanaka, 1978, "Particle Decay Widths and Charge Form Factors of 9Be by the Molecular Model," Prog. Theor. Phys. **59**, 315.
Okolowicz, J., W. Nazarewicz, and M. Ploszajczak, 2013, "Toward understanding the microscopic origin of nuclear clustering," Fortschr. Phys. **61**, 66–79.
Okolowicz, J., M. Ploszajczak, and I. Rotter, 2003, Phys. Rep. **374**, 271–383.
Ono, A., H. Horiuchi, T. Maruyama, and A. Ohnishi, 1992a, "Fragment formation studied with antisymmetrized version of molecular dynamics with two nucleon collisions," Phys. Rev. Lett. **68**, 2898–2900.
Ono, Akira, Hisashi Horiuchi, Toshiki Maruyama, and Akira Ohnishi, 1992b, "Antisymmetrized version of molecular dynamics with two nucleon collisions and its application to heavy ion reactions," Prog. Theor. Phys. **87**, 1185–1206.
Ono, Akira, and Hisashi Horiuchi, 1996, "Statistical properties of antisymmetrized molecular dynamics for nonnucleon emission and nucleon emission processes," Phys. Rev. C **53**, 2341–2351.
Ono, Akira, and Hisashi Horiuchi, 2004, "Antisymmetrized molecular dynamics for heavy ion collisions," Prog. Part. Nucl. Phys. **53**, 501–581.
Orlandini, Giuseppina, *et al.*, 2014, "Coupling the Lorentz Integral Transform (LIT) and the Coupled Cluster (CC) Methods: A Way Towards Continuum Spectra of 'Not-So-Few-Body' Systems," Few-Body Syst. **55**, 907–911.
Overway, D., J. Jnecke, F. D. Becchetti, C. E. Thorn, and G. Kekelis, 1981, "Reaction dependence of nuclear decay linewidths," Nucl. Phys. A **366**, 299–319.
Pain, S. D., *et al.*, 2006, "Structure of Be^{12}: Intruder d—wave strength at $N=8$," Phys. Rev. Lett. **96**, 032502.
Papadimitriou, G., J. Rotureau, N. Michel, M. Płoszajczak, and B. R. Barrett, 2013, "Ab initio," Phys. Rev. C **88**, 044318.
Pieper, Steven C., K. Varga, and Robert B. Wiringa, 2002, "Quantum Monte Carlo calculations of A=9, $A=10$ nuclei," Phys. Rev. C **66**, 044310.
Pieper, Steven C., and Robert B. Wiringa, 2001, "Quantum Monte Carlo calculations of light nuclei," Annu. Rev. Nucl. Part. Sci. **51**, 53–90.
Pieper, Steven C., Robert B. Wiringa, and V. R. Pandharipande, 1992, "Variational calculation of the ground state of O-16," Phys. Rev. C **46**, 1741–1756.
Pine, Michelle, Dean Lee, and Gautam Rupak, 2013, "Adiabatic projection method for scattering and reactions on the lattice," Eur. Phys. J. A **49**, 151.
Quaglioni, Sofia, and Petr Navrátil, 2008, "Ab Initio Many-Body Calculations of n-H-3, n-He-4, p-He-3,4, and n-Be-10 Scattering," Phys. Rev. Lett. **101**, 092501.
Quaglioni, Sofia, Petr Navrátil, and Robert Roth, 2010, "Scattering of light nuclei," Eur. Phys. J. Web Conf. **3**, 01012.
Quaglioni, Sofia, Carolina Romero-Redondo, and Petr Navrtil, 2013, "Three-cluster dynamics within an ab initio framework," Phys. Rev. C **88**, 034320; **94**, 019902(E) (2016).
Raimondi, Francesco, Guillaume Hupin, Petr Navrtil, and Sofia Quaglioni, 2016, "Deuteron-induced nucleon transfer reactions within an ab initio framework: First application to p-shell nuclei," Phys. Rev. C **93**, 054606.
Rana, T. K., *et al.*, 2013, "Estimation of direct components of the decay of the Hoyle state," Phys. Rev. C **88**, 021601(R); Addendum: **88**, 029904 (2013).

Rodrigues, M. R. D., T. BorelloLewin, L. B. HorodynskiMatsushigue, A. Cunsolo, F. Cappuzzello, J. L. M. Duarte, C. L. Rodrigues, G. M. Ukita, M. A. Souza, and H. Miyake, 2010, "Alpha resonances in 13c excited by the 9be (6li,d) reaction," AIP Conf. Proc. **1245**, 141–144.

Rokash, Alexander, Michelle Pine, Serdar Elhatisari, Dean Lee, Evgeny Epelbaum, and Hermann Krebs, 2015, "Scattering cluster wave functions on the lattice using the adiabatic projection method," Phys. Rev. C **92**, 054612.

Romero-Redondo, Carolina, Sofia Quaglioni, Petr Navrátil, and Guillaume Hupin, 2016, "How many-body correlations and α-clustering shape ^{6}He," Phys. Rev. Lett. **117**, 222501.

Romero-Redondo, Carolina, Sofia Quaglioni, Petr Navrtil, and Guillaume Hupin, 2014, "$^4\mathrm{He} + n + n$ continuum within an ab initio framework," Phys. Rev. Lett. **113**, 032503.

Röpke, G., A. Schnell, P. Schuck, and P. Noziéres, 1998, "Four-particle condensate in strongly coupled fermion systems," Phys. Rev. Lett. **80**, 3177.

Roth, Robert, Joachim Langhammer, Angelo Calci, Sven Binder, and Petr Navrátil, 2011, "Similarity-Transformed Chiral NN+3N Interactions for the Ab Initio Description of 12-C and 16-O," Phys. Rev. Lett. **107**, 072501.

Roth, Robert, Thomas Neff, and Hans Feldmeier, 2010, "Nuclear Structure in the Framework of the Unitary Correlation Operator Method," Prog. Part. Nucl. Phys. **65**, 50–93.

Rowe, D. J., and G. Rosensteel, 1980, "On the Algebraic Formulation of Collective Models. II. Collective and Instrinsic Submanifolds," Ann. Phys. (N.Y.) **126**, 198–233.

Rowe, D. J., and J. L. Wood, 2010, *Fundamentals of Nuclear Models* (World Scientific, Singapore).

Rupak, Gautam, and Dean Lee, 2013, "Radiative capture reactions in lattice effective field theory," Phys. Rev. Lett. **111**, 032502.

Rutherford, E., 1899, "Uranium radiation and the electrical conduction produced by it," Philos. Mag. **47**, 109.

Schuck, P., Y. Funaki, H. Horiuchi, G. Röpke, A. Tohsaki, and T. Yamada, 2016, "Alpha particle clusters and their condensation in nuclear systems," Phys. Scr. **91**, 123001.

Seya, M., N. Kohno, and S. Nagata, 1981, "Nuclear Binding Mechanism and Structure of Neutron-Rich Be and B Isotopes by Molecular-Orbital Model," Prog. Theor. Phys. **65**, 204.

Shimizu, Noritaka, Takashi Abe, Yusuke Tsunoda, Yutaka Utsuno, Tooru Yoshida, Takahiro Mizusaki, Michio Honma, and Takaharu Otsuka, 2012, "New Generation of the Monte Carlo Shell Model for the K Computer Era," Prog. Theor. Exp. Phys. **2012**, 01A205.

Shimizu, Noritaka, Yutaka Utsuno, Takahiro Mizusaki, Michio Honma, Yusuke Tsunoda, and Takaharu Otsuka, 2012, "Variational procedure for nuclear shell-model calculations and energy-variance extrapolation," Phys. Rev. C **85**, 054301.

Shimizu, Noritaka, Yutaka Utsuno, Takahiro Mizusaki, Takaharu Otsuka, Takashi Abe, and Michio Honma, 2010, "Novel Extrapolation Method in the Monte Carlo Shell Model," Phys. Rev. C **82**, 061305.

Shimoura, S., *et al.*, 2003, "Isomeric 0+ state in 12Be," Phys. Lett. B **560**, 31–36.

Sick, I., and J. S. Mccarthy, 1970, "Elastic electron scattering from c-12 and o-16," Nucl. Phys. A **150**, 631–654.

Smith, R., *et al.*, 2017, "New Measurement of the Direct 3α Decay from the ^{12}C Hoyle State," Phys. Rev. Lett. **119**, 132502.

Soic, N., *et al.*, 2003, "Cluster structure of C-13 probed via the Li-7(Be-9, C*-13 → Be-9 + alpha) reaction," Nucl. Phys. A **728**, 12.

Stoof, H. T. C., 1994, "Atomic Bose gas with a negative scattering length," Phys. Rev. A **49**, 3824–3830.

Strehl, P., and Th. H. Schucan, 1968, "Study of monopole transitions in 12 C, 24 Mg, 28 Si, 32 S and 40 Ca by inelastic electron scattering," Phys. Lett. B **27**, 641–643.

Suhara, T., N. Itagaki, J. Cseh, and M. Poszajczak, 2013, "Novel and simple description for a smooth transition from α-cluster wave functions to jj-coupling shell model wave functions," Phys. Rev. C **87**, 054334.

Suhara, T., and Y. Kanada-En'yo, 2010, "Cluster structures of excited states in 11B," Prog. Theor. Phys. **123**, 303.

Suhara, Tadahiro, and Yoshiko Kanada-En'yo, 2010a, "Cluster structures of excited states in ^{14}C," Phys. Rev. C **82**, 044301.

Suhara, Tadahiro, and Yoshiko Kanada-En'yo, 2010b, "Quadrupole Deformation β and γ Constraint in a Framework of Antisymmetrized Molecular Dynamics," Prog. Theor. Phys. **123**, 303–325.

Suhara, Tadahiro, and Yoshiko Kanada-En'yo, 2015, "Effects of α-cluster breaking on 3α cluster structures in ^{12}C," Phys. Rev. C **91**, 024315.

Suzuki, D., *et al.*, 2013, "Resonant alpha scattering of ^{6}He: Limits of clustering in ^{10}Be," Phys. Rev. C **87**, 054301.

Suzuki, Toshio, and Takaharu Otsuka, 1997, "Gamow-Teller transitions from Li-11 and Be-12," Phys. Rev. C **56**, 847–856.

Suzuki, Y., H. Horiuchi, and I. Ikeda, 1972, "Study of α Chain States through Their Decay Widths," Prog. Theor. Phys. **47**, 1517.

Tang, Y. C., M. Lemere, and D. R. Thompson, 1978, "Resonating-group method for nuclear many-body problems," Phys. Rep. **47**, 167–223.

Taniguchi, Yasutaka, Masaaki Kimura, and Hisashi Horiuchi, 2004, "New constraint of clustering for AMD and its application to the study of 2 alpha—C-12 structure of Ne-20," Prog. Theor. Phys. **112**, 475.

Tanihata, I., H. Hamagaki, O. Hashimoto, Y. Shida, N. Yoshikawa, K. Sugimoto, O. Yamakawa, T. Kobayashi, and N. Takahashi, 1985, "Measurements of Interaction Cross-Sections and Nuclear Radii in the Light p Shell Region," Phys. Rev. Lett. **55**, 2676–2679.

Thompson, D. R., M. Lemere, and Y. C. Tang, 1977, "Systematic investigation of scattering problems with the resonating-group method," Nucl. Phys. A **286**, 53–66.

Tilley, D. R., H. R. Weller, and C. M. Cheves, 1993, "Energy levels of light nuclei A=16-17," Nucl. Phys. A **564**, 1–183.

Tohsaki, A., H. Horiuchi, P. Schuck, and G. Röpke, 2001, "Alpha cluster condensation in C-12 and O-16," Phys. Rev. Lett. **87**, 192501.

Tohsaki, A., H. Horiuchi, P. Schuck, and G. Röpke, 2017, "Colloquium: Status of α-particle condensate structure of the Hoyle state," Rev. Mod. Phys. **89**, 011002.

Uegaki, E., Y. Abe, S. Okabe, and H. Tanaka, 1979, "Structure of the Excited States in ^{12}C. II," Prog. Theor. Phys. **62**, 1621.

Uegaki, E., S. Okabe, Y. Abe, and H. Tanaka, 1977, "Structure of the Excited States in ^{12}C. I," Prog. Theor. Phys. **57**, 1262.

Varga, K., and Y. Suzuki, 1995, "Precise solution of few body problems with stochastic variational method on correlated Gaussian basis," Phys. Rev. C **52**, 2885–2905.

Varga, K., Y. Suzuki, and R. G. Lovas, 1994, "Microscopic multicluster description of neutron halo nuclei with a stochastic variational method," Nucl. Phys. A **571**, 447–466.

Varga, K., Y. Suzuki, and I. Tanihata, 1995, "Microscopic four cluster description of the Li-9 and C-9 mirror nuclei," Phys. Rev. C **52**, 3013–3025.

Volkov, A., 1965, "Equilibrium deformation calculations of the ground state energies of 1p shell nuclei," Nucl. Phys. **74**, 33–58.

Volya, Alexander, and Yury M. Tchuvil'sky, 2015, "Nuclear clustering using a modern shell model approach," Phys. Rev. C **91**, 044319.

Volya, Alexander, and Vladimir Zelevinsky, 2005, "Discrete and continuum spectra in the unified shell model approach," Phys. Rev. Lett. **94**, 052501.

von Oertzen, W., 1996, "Two-center molecular states in ^{9}B, ^{9}Be, ^{10}Be, and ^{10}B," Z. Phys. A **354**, 37.

von Oertzen, W., 1997a, "Dimers based on the $\alpha + \alpha$ potential and chain states of carbon isotopes," Z. Phys. A **357**, 355–365.

von Oertzen, W., 1997b, "Dimers and polymers in extremely deformed neutron-rich light nuclei," Il Nuovo Cimento A **110**, 895–906.

von Oertzen, W., M. Freer, and Y. Kanada-En'yo, 2006, "Nuclear clusters and nuclear molecules," Phys. Rep. **432**, 43.

von Oertzen, W., *et al.*, 2004, "Search for cluster structure of excited states in 14c," Eur. Phys. J. A **21**, 193–215.

von Stecher, J., J. P. D'Incao, and Chris H. Greene, 2009, "Signatures of universal four-body phenomena and their relation to the efimov effect," Nat. Phys. **5**, 417–421.

Weinberg, Steven, 1990, "Nuclear forces from chiral lagrangians," Phys. Lett. B **251**, 288–292.

Weinberg, Steven, 1991, "Effective chiral lagrangians for nucleon—pion interactions and nuclear forces," Nucl. Phys. B **363**, 3–18.

Wheeler, John A., 1937a, "On the Mathematical Description of Light Nuclei by the Method of Resonating Group Structure," Phys. Rev. **52**, 1107–1122.

Wheeler, John Archibald, 1937b, "Molecular Viewpoints in Nuclear Structure," Phys. Rev. **52**, 1083–1106.

Wheldon, C., *et al.*, 2011, "High-resolution measurement of absolute alpha-decay widths in O-16," Phys. Rev. C **83**, 064324.

Wigner, E., 1937, "On the Structure of Nuclei Beyond Oxygen," Phys. Rev. **51**, 947–958.

Wildermuth, K., and Th. Kanellopoulos, 1958, "The cluster model of the atomic nuclei," Nucl. Phys. **7**, 150–162.

Wiringa, Robert B., Steven C. Pieper, J. Carlson, and V. R. Pandharipande, 2000, "Quantum Monte Carlo calculations of A=8 nuclei," Phys. Rev. C **62**, 014001.

Wiringa, Robert B., V. G. J. Stoks, and R. Schiavilla, 1995, "An Accurate nucleon-nucleon potential with charge independence breaking," Phys. Rev. C **51**, 38–51.

Yamada, Taiichi, Yasuro Funaki, Takayuki Myo, Hisashi Horiuchi, Kiyomi Ikeda, Gerd Röpke, Peter Schuck, and Akihiro Tohsaki, 2012, "Isoscalar monopole excitations in ^{16}O: α-cluster states at low energy and mean-field-type states at higher energy," Phys. Rev. C **85**, 034315.

Yamaguchi, H., *et al.*, 2017, "Experimental investigation of a linear-chain structure in the nucleus 14c," Phys. Lett. B **766**, 11–16.

Yoshida, T., N. Shimizu, T. Abe, and T. Otsuka, 2013, "Intrinsic Structure of Light Nuclei in Monte Carlo Shell Model Calculation," Few-Body Syst. **54**, 1465–1468.

Youngblood, D. H., Y. W. Lui, and H. L. Clark, 1998, "High lying E-0 strength in C-12," Phys. Rev. C **57**, 2748–2751.

Zhou, B., Y. Funaki, H. Horiuchi, Z. Ren, G. Röpke, P. Schuck, A. Tohsaki, C. Xu, and T. Yamada, 2013, "Nonlocalized clustering: A new concept in nuclear cluster structure physics," Phys. Rev. Lett. **110**, 262501.

Zhou, B., Y. Funaki, H. Horiuchi, Z. Ren, G. Röpke, P. Schuck, A. Tohsaki, C. Xu, and T. Yamada, 2014, "Nonlocalized cluster dynamics and nuclear molecular structure," Phys. Rev. C **89**, 034319.

Zhou, B., Y. Funaki, A. Tohsaki, H. Horiuchi, and Z. Ren, 2014, "The container picture with two-alpha correlation for the ground state of 12C," Prog. Theor. Exp. Phys. **2014**, 101D01.

Zhou, B., Z. Ren, C. Xu, Y. Funaki, T. Yamada, A. Tohsaki, H. Horiuchi, P. Schuck, and G. Röpke, 2012, "New concept for the ground-state band in 20ne within a microscopic cluster model," Phys. Rev. C **86**, 014301.

Zhou, Bo, Akihiro Tohsaki, Hisashi Horiuchi, and Zhongzhou Ren, 2016, "Breathing-like excited state of the Hoyle state in ^{12}C," Phys. Rev. C **94**, 044319.

Zimmerman, W. R., 2013, Direct Observation of the Second 2+ State in 12C, Ph.D. thesis (University of Connecticut).

Zimmerman, W. R., N. E. Destefano, M. Freer, M. Gai, and F. D. Smit, 2011, "Further evidence for the broad 2_2^+ state at 9.6 MeV in ^{12}C," Phys. Rev. C **84**, 027304.

Zimmerman, W. R., *et al.*, 2013, "Unambiguous Identification of the Second 2^+ State in C^{12} and the Structure of the Hoyle State," Phys. Rev. Lett. **110**, 152502.